Cone and Cellular Solar Concentrator Model

INTERIM SUMMARY PROGRESS REPORT

GER 12114

FEBRUARY 1965

CONTRACT NAS 1-4341

NATIONAL AERONAUTICS AND SPACE ADMINISTRATION
LANGLEY RESEARCH CENTER
HAMPTON, VIRGINIA

GOODYEAR AEROSPACE

GER-12114

CONE AND COLUMN SOLAR CONCENTRATOR MODEL

INTERIM SUMMARY PROGRESS REPORT

February 1965

By Thomas J. McCusker

Prepared under Contract No. NAS-1-4341,
Control No. L-4733 by

GOODYEAR AEROSPACE CORPORATION
Akron, Ohio

for

NATIONAL AERONAUTICS AND SPACE ADMINISTRATION
LANGLEY RESEARCH CENTER
HAMPTON, VIRGINIA

FOREWORD

This report summarizes the design feasibility analysis conducted by Goodyear Aerospace Corporation (GAC) for NASA, Langley Research Center, under Contract NAS 1-4341 for the development of supporting structure and the design, development, and fabrication of a preprototype, five-foot diameter cone and column solar concentrator model.

The work was performed by the Space Systems and Analytics Division with T. J. McCusker as project engineer. The structural analysis was performed by J. E. Houmard. The thermal analysis was performed by R. L. Ginter.

TABLE OF CONTENTS

LIST OF ILLUSTRATIONS

LIST OF TABLES

CONE AND COLUMN SOLAR CONCENTRATOR MODEL

INTERIM SUMMARY PROGRESS REPORT

By Thomas J. McCusker
Goodyear Aerospace Corporation

SUMMARY

This Interim Summary Progress Report summarizes the studies made in the design feasibility analysis of the cone and column solar concentrator. The studies are based on a 60 foot diameter concentrator with the capability of focusing 95 percent of the focal plane energy within a 1.9 foot diameter circle.

An optical analysis is made to translate the performance requirements into structural sizes and tolerances. Based on these structural requirements, a packaging/erection scheme is detailed which can be analyzed structurally and thermally.

The optical analysis shows that the concentrator will intercept 368 kW of solar energy in space. Of this, 230 kW will reach the focal plane. With a receiver efficiency of 75 percent, 172 kW will be available for energy conversion. The specified rms average errors for attaining this performance are 30 minutes and 15 minutes for the cone tangential and radial errors and 16 minutes for the column radial error. The maximum column diameter required is 2.13 feet.

The packaging study shows that it is feasible to package the concentrator within a volume 9 feet diameter by 25.33 feet long.

Weight calculations show that the weight objective of 0.2 pounds per square foot is feasible.

The packaging and erection of the concentrator are shown to be feasible. Problems in the area of maintaining the required tangential accuracy of the cone reflector are analyzed. Experimental investigations are still in progress in this area.

The thermal analysis shows the temperature distributions which can be expected in the concentrator and their effect on geometry.

INTRODUCTION

General

The cone and column concentrator is a combination of reflectors designed to be the optical equivalent of a paraboloidal reflector. The concentrator is shown schematically in Figure 1. Its purpose is to concentrate solar energy to a focal point that can be used for electrical power generation or for other applications.

The concentrator consists of a conical reflector with a stepped column reflector located on its axis. When the concentrator axis is pointed to the sun, solar energy incident on the cone is reflected to the column reflector, back to the cone, and thence to the focal point. The focal point lies on the axis of the concentrator beyond the end of the column.

Theoretical analysis and tests of an optical demonstration model were made under NASA contract NAS 1-3140. This work has served to establish the optical principles of the concept and has shown that the cone and column concentrator can be competitive with established concentrator designs provided that lightweight construction can be used without loss of optical accuracy.

Scope

Described in this report is the conceptual design of a deployment system for a 60 foot diameter cone and column concentrator. Only sufficient detail has been included in the design to show that such a system is feasible. Included with this design is a weight breakdown.

The structural analysis includes the investigations of the membrane type cone reflector and a folding support ring for the cone reflector. Since these two components require the more extensive development, most of the analysis was devoted to these items.

A thermal analysis was made to determine the temperature distribution in the reflector surfaces under various operating conditions. The effect of this distribution on cone geometry is investigated.

An overall evaluation is made of the cone and column concentrator concept and conclusions and recommendations are presented.

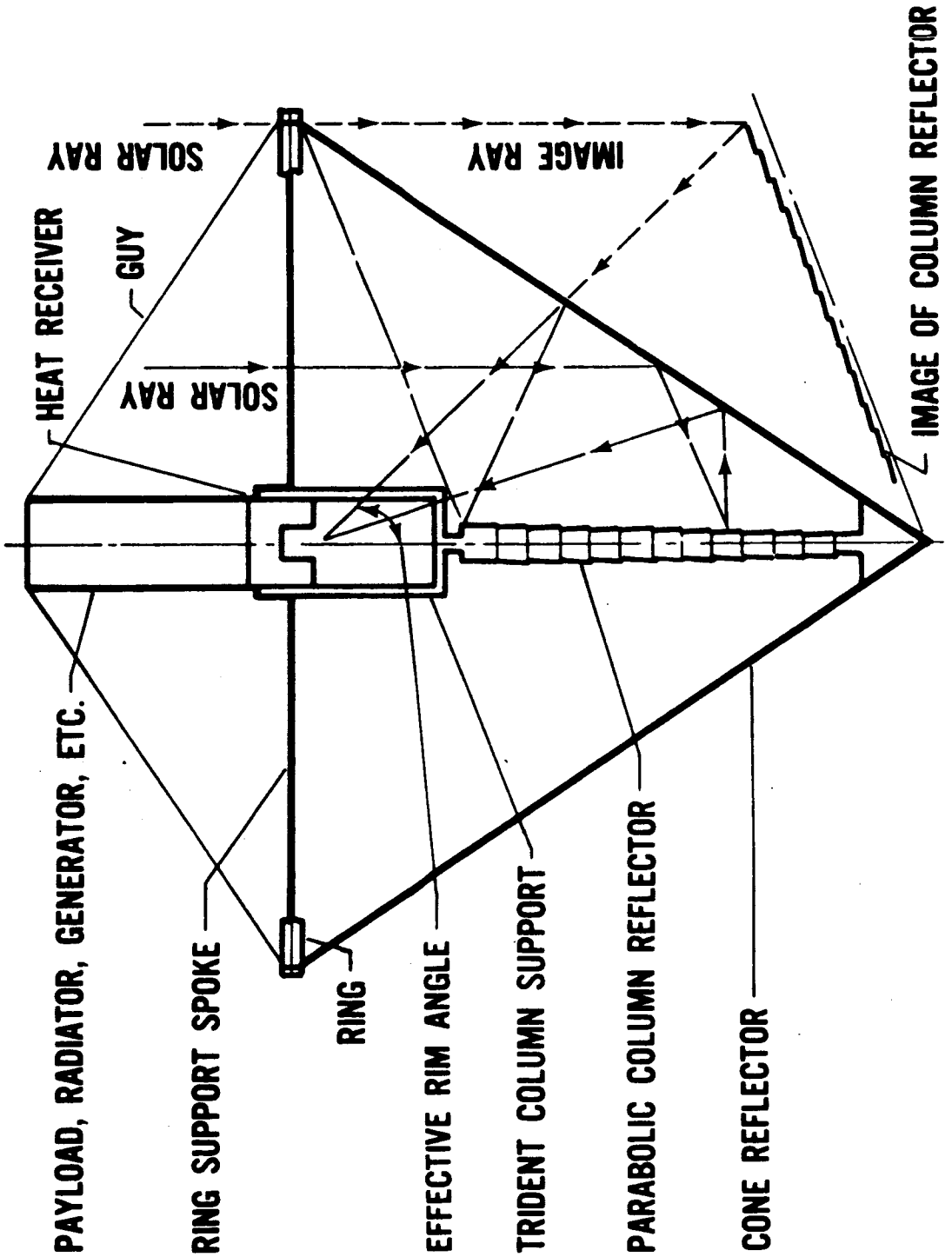

FIGURE 1. CONE AND COLUMN SOLAR CONCENTRATOR

OPTICAL DESIGN

The optical design of the 60-foot diameter cone and column concentrator should be made in accordance with the design equations developed under the preceding contract and reported in GER-11292[1]. The effective aperture of the receiver defines the accuracy requirements of the concentrator surfaces. The specified aperture is 1.9 inches for a 60 inch diameter concentrator with the aperture collecting 95 percent of the focal plane energy. The effective aperture diameter as defined in the reference is then 2.124 inches.* For a concentrator radius of 30 feet, as specified for the feasibility study, the corresponding effective aperture radius will be 1.062 feet.

Equation 42 of Reference 1 gives the effective image radius as:

$$d_r = \frac{R_o}{3440}\left[(1.60 \times 16)^2 + (6.26\,\sigma_{\bar{\theta}_r})^2 + (4.51\,\sigma_{\bar{\alpha}_r})^2\right]^{1/2}$$

where:

d_r = effective image radius as determined from radial error considerations

R_o = concentrator radius

$\sigma_{\bar{\theta}_r}$ = rms average radial slope error in the cone reflector, minutes

$\sigma_{\bar{\alpha}_r}$ = rms average radial slope error in the column reflector, minutes

Substituting $d_r = 1.062$ and $R_o = 30.00$, and rearranging we obtain:

---

1 GER 11292, Investigation of the Optical Characteristics of the Cone-and- Column Double Reflector Solar Concentrator, Goodyear Aerospace Corporation, Akron, Ohio. November 1963.

* Assuming the receiver efficiency to be 75 percent, the effective aperture is that aperture which will radiate 25 percent of the focal plane energy.

$$(6.26\ \sigma_{\bar{\theta}_r})^2 + (4.57\ \sigma_{\bar{\alpha}_r})^2 = 14{,}180$$

from which a combination of $\sigma_{\bar{\theta}_r}$ and $\sigma_{\bar{\alpha}_r}$ may be specified. When $\sigma_{\bar{\theta}_r}$ is taken as 15.0 minutes, the corresponding value of $\sigma_{\bar{\alpha}_r}$ is 16.02 minutes. This allocation of accuracy requirements appears to be practical.

Equation 43 of Reference 1 may be used to determine an acceptable value of tangential cone error, $\sigma_{\bar{\theta}_t}$. Image radius is

$$d_t = \frac{R_o}{3440}\left[(1.60 \times 16)^2 + (3.21\ \sigma_{\bar{\theta}_t})^2 \right]^{\frac{1}{2}}.$$

Substituting d_t and R_o as before, we obtain $\sigma_{\bar{\theta}_t} = 37.10$ minutes.

In order to ensure that only one of the quantities d_t and d_r governs the image radius, one should be made smaller than the other. This can be done by reducing $\sigma_{\bar{\theta}_t}$ to 30 minutes.

This value of $\sigma_{\bar{\theta}_t}$ can be used in Equation 31 of Reference 1 to obtain the radius of the top column section.

$$p_o = 0.01\ R_o \left[4.6 + 0.267\ \sigma_{\bar{\theta}_t} \right]^{\frac{1}{2}}$$

Substitution gives $p_o = 1.065$ feet radius. The radius of the next column section is $0.725\ p_o = 0.772$ feet radius. The radius of the bottom column section is $0.415\ p_o = 0.442$ feet radius. Since these are practical column radii there is no need to further lower the allowable tangential slope error of the cone.

In summary, the slope accuracy requirements are:

Cone tangential error	=	30 min rms average
Cone radial error	=	15 min rms average
Column radial error	=	16 min rms average

The column dimensions are shown in Figure 2. The column will accommodate solar rays from that part of the cone between radii of 3 feet and 30 feet. The column has been lengthened to intercept rays up to 0° - 30' from the paths of the ideal rays as shown.

The focal point is located by tracing the path of the ideal rim ray. The image of the column in the cone reflector is located as shown in Figure 3. The rim ray is drawn from the column image so that it approaches the focal plane at an angle (effective rim angle) of 45 degrees. Solution of the resulting geometry shown locates the focal point 1.319 feet below the rim of the cone.

Figures 4 and 5 show the paths of rays grazing the top of the column and entering the center of the aperture and the edge of the aperture. The ray shown entering the edge of the aperture is in the position beyond which there is no loss due to interference by the top of the column. The ray entering the center of the aperture is in a position where the interference loss is approximately 50%. By assuming a linear relationship between fraction of power lost and concentrator radius, an estimate of the total power loss can be made.

The fraction of power loss from rays originating at radius r is:

$$f = .50 \frac{r_o - r}{r_o - r_{.50}}$$

where:

r_o = radius of origin of rays having no interference loss

$r_{.50}$ = radius of origin of rays having 50 percent interference loss

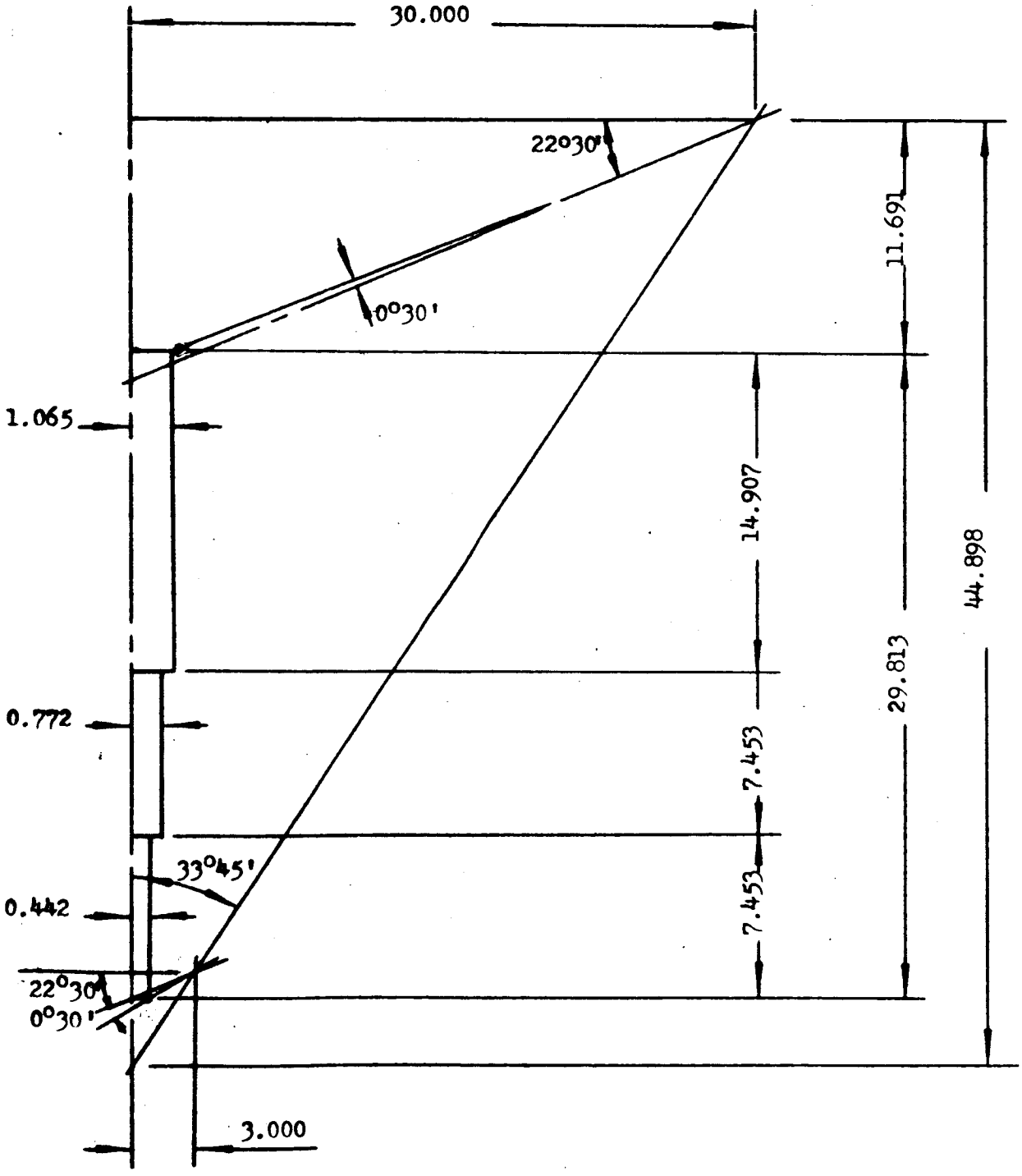

FIGURE 2. COLUMN DIMENSIONS

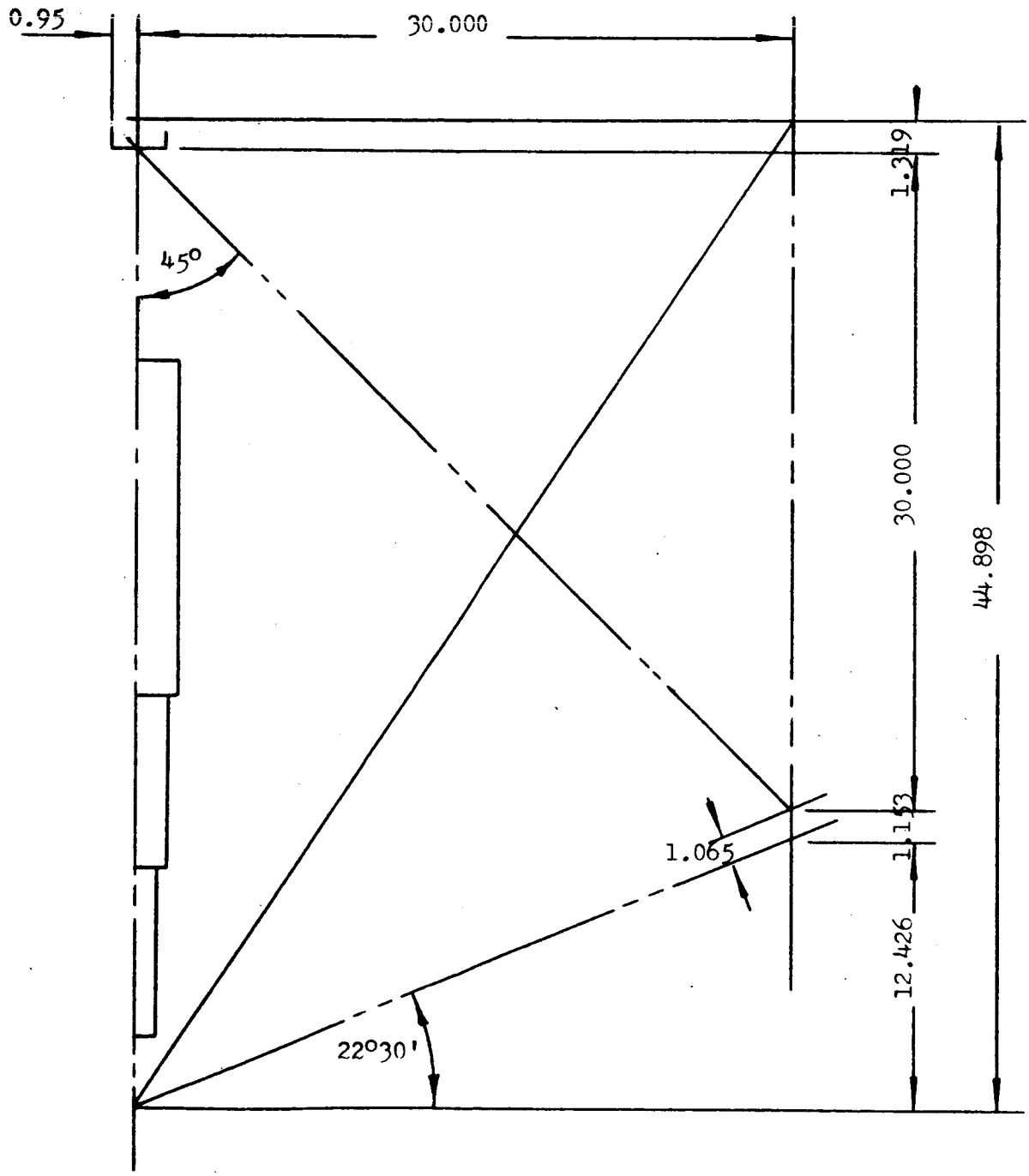

FIGURE 3. FOCAL POINT LOCATION

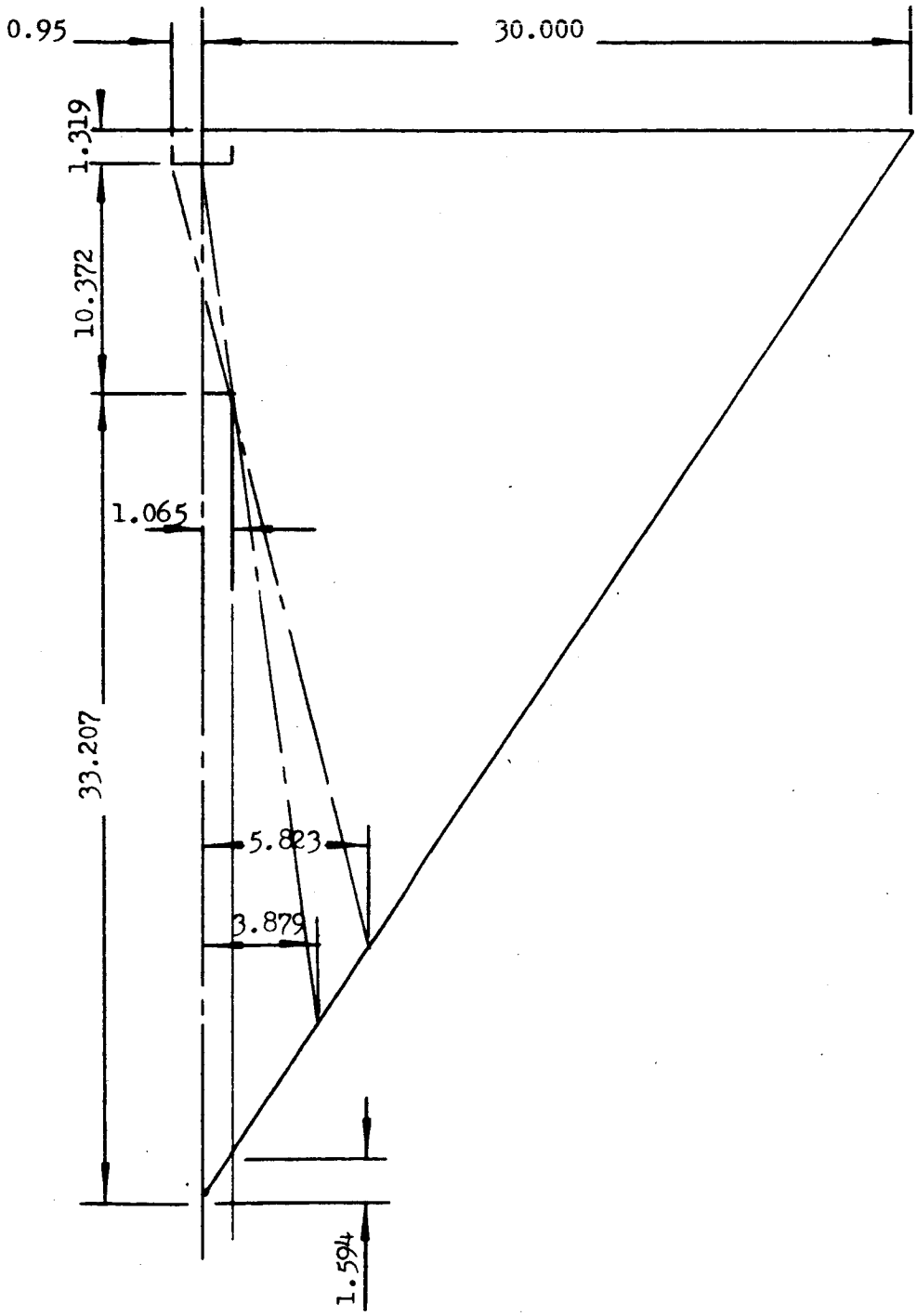

FIGURE 4. COLUMN INTERFERENCE

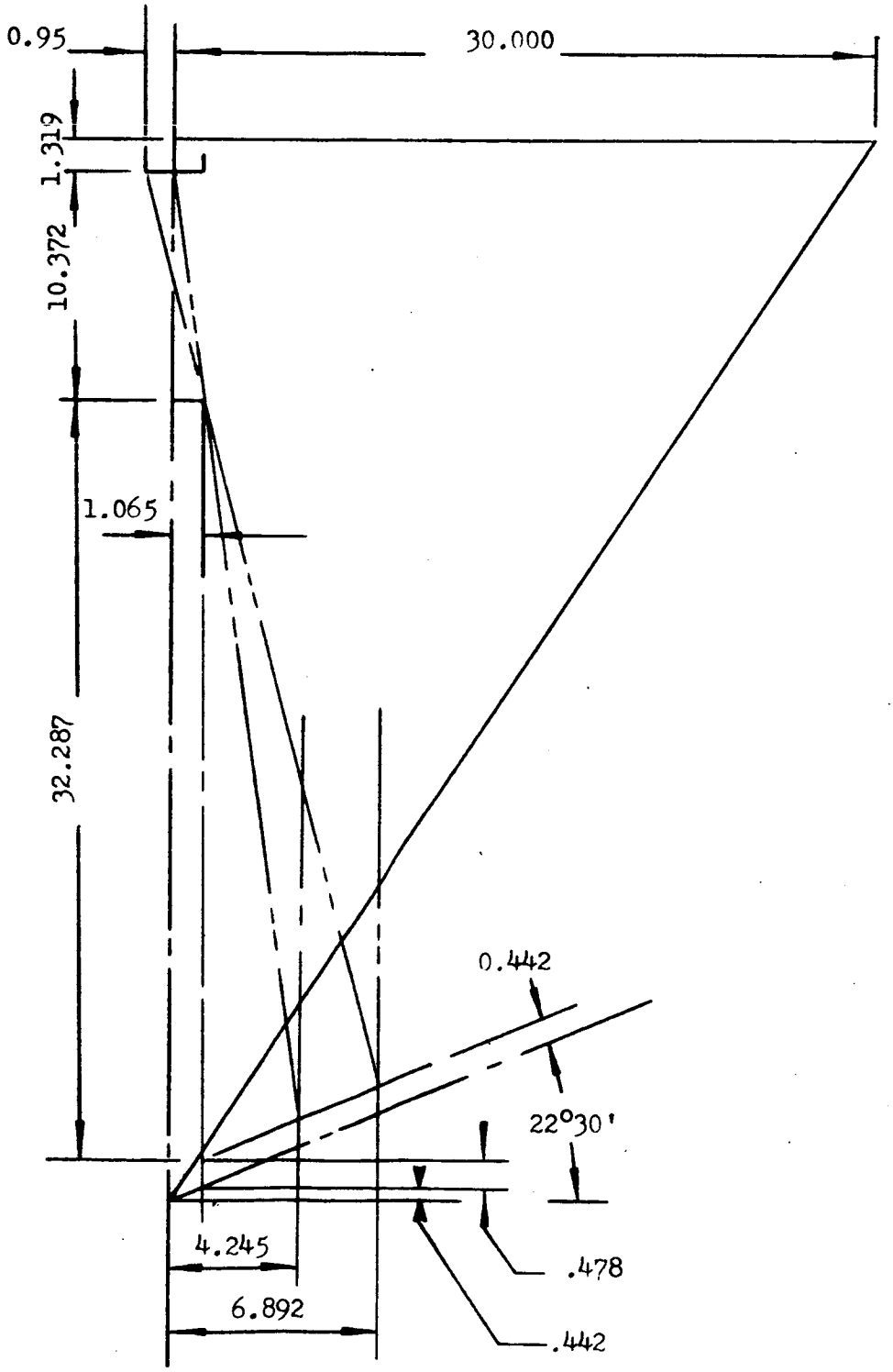

FIGURE 5. COLUMN INTERFERENCE RAY ORIGIN

The fraction of power lost from the cone is then:

$$F = \frac{\int f \, dA}{A}$$

where A is cone area. Where R_i and R_o are the inside and outside cone radii, the loss becomes:

$$F = \frac{\int_{R_i}^{r_o} f \, 2 \pi r \, dr}{\pi (R_o^2 - R_i^2)}$$

$$= \frac{\int_{R_i}^{r_o} .50 \, \frac{r_o - r}{r_o - r_{.50}} \, 2 r \, dr}{R_o^2 - R_i^2}$$

$$= \frac{1}{(R_o^2 - R_i^2)(r_o - r_{.50})} \left[\left(\frac{r_o^3}{2} - \frac{r_o R_i^2}{2} \right) - \left(\frac{r_o^3}{3} - \frac{R_i^3}{3} \right) \right]$$

Substituting $r_o = 6.892$, $r_{.50} = 4.245$, $R_o = 30$, and $R_i = 3$, we obtain $F = 0.0138$. Considering the approximations made in the calculation, we may conclude that the top of the column intercepts between 1¼ and 1½ percent of the energy focused on the heat receiver.

The column is supported from the heat receiver by 3 one-inch tubes equally spaced on a 2.83-foot radius circle. The top of the column is connected to these tubes by a spider of 3 one-inch tubes. These structural members interfere with solar rays focused on the receiver aperture. The fractional power blocked can be closely estimated by taking the ratio of the view factor of the structure to the view factor of the incident rays as viewed from the aperture. This ratio has been calculated to be 0.00429/0.2877 = 0.0149. Thus, the column support structure has been found to block about 1½ percent of the energy focused on the heat receiver.

The ring support wires (120 at 0.020 inch diameter) will block 0.21 percent of the incident solar energy.

The various shadowing losses can then be summarized as follows:

Receiver blockage	1.0 percent loss
Top of column	1.4 percent loss
Column support structure	1.5 percent loss
Ring support structure	0.2 percent loss
Total shadow loss*	4.0 percent

This total is a reasonable one for solar concentrators.

The triple reflectance for aluminum as determined in Reference 1 is 80.3 percent. Various factors such as diffuse reflection, surface coatings for temperature control, loss of quality obtainable on large areas, etc., make this reflectance difficult to obtain. A reasonable objective for reflectance has been specified at 65 percent. Combining this value with a 4 percent shadow loss gives 62.4 percent of the intercepted energy reaching the focal plane. At 1 A.U., a 60-foot concentrator will intercept 368 kW, 230 kW will reach the focal plane, and 218 kW will enter the receiver aperture. With a receiver efficiency of 75 percent, 172 kW will be available for energy conversion.

---

1 op. cit. - GER 11292

* Total shadow loss is calculated from total transmittance, where transmittance is defined as the complement of the shadow loss and total transmittance is the product of the several transmittances.

DEPLOYMENT CONCEPT

Packaging Objectives

Since the cone and column concentrator is to be used in space, means must be provided for packaging the concentrator, transporting it to space, and erecting the concentrator. The general objectives of the deployment system are to meet the packaging and erection requirements and to support the packaged concentrator during launch.

The package dimensions for large diameter concentrators should be about 10 to 20 percent of the concentrator diameter.

The package should deploy automatically on command in a zero-g space environment. It is desirable that some, if not all phases of deployment, can be demonstrated and checked on the ground.

The concentrator and packaging accessories should be lightweight. The weight objective is 0.2 lb/ft^2 of frontal area.

The mechanisms for the deployment of the concentrator should require a minimum of power and energy.

Approach

Fabricating the cone of a thin flexible film permits the cone to be folded to fit in the package. The film cone can be supported between a rim ring and a ring near its apex. Because of its size, the rim ring must be folded to fit in the package. The approach taken for folding the rim ring is to incorporate longitudinal hinges in the ring so that the cross-section can be collapsed. The ring can then be folded elastically.

The rim ring can be supported by flexible wire spokes from the central structure in the vicinity of the heat receiver. The extension of the ring will be controlled by regulating the deployment of the spokes.

The two lower sections of the column can be telescoped into the upper section of the column. The package length can further be reduced by moving the column assembly toward the heat receiver. The resulting package length is somewhat longer than the more desirable 10 to 20 percent of the concentrator diameter suggested as an objective, but further telescoping yields only a small decrease in length at a considerable penalty in complexity.

Description Of Packaging/Erection Scheme

A conceptual design of a cone and column concentrator is shown in Figures 6, 7, and 8. The design incorporates means for folding the concentrator for packaging and a means for controlling the erection of the concentrator in space. Sufficient detail is shown in these figures to evaluate the feasibility of the concept.

The principal parts of the concentrator are:

(1) Apex Ring
(2) Rim Ring
(3) Cone
(4) Lower Column Section
(5) Middle Column Section
(6) Upper Column Section
(7) Ball Bushings
(8) Lower, Middle, and Upper Support Tubes
(9) Column Support Tube
(10) Column Drive Cable
(11) Spokes
(12) Spoke Reel
(13) Column Drive Cable Reel
(14) Receiver
(15) Drive Motor

Figure 6 shows the arrangement of parts with the concentrator in the erected position. Figure 7 shows various details of the erection mechanism and the structure. The packaged concentrator is shown in Figure 8. The overall dimensions of the packaged concentrator are 9 feet diameter by 25.33 feet long.

Packaging/Erection of Ring. - The ring design utilizes a collapsible diamond cross-section to permit folding. With the cross-section collapsed the ring becomes flexible and can be folded into loops to fit its storage compartment as shown in Figure 8.

For control of ring erection, it is desirable to have each loop attached to a spoke. This is accomplished by the design shown. To erect the ring, the spoke reels are rotated allowing the spokes to extend. Spring loading in the ring will cause the ring to extend toward its erected position. A pressure must be applied to the inside of the ring cross-section to open the ring to its final diamond cross-section. As opening of the cross-section progresses, the ring will take its circular shape.

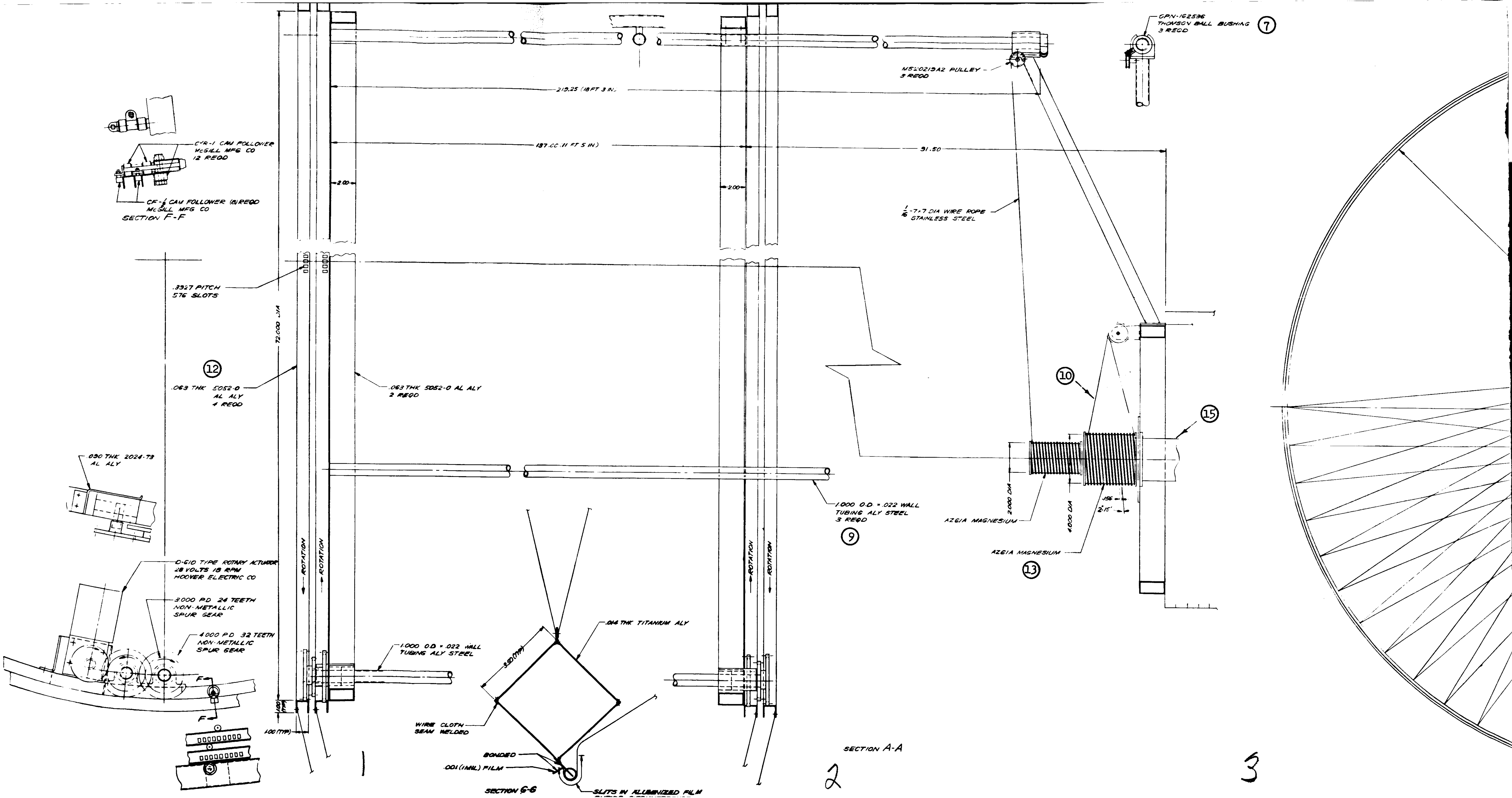

GPN-162536
THOMSON BALL BUSHING
3 REQD
7
MS20215A2 PULLEY
3 REQD
219.25 (18 FT 3 IN)
137.00 (11 FT 5 IN)
91.50
2.00
CYR-1 CAM FOLLOWER
McGILL MFG CO
12 REQD
CF-1/2 CAM FOLLOWER (8) REQD
McGILL MFG CO
SECTION F-F
1/16-7×7 DIA WIRE ROPE
STAINLESS STEEL
.3927 PITCH
576 SLOTS
72.000 DIA
12
.063 THK 5052-0
AL ALY
4 REQD
.063 THK 5052-0 AL ALY
2 REQD
10
15
.090 THK 2024-T3
AL ALY
1.000 O.D × .022 WALL
TUBING ALY STEEL
3 REQD
9
2.000 DIA
4.000 DIA
.156
2.15
AZ61A MAGNESIUM
AZ61A MAGNESIUM
13
ROTATION
D-610 TYPE ROTARY ACTUATOR
28 VOLTS 18 RPM
HOOVER ELECTRIC CO
3.000 P.D. 24 TEETH
NON-METALLIC
SPUR GEAR
4.000 P.D. 32 TEETH
NON-METALLIC
SPUR GEAR
F
.014 THK TITANIUM ALY
3.50 (TYP)
1.000 O.D × .022 WALL
TUBING ALY STEEL
1.00 (TYP)
WIRE CLOTH
SEAM WELDED
BONDED
.001 (1MIL) FILM
SLITS IN ALUMINIZED FILM
SECTION G-G
SECTION A-A
1
2
3

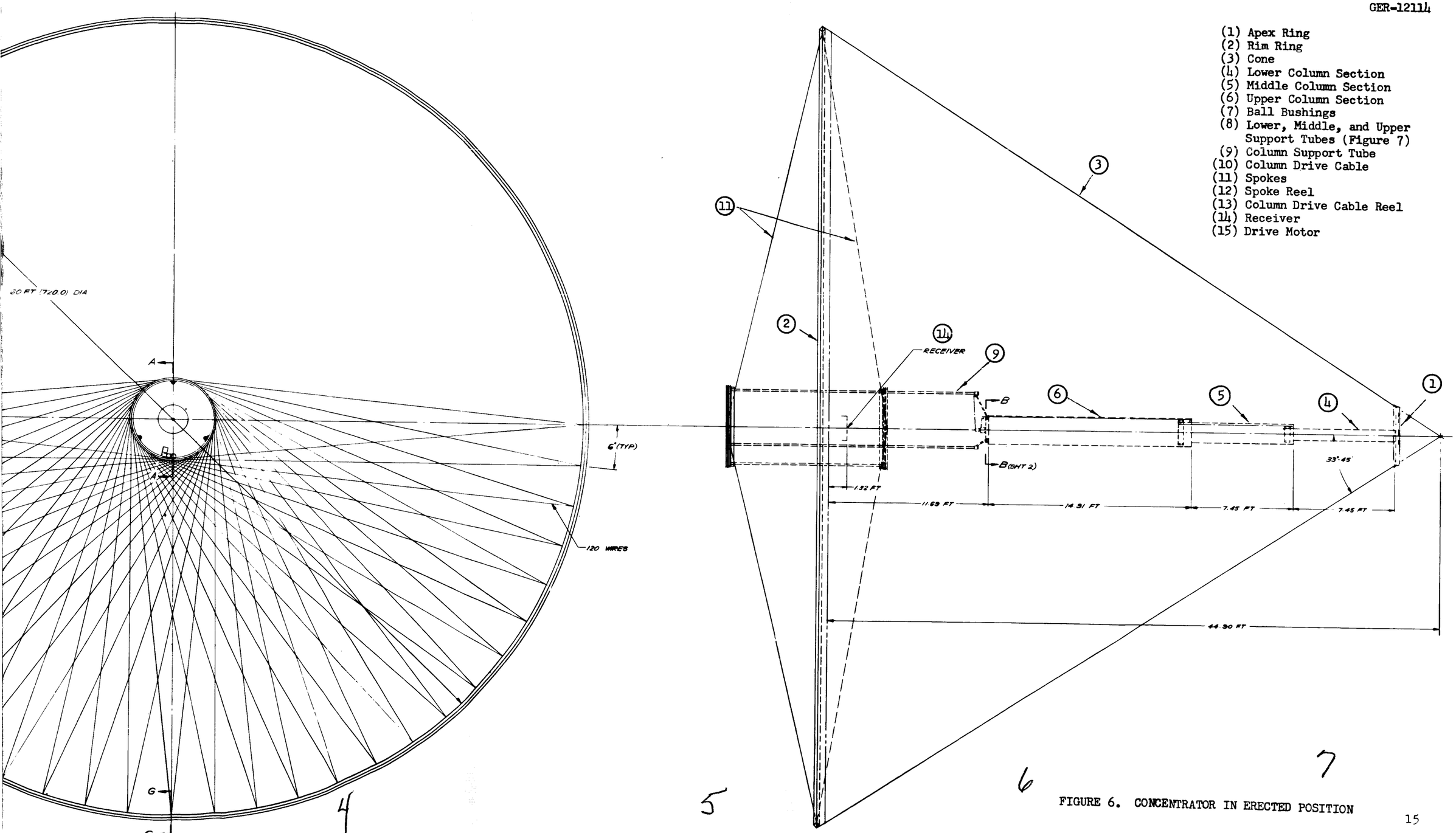

FIGURE 6. CONCENTRATOR IN ERECTED POSITION

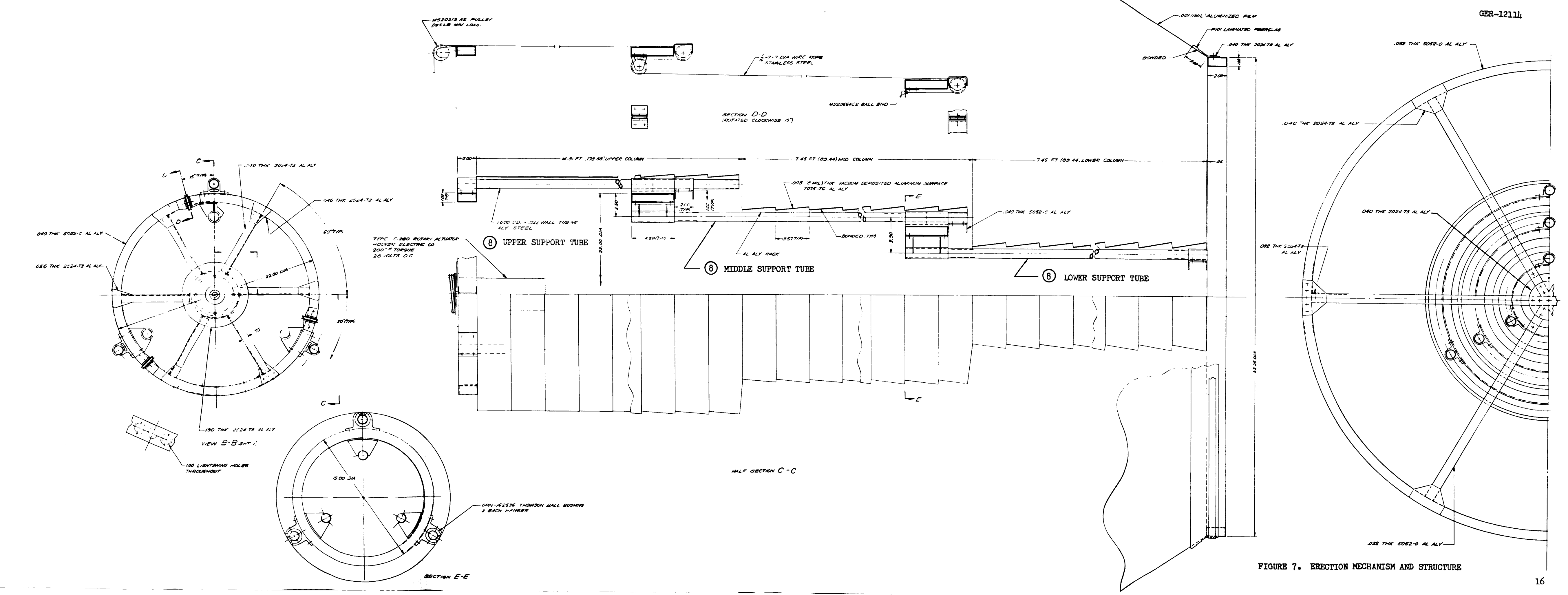

FIGURE 7. ERECTION MECHANISM AND STRUCTURE

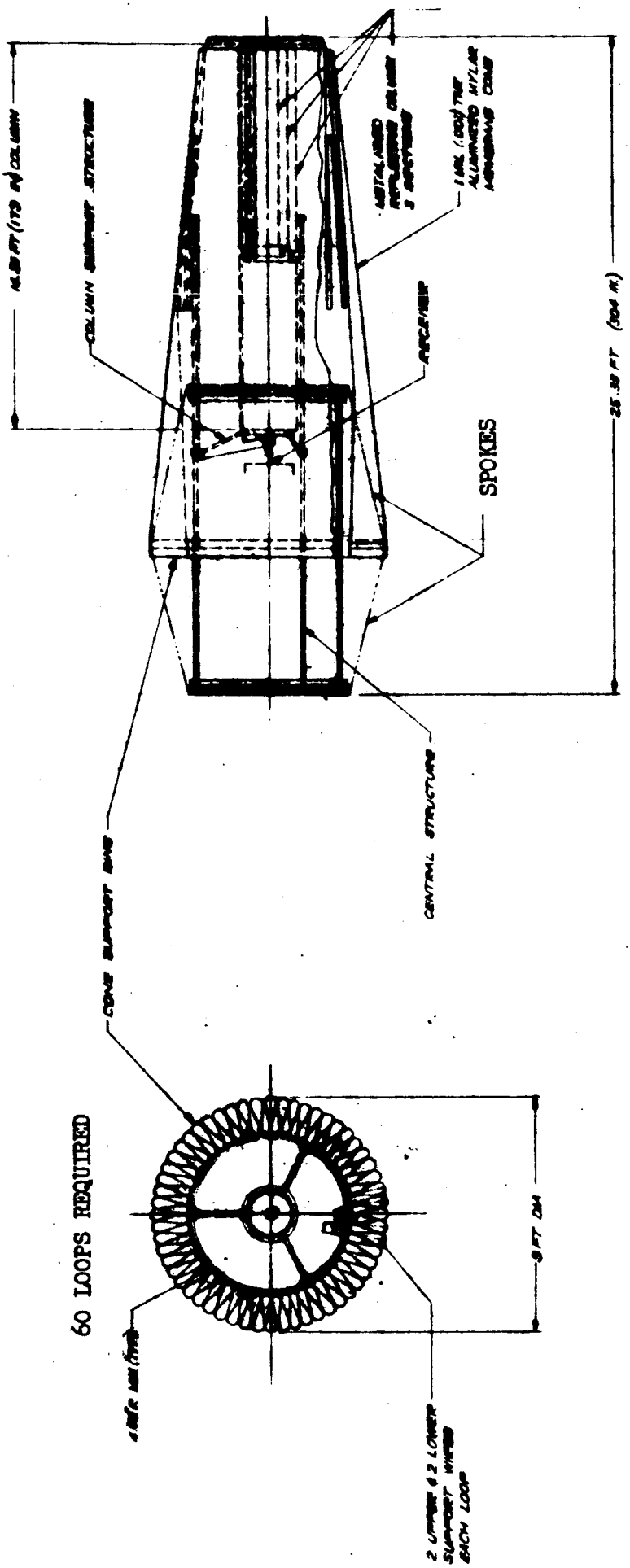

FIGURE 8. PACKAGED CONCENTRATOR

The opening pressure can be either pneumatic or mechanical. A pneumatic system will take the form of a gas bottle attached to the ring with the gas pressurizing the ring as required. A mechanical system will utilize springs inside the cross-section to provide the required opening pressure. The spokes will probably have to be overextended temporarily to facilitate the opening of the ring cross-section.

Packaging/Erection of Column. - The column is packaged by a telescoping mechanism. The reflectors of each column section are supported by three support tubes. Ball bushings attached to the lower and middle support tubes allow these column sections to be telescoped inside the upper column section. Ball bushings mounted on arms extending from the top column section allow the column assembly to roll up the column support tubes for more compact packaging.

The column is erected by means of cables rigged to extend the sections as the cables are reeled on a motor-driven drum mounted on the top column section. One set of cables extends the lower and middle column section while another set positions the column assembly with respect to the receiver.

Packaging/Erection of Cone. - The membrane cone must be reduced in length as well as diameter for packaging. Diametral reduction may be accomplished by pleating the cone as the rim ring is folded for packaging. In order to accomplish a reduction in length, additional circumferential folds may be made. As an alternate method, the membrane may be wrapped spirally around the collapsed column assembly simultaneously with the folding of the ring.

The folded membrane must be clamped in place at several points for support. These clamps can be released prior to the extension of the cone. The cone will be positioned for operation as the rim ring and the apex ring are erected.

Weight Breakdown

The conceptual design of the packaging/erection system for a 60 foot diameter concentrator was made in sufficient detail to permit the calculation of the system weight. The weight breakdown is given in Table I. The total weight was calculated to be 319.54 pounds exclusive of the opening mechanism for the rim ring and the structure required to support the concentrator in the vehicle. Estimating the opening mechanism weight at 15 pounds brings the total to 335 pounds exclusive of supporting structure. The effective frontal area of the concentrator is the area of a 60 foot diameter disc or 2827.4 square feet. The specific weight is then 0.1185 pounds per square foot exclusive of supporting structure. The supporting structure weight cannot be accurately estimated at this time because of its dependence on

vehicle configuration which is not defined. The design objective for the concentrator is 0.2 pounds per square foot or a total weight of 565 pounds for the 60 foot diameter. Thus, 230 pounds remain available to be used for supporting the concentrator in the vehicle. This structural weight allowance appears to be adequate.

TABLE I

WEIGHT BREAKDOWN FOR 60 FOOT DIAMETER CONCENTRATOR

Component	Number Required	Material	Weight (Lbs)
Central Structure			
Spoke Reels	4	Aluminum	17.00
Support Channels	2	Aluminum	16.80
Support tubes	3	Steel	12.70
Drive Tube	1	Steel	2.70
Actuator, D-610 Hoover	1		3.75
Cams, CF - 1/2 McGill	8		.20
Cams, CYR-1 McGill	12		1.64
Motor Actuator	1	Aluminum	.24
Gears	13	Aluminum	2.15
Stand-Off	3	Aluminum	.15
Drive Hangers	2	Aluminum	1.26
Hangers	3	Aluminum	.70
			59.29
Rim Ring			
Sides	4	Titanium	111.63
Cone Mount	1	Polyethylene	5.43
Cables, 20 Mil	120	Steel	3.84
			120.90
Cone			
Membrane, 1 Mil	1	Mylar	35.45
			35.45
Carriage And Upper Column Section			
Tubes	3	Aluminum	1.29
Mounting Plates	6	Aluminum	.12
Housings	3	Aluminum	.93
Ball Bushings, OPN-162536 Thompson	3		.96
Drum, 2 Inch	1	Magnesium	.72
Drum, 4 Inch	1	Magnesium	1.92
Motor Mounting Plate	1	Aluminum	.72
Actuator, C-280 Hoover	1		7.50
Box Ring	1	Aluminum	1.62
Channels	6	Aluminum	.59

TABLE I (CONTINUED)

Component	Number Required	Material	Weight (Lbs)
Angles	12	Aluminum	.14
Gussets	6	Aluminum	.10
Pulleys	15		.58
Pulley Brackets	12	Aluminum	.28
Tubes	3	Steel	10.50
Channel Ring	1	Aluminum	1.12
Hangers	6	Aluminum	1.40
Reflectors	50	Aluminum	11.50
			42.00
Middle Column Section			
Tubes	3	Steel	5.80
Box Ring	1	Aluminum	2.98
Channel Ring	1	Aluminum	.77
Reflectors	25	Aluminum	4.22
Hangers, Lower	3	Aluminum	.70
Hangers, Upper	3	Aluminum	2.66
Ball Bushings	6		1.92
Pulleys	6		.39
Pulley Brackets	6		.16
Rack	3	Aluminum	6.56
			26.16
Lower Column Section			
Tubes	3	Steel	5.40
Box Ring	1	Aluminum	2.06
Channel Ring	1	Aluminum	.39
Reflectors	25	Aluminum	2.53
Hangers, Upper	3	Aluminum	2.66
Ball Bushings	6		1.92
Rack	3	Aluminum	6.56
Box Ring	1	Aluminum	3.08
Angles	6	Aluminum	.06
Gussets	6	Aluminum	.23
Disc	1	Aluminum	.67
Box Stiffener	6	Aluminum	2.72
Apex Ring	1	Fiberglass	7.00
Apex Ring Retainer	1	Aluminum	.46
			35.74
TOTAL WEIGHT			319.54

SUMMARY OF STRUCTURAL ANALYSIS

Analyses Conducted

The concept of the cone and column concentrator, wherein the cone is subjected to only axial tension along with the fabrication, packaging and deployment techniques, present several unique structural problems. These problems are discussed in detail in Appendix A.

Of the four basic structural components that make up the concentrator, the unique problems arise in the analyses of the large foldable ring and of the film cone. General equations are developed for the structural analysis of these two components and are then applied to a 60 foot diameter cone and ring. These analyses indicate that, while a functional ring of adequate structural strength is feasible for an arbitrary column load of 60 lbs, it is not possible to obtain a sufficiently smooth surface on a simple membrane cone by applying only axial load.

This study indicates that a smooth surface may be obtained by deviating from a true cone to a membrane of revolution of anticlastic curvature. However, fabrication of such non-developable surfaces becomes difficult. If the surface is initially fabricated with single-curved gores so that the unstressed cross-section is polygonal, analysis indicates that the desired membrane of revolution cannot be obtained by application of axial load.

Alternate Approaches to Cone Construction

Another method of fabricating a true cone that will have the required smooth surface under axial load only is presently being investigated experimentally. The concept is based upon the application of collapsible circumferential structural members distributed over the external surface of the cone. These members will provide the circumferential compressive and flexural stiffnesses required to restrain the compressive strains that induce wrinkles in an unstiffened membrane cone. The results of these investigations will be included in another report.

THERMAL ANALYSIS

Summary

A thermal analysis was made to determine typical temperature distributions in the cone while operating in various positions in a near-earth orbit and also while outside the influence of the earth. The details of this analysis are included in Appendix B. Factors which were considered in this analysis are:

(1) Solar energy
(2) Earth albedo
(3) Earth radiation
(4) Heat receiver aperture re-radiation
(5) Interchanges within the cone

The thermal analysis incorporates reasonable simplifying assumptions and/or approximations to reduce this effort to a level suitable for a feasibility study without notably degrading the analysis accuracy. The thermal areas affected are:

(1) Reflections within the cone of system emitted IR radiation, planetary radiation, and albedo. These items are partially diffuse before striking the cone internal surfaces, and will remain so after reflection. By assuming the reflections as perfectly diffuse, view factor routines will be adequate to handle these reflections.

(2) Dividing the cone into axial and circumferential nodes may result in an excessive number of nodes with resultant analysis complexity. A hybrid system of nodes and infinitesimal areas may be introduced to expedite the analysis.

Transient considerations do not appear to be a serious factor as the thermal response time for the cone material would be 1 to 2 minutes. The structural support response time would be considerably longer, however, this consideration is beyond the scope of this program.

Thermal Analysis Results

Cases Investigated. - In addition to the sample temperature distributions obtained as part of the development of the thermal analysis program, temperature distributions were calculated for the cases listed in Table II.

TABLE II

PARAMETER VALUES FOR COMPUTER RUNS

Run No.	Internal Surface		External Surface		Planet Angle (deg)
	α (%)	ϵ (%)	α (%)	ϵ (%)	
1	12	4	any	40	none
2	12	4	any	90	none
3	12	4	15	40	0
4	12	4	15	40	45
5	12	4	any	40	90
6	any	4	any	40	180
7	12	4	25	90	0
8	12	4	25	90	45
9	12	4	any	90	90
10	any	4	any	90	180
11	12	4	90	90	0
12	12	4	90	90	45
13	15	40	15	5	0
14	15	40	15	5	45
15	15	40	15	40	45
16	15	40	90	90	45

The combinations of absorptance and emittance selected are typical of various surfaces which could be used in the concentrator construction. The properties of some typical materials are shown in Table III.

TABLE III

PROPERTIES OF TYPICAL MATERIALS

Material	α	ϵ
Aluminized Mylar	0.13	0.04
SiO on Aluminized Mylar	0.15	0.40
Black Paint	0.9	0.9
Solar Reflector Paint	0.25	0.9
Flat Reflector Paint	0.25	0.25
Mylar (1 mil clear)	0.20	0.7

Calculations were made for operation in a 300-mile orbit about the earth and for operation at 1 A.U. removed from the influence of the earth.

For earth orbit cases, calculations were made with the concentrator on the earth-sun line and at locations 45 degrees, 90 degrees and 180 degrees from this line (the last case locates the concentrator in the shade of the earth). In all cases, the concentrator is oriented to the sun.

Result Sheets. - The thermal analysis computer output data is presented in Appendix C. Each set of results is identified with the proper input data.

Graphs. - Figures 9, 10 and 11 show the effect of surface properties on the radial temperature distribution of the cone. A temperature discontinuity occurs at a radius of about 58 percent of the outside radius because of the second incidence of solar energy inside this radius. The temperature plots terminate at radii of 10 and 100 percent of outside radius at the extremities of the conical surface.

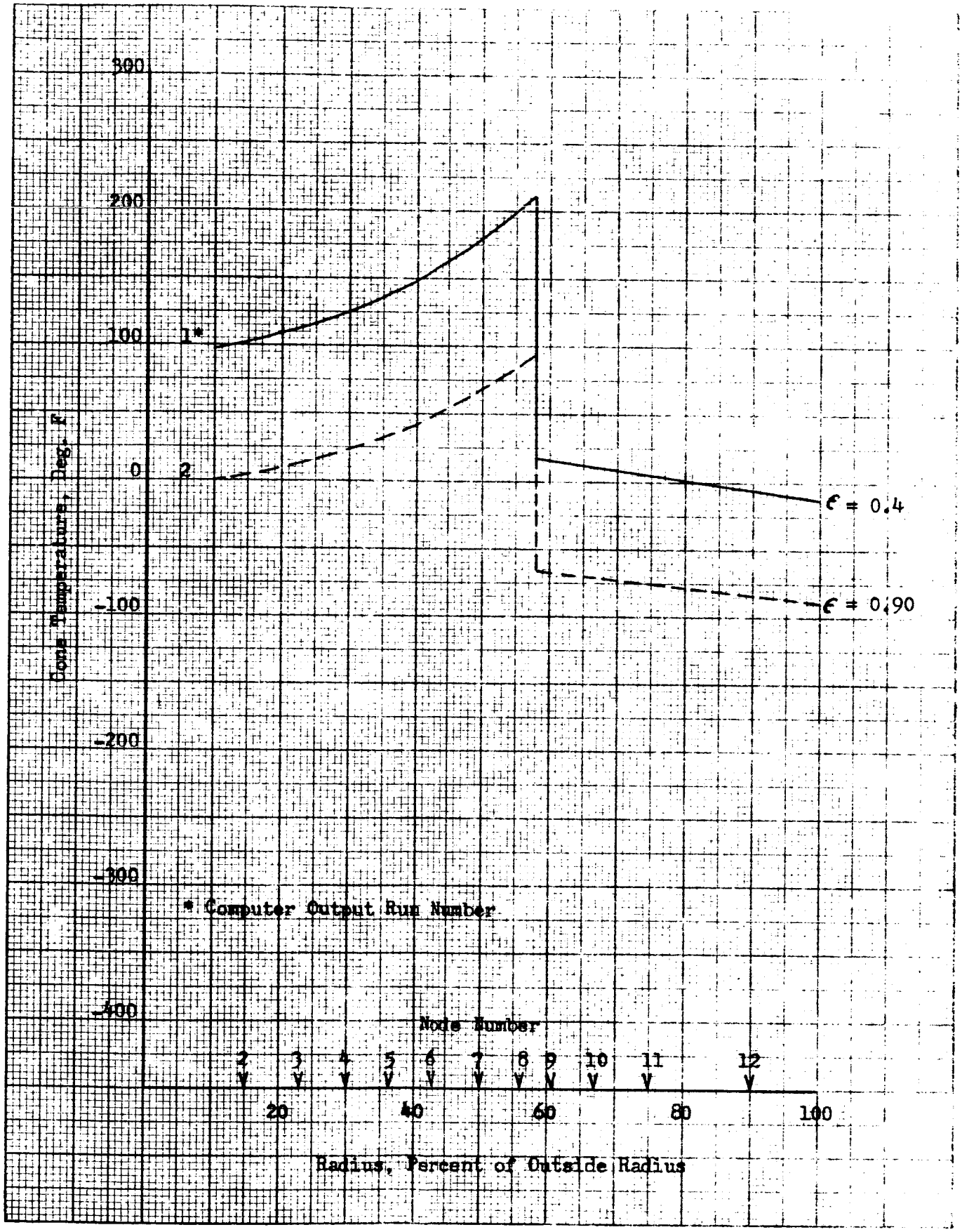

FIGURE 9. CONE TEMPERATURE DISTRIBUTION WITH NO PLANET IN THE VICINITY

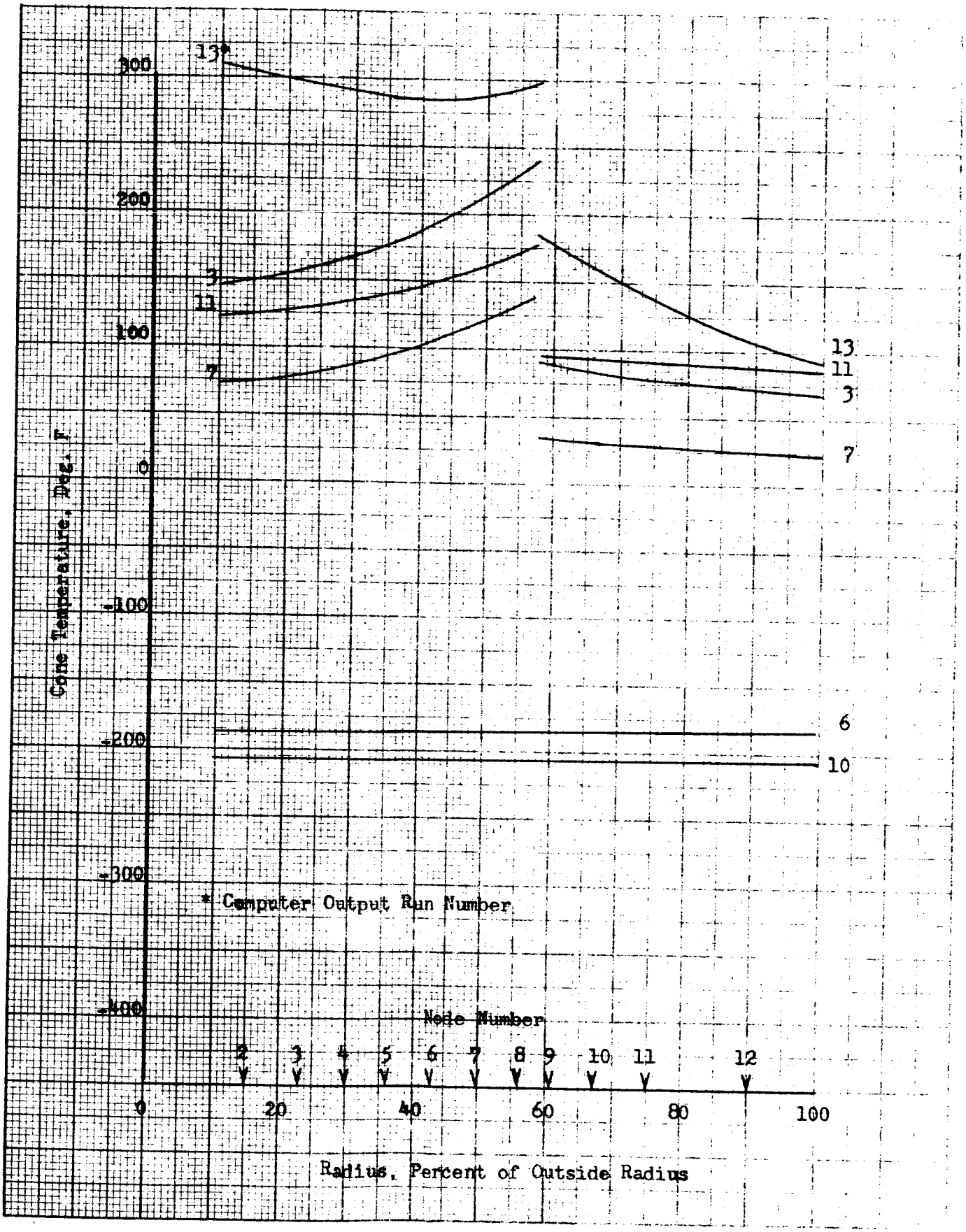

FIGURE 10. CONE TEMPERATURE DISTRIBUTION AT 90 DEGREE ANGLE TO TWILIGHT PLANE

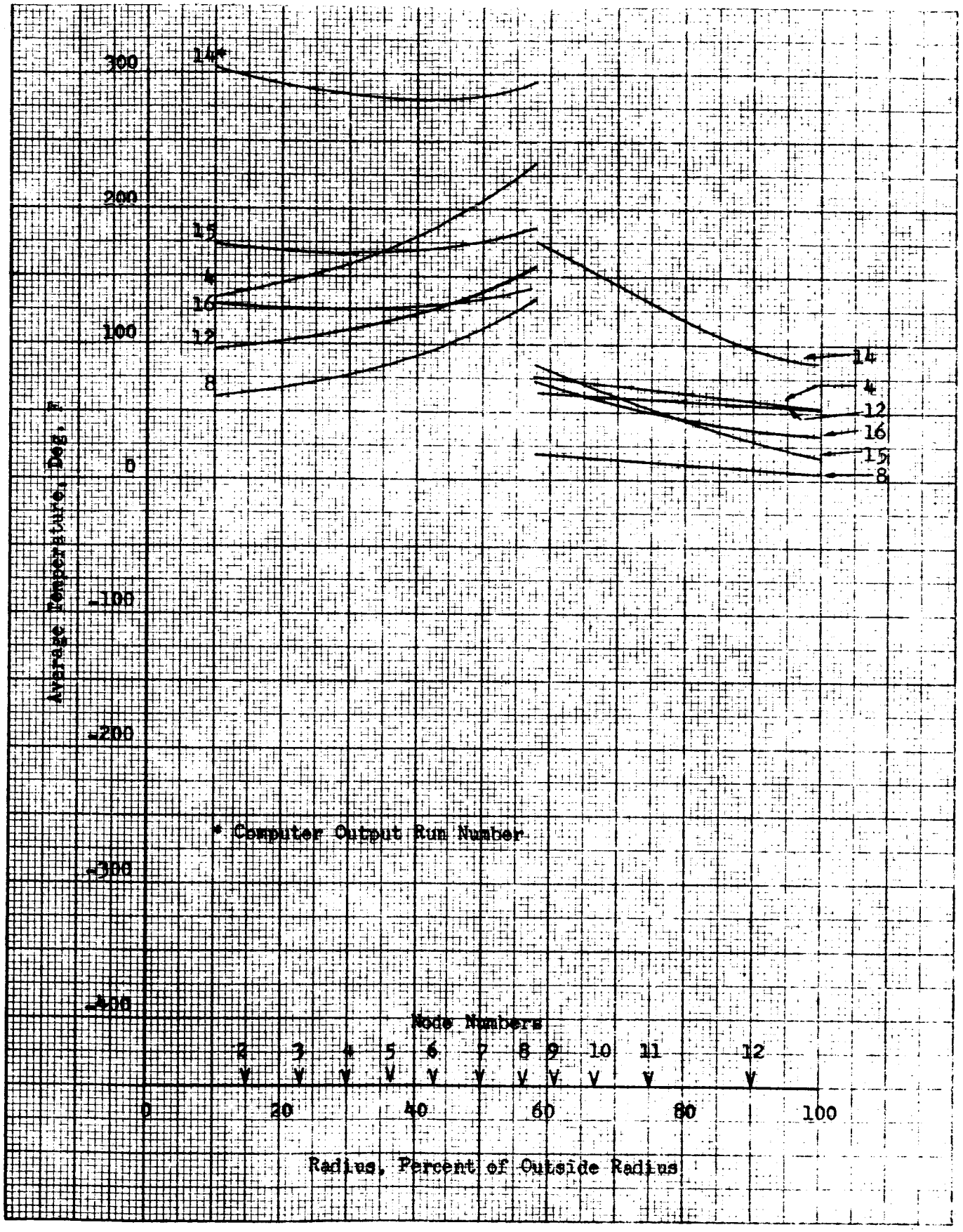

FIGURE 11. CONE TEMPERATURE DISTRIBUTION AT 45 DEGREE ANGLE TO TWILIGHT PLANE

When the concentrator is not on the earth-sun line, the temperature distribution is not radially symmetric. In these cases, the temperature distribution is best shown by a plot of isotherms (constant temperature lines) on the cone.

Figures 12 through 16 are plots of isotherms on the cone. The polar grid represents a view looking into the cone. Since the temperature distribution is symmetrical with respect to the azimuth of the earth, only half the cone is shown.

Effects of Thermal Expansion on Cone Geometry. - The temperature variations from one part of the cone reflector to another can cause thermal distortion which will affect the reflector accuracy and performance.

If the reflector is a true cone at one temperature, it will expand (or contract) to a cone shape at any other uniform temperature. The new cone shape will have the same apex angle as the previous one as illustrated in Figure 17, view A.

Where a temperature discontinuity exists between two parts of the cone, the two parts will tend to be physically discontinuous. This tendency will be resisted by stresses due to strains where the two parts are connected. View B of Figure 17 shows the effect of a radial temperature discontinuity and view C shows the effect of a circumferential discontinuity.

Where a uniform temperature gradient exists along a meridian of the cone, the meridian will curve. The curvature will be concaved outward when the temperature increases with radius and inward with decreasing temperature. Outward curvature of the meridian produces an anticlastic surface and inward curvature produces a synclastic surface.

In general, the curvature may be expressed as:

$$1/\rho = \alpha \sin^2\theta \sec\theta \left(\frac{dT}{dr} + r \frac{d^2T}{dr^2} \right) \qquad (1)$$

where:

r = cone radius
$1/\rho$ = Curvature (inverse of radius of curvature) at radius r
α = linear coefficient of thermal expansion
θ = cone half-angle
T = temperature at radius r

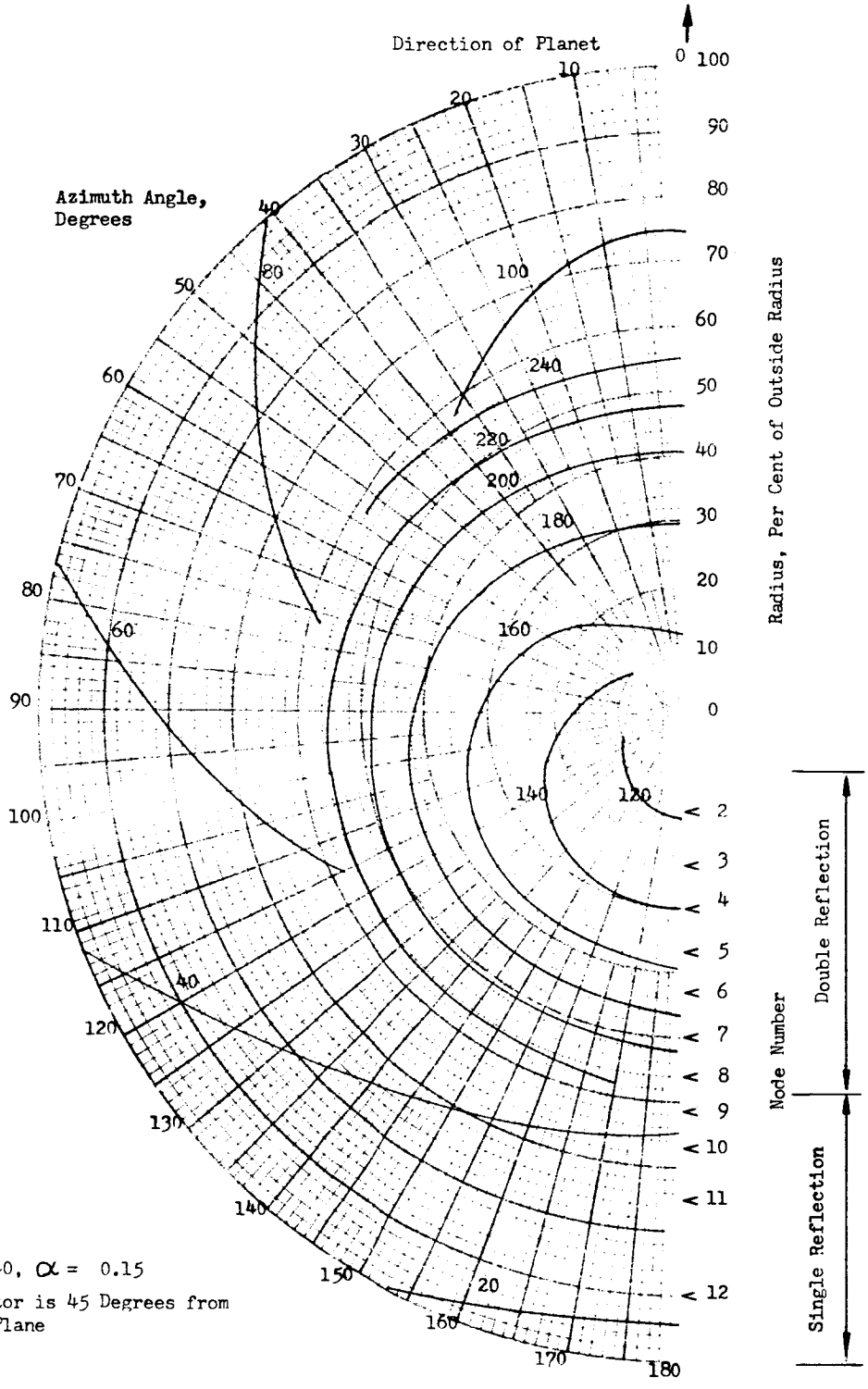

FIGURE 12. CONE ISOTHERMS, RUN NO. 4

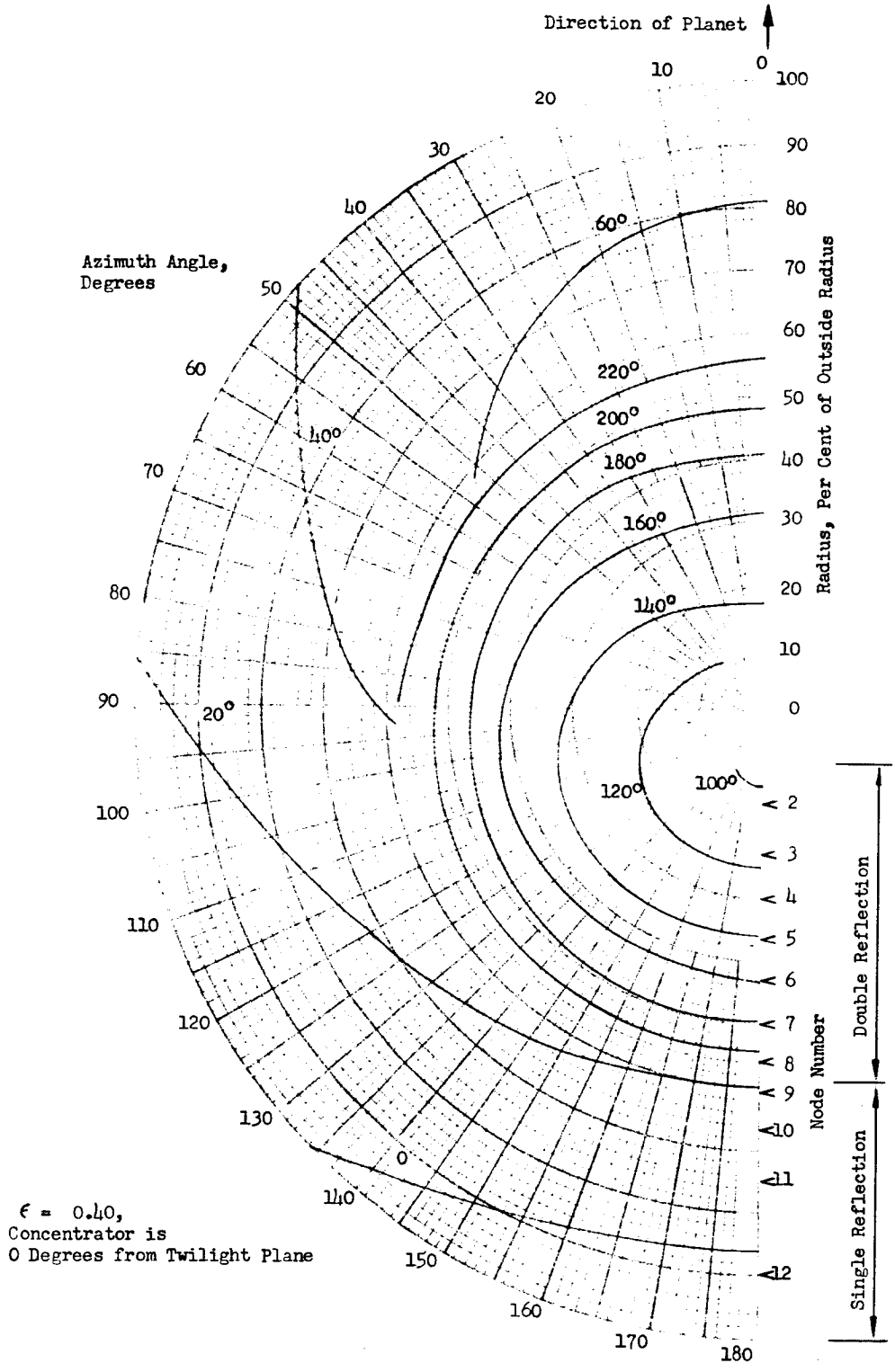

FIGURE 13. CONE ISOTHERMS, RUN NO. 5

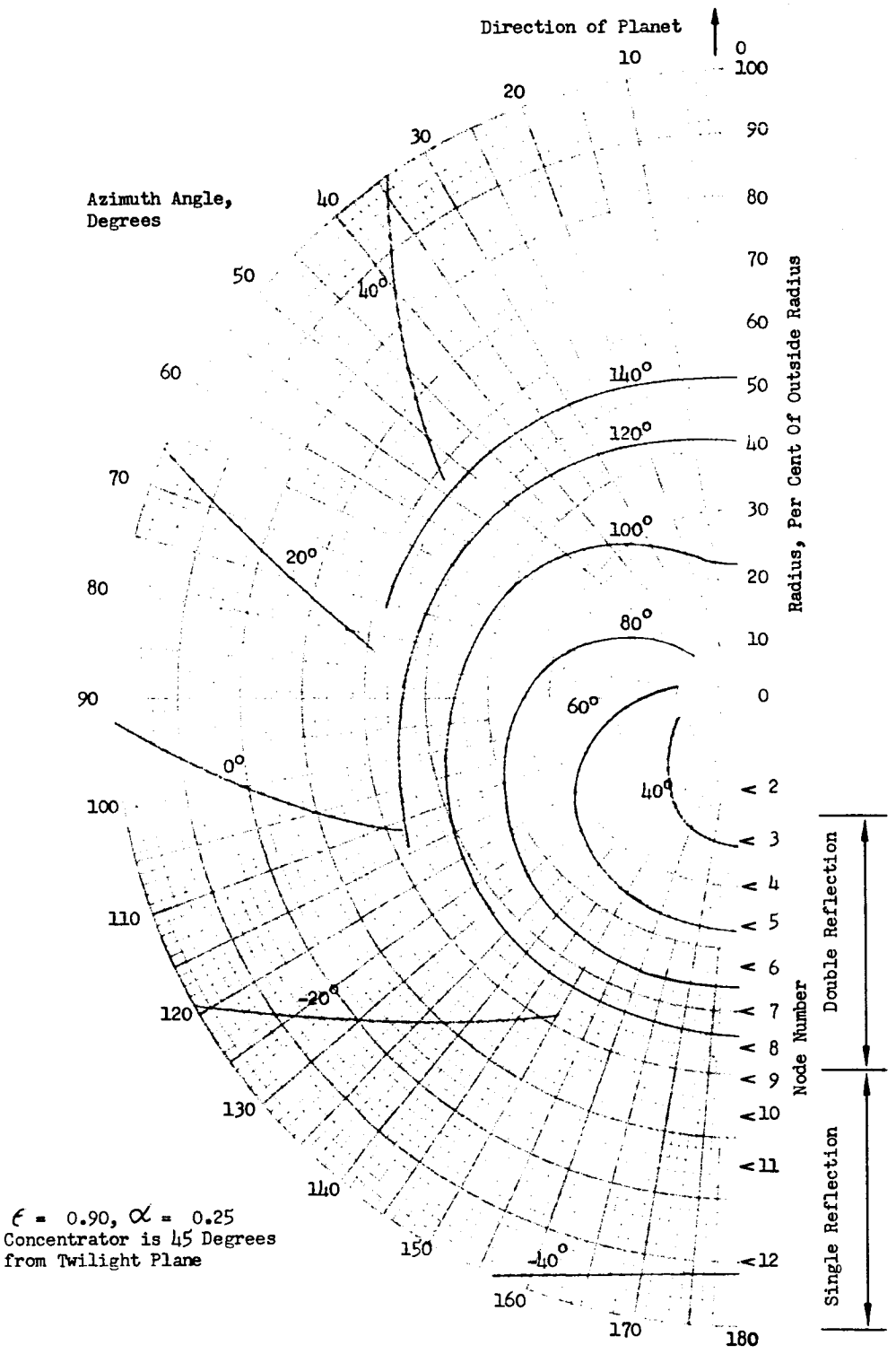

FIGURE 14. CONE ISOTHERMS, RUN NO. 8

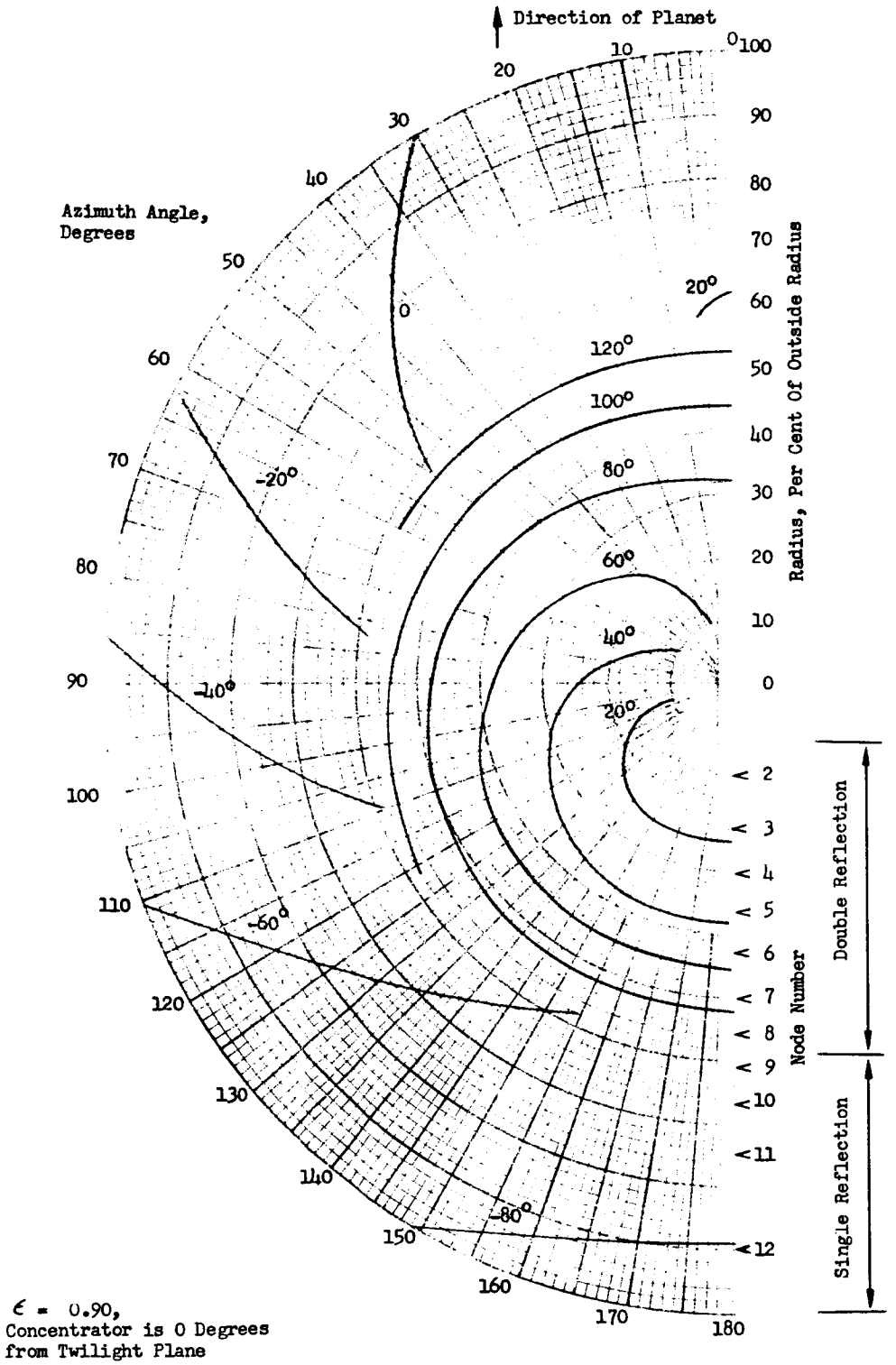

FIGURE 15. CONE ISOTHERMS, RUN NO. 9

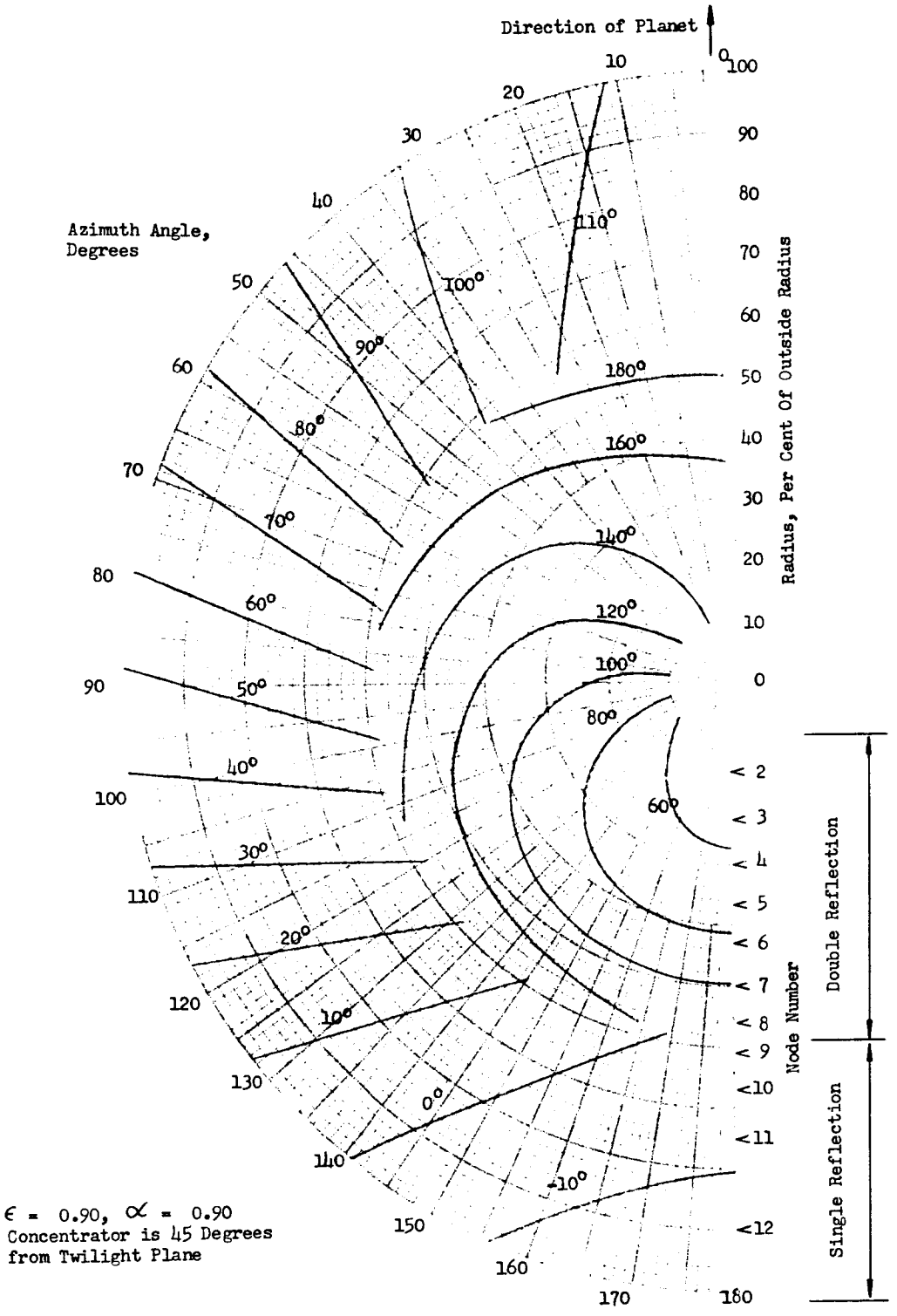

FIGURE 16. CONE ISOTHERMS, RUN NO. 12

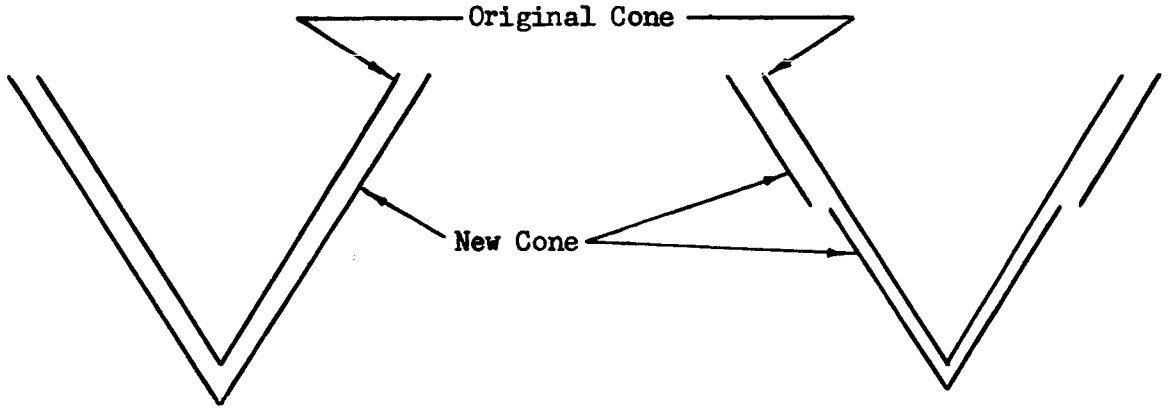

A. UNIFORM TEMPERATURE CHANGE

B. RADIAL TEMPERATURE DISCONTINUITY

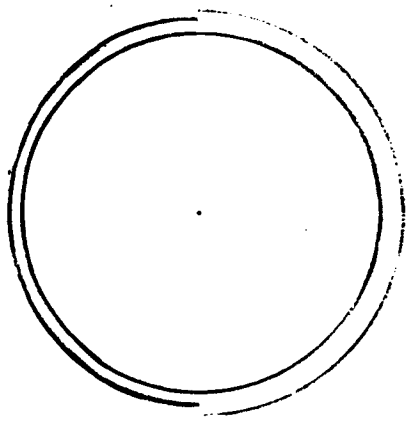

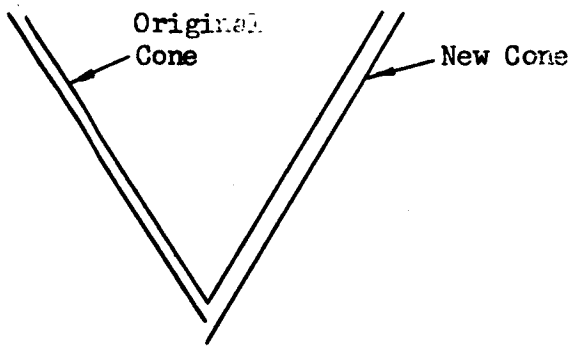

C. CIRCUMFERENTIAL TEMPERATURE DISCONTINUITY

FIGURE 17. EFFECTS OF THERMAL EXPANSION ON CONE GEOMETRY

As long as the curvature is positive (concave outward), the cone surface cannot become synclastic and there will be no danger of compression in the surface accompanying the application of meridional tension. The limiting case is when the curvature is zero. Solution of the resulting differential equation gives:

$$T = C_1 \ln r + C_2$$

where C_1 and C_2 are constants of integration. The uniform temperature condition is obtained when $C_1 = 0$.

An alternate form of equation (1) is:

$$1/\rho = \alpha \sin^2\theta \sec\theta \frac{1}{r} \frac{d^2T}{d(\ln r)^2} \qquad (2)$$

This form makes it possible to check for cone curvature by plotting the temperature against the logarithm of the radius. The curve obtained should be concave upward to ensure deformation in the direction of an anticlastic surface. An example of such a plot is shown in Figure 18 for the case of concentrator operation not in the vicinity of a planet, (runs no. 1 and no. 2). The curves are concave upward in the central part of the cone but tends to be concave downward in the outer part of the cone. Thus, the meridians in the outer part will tend to curve inward and put the membrane in compression in the circumferential direction. Unless there is a counteracting membrane tension, the membrane will buckle under compression and wrinkles will result.

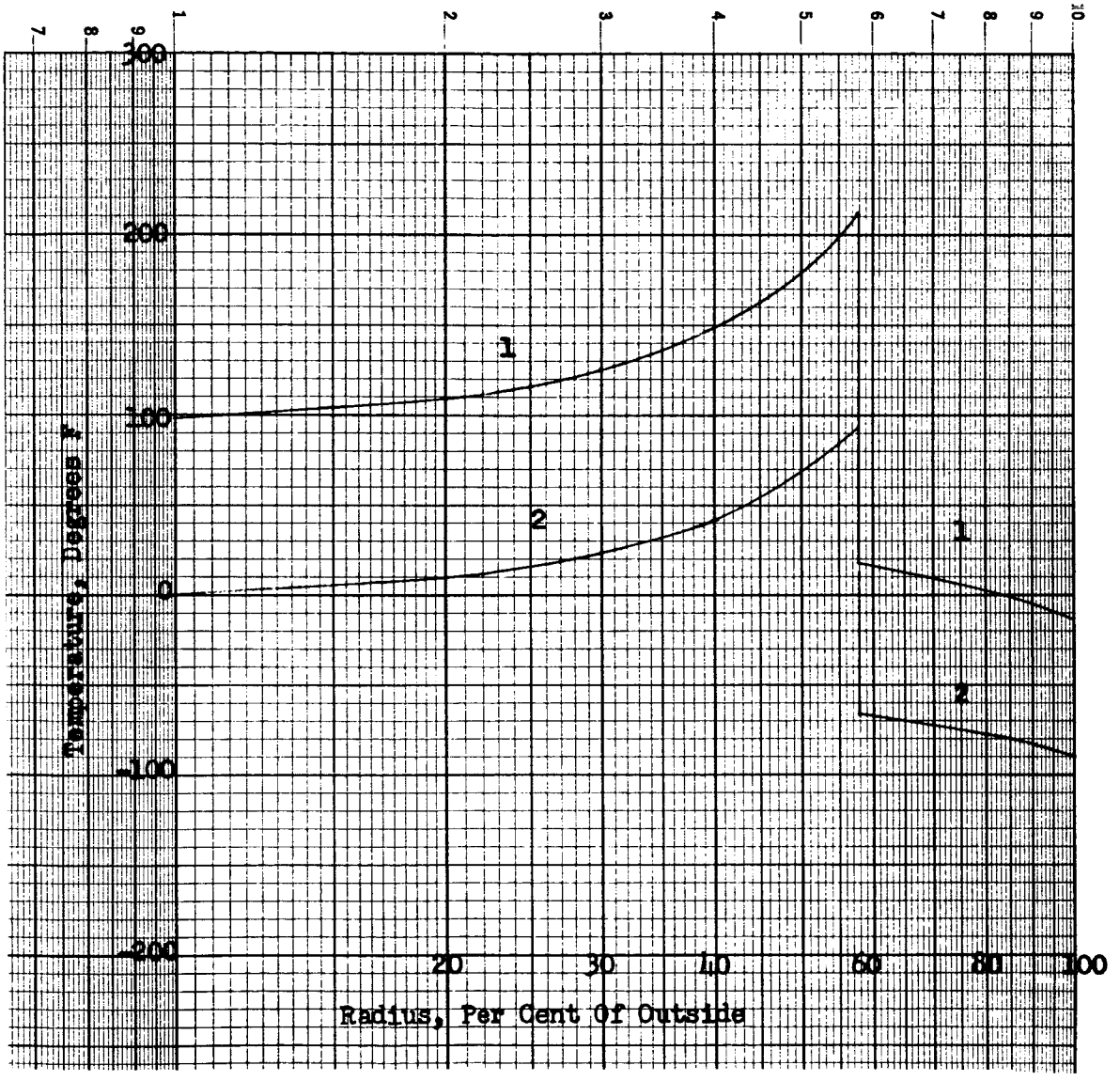

FIGURE 18. TEMPERATURE DISTRIBUTION FOR CONE CURVATURE DETERMINATION

CONCLUSIONS AND RECOMMENDATIONS

Structural Feasibility

An analysis was made of the structure required for erection of a lightweight cone-and-column concentrator in space. This analysis showed that all parts of the structure can be designed to carry erection loads and at the same time be made foldable. The erection load assumed for the analysis was sixty pounds axial compression load in the column with the reaction carried through the conical membrane and the support ring. This load was selected arbitrarily since the loading required to position the surface of the conical membrane is not yet established. This load is near the weights of the principal components and so is representative of the structural loading associated with accelerations near 1-g.

The weight of the system was calculated to be 335 pounds, exclusive of structure required to support the system in the vehicle. This is nearly 0.12 lb/ft^2 concentrator frontal area as compared to the design objective of 0.2 lb/ft^2. Should the required membrane tension be greater than that provided for by this design, the various structural parts will have to be stiffened and strengthened at an increase in weight. Other factors which may lead to an increase in structural weight are inertial loads associated with orientation and structural adaptation of the concentrator package to the launch vehicle. Packaging of the concentrator into a space 9 feet in diameter by 25.33 feet in length was determined to be feasible.

Studies were made of methods of introducing a circumferential tension in the cone in order to smooth out longitudinal creases and wrinkles. Anticlastic surfaces were investigated to determine their suitability in generating circumferential tension and to determine the feasibility of making such surfaces of flat gores.

A surface with both meridional and circumferential curvature was found to produce sufficient circumferential stress to smooth out longitudinal wrinkles and at the same time to be sufficiently near a cone to preserve the optical principles of the cone-and-column concentrator. However, the investigation concluded that it is practically impossible to achieve circumferential curvature in a near-conical surface made of flat gores seamed together.

Optical Considerations

The cone-and-column concentrator, 60 feet in diameter, will focus 95 per cent of the focal plane energy into a 1.9-foot diameter aperture if the

optical components are constructed with the following accuracies:

cone tangential error	-	30 min rms average
cone radial error	-	15 min rms average
column radial error	-	16 min rms average

The column diameters required are:

top half of length	-	2.130 ft. diameter
third quarter of length	-	1.544 ft. diameter
lower quarter of length	-	0.884 ft. diameter

The shadow loss was calculated to be 4 per cent. When combined with the specified reflectance of 65 per cent, an overall efficiency figure of 62.4 per cent is obtained for the concentrator.

Thermal Effects

Temperature variation over the surface of the cone results in non-uniform expansion of the cone. The temperature variation is primarily along meridians of the cone because of the radial variation of incident solar flux on the cone. The largest variation is the discontinuity at the line of demarcation between singly reflecting surface and doubly reflecting surface. The differential expansion there can be compensated in the construction of the cone.

When the temperature of the cone is influenced by the presence of a planet, circumferential variation in temperature will exist. The resulting thermal expansion will generate shear stresses which will buckle the surface of the cone. The likelihood of overcoming these stresses with bi-axial tensile stresses is small because of the low level of circumferential tensile stress which can be attained.

Conclusions

A conical reflector made by seaming plastic film into a conical shape will not perform satisfactorily in a cone-and-column concentrator. This is because there is no practical method of introducing a sufficiently high circumferential stress to remove meridianal wrinkles which may result from packaging creases, thermal distortion, or practical limitations on accuracy of fabrication. The latter two sources of wrinkles may be attacked by making the cone of unseamed meridianal strips. This method, however, introduces the problems of curling and twisting of the strips.

Other parts of the system appear to be feasible. The component requiring the most development next to the cone is the collapsible rim ring. This is due to the novelty of the concept. Parts of the ring concept appearing to require development are: (1) the hinges which permit collapse of the cross section but which must carry high shear loads during folding and after erection, and (2) the opening mechanism.

Recommendations

The means of constructing a lightweight conical reflector require further analytical and experimental investigation to establish the feasibility of this concentrator component.

The folding and erection principles of the rim support ring require some form of experimental verification. The cone is being developed as part of the present program. The folding support ring development is not included in the present program. Future program plans should include this item.

APPENDIX A

STRUCTURAL ANALYSIS

TABLE OF CONTENTS

TABLE OF CONTENTS (Continued)

TABLE OF CONTENTS (Continued)

LIST OF FIGURES

LIST OF FIGURES (CONT)

LIST OF SYMBOLS

Symbol		Units	Defined by Equation No.
A, B, C	The moduli in the general equation of a parabola		124
a, b	The radii of the small & large bases of the "conical" frustum, respectively	in.	
c	Compressive force in the support ring	lbs.	5
C_1, C_2	Constants of integration		25, 27
E	Modulus of elasticity	psi	
F	Resultant of the combined cable reactions at each support point on the supporting ring	lbs.	3, 4
F.S.	Denotes the factory of safety		
F_{ty}	Tensile yield strength	psi	
f	Calculated stress	psi	
f_a	Allowable working stress	psi	
f_b	Calculated bending stress	psi	
f_s	Calculated shear stress	psi	
G	Modulus of rigidity (shear modulus)	psi	
H	Height of the "conical" frustum	in.	
h	Thickness of the film (Mylar)	in.	
I	Moment of inertia	$in.^4$	

LIST OF SYMBOLS (CONT)

Symbol		Units	Defined by Equation No.
J	The torsion constant of the ring	$in.^4$	
j	A simplifying constant		136
K	A simplifying substitution	$in.^{-1}$	114
k	A simplifying substitution	$in.^{-3}$	93
L	The horizontal projection of the deflected cantilevered beam (Refer to Figure 8)	in.	
ℓ	The projected length between a crease and the mid-point between creases (Refer to Figure 9)	in.	
ℓ_c, ℓ_r	The projections of the half length of the creased area taken parallel and normal to the uncreased area, respectively (Refer to Figure 9)	in.	
ℓ_1, ℓ_2 ℓ_3	The projected lengths of the first, second and third cantilevered beams making up half the creased area and taken parallel to the uncreased area (Refer to Figure 9)	in.	
M	Bending moment	in-lbs.	
m	A simplifying constant	in.	73
N	Denotes unit membrane forces when used with subscripts and also used to denote the number of meridian creases when used without subscripts	lbs/in.	
n	Number of cable attachments on the ring		
p	Length of one side of the diamond cross-section	in.	
Q	Total axial compression load in the column	lbs.	

LIST OF SYMBOLS (CONT)

Symbol		Units	Defined by Equation No.
q	Denotes the distributed ring loading when used with subscripts and also used as the unit meridian membrane load at the small base of the frustum when given without subscripts	lbs/in.	1, 2, 52
R	A simplifying substitution		158
R_p	The resultant of cable pretensions at each point, n, in either conical surfaces 1 or 2	lbs.	4
R_θ	Radius of the circle that the side of regular polygon, cut by a plane normal to the axis of symmetry, taken during deformation	in.	154
R_1, R_2	Resultant cable tension at each point, n, in conical surfaces 1 and 2, respectively	lbs.	
r	The number of sides of the regular polygon cut by a plane normal to the axis of symmetry (Refer to Figure 17)		
r_o	Radius of a circle cut by a plane normal to the rotational axis of symmetry of the "conical" frustum	in.	53
S	Denotes arc length, the length of the cantilevered beam, (Refer to Figure 8) and also used as a simplifying substitution	in.	158
S_c	Total length of the three cantilever beams making up the half length of a crease (Refer to Figure 9)	in.	
T	Denotes torque, temperature (Refer to Figure 6), the tension in a meridian seam, and also used as a simplifying substitution	in-lbs. F° lbs.	 131 158

LIST OF SYMBOLS (CONT)

Symbol		Unit	Defined by Equation No.
t	A simplifying subsitution		118, 119
t_r	Wall thickness of the diamond cross-section	in.	
U	Energy required to fold or open the diamond cross-section, and also used as a simplifying substitution	in-lbs	40, 158
u, z	Coordinates of the deflected meridian taken parallel and normal to the undeflected meridian in the true conical frustum (Refer to Figure 7)	in.	66, 67
V	Denotes shear force when used with subscripts and used as a simplifying substitution without subscripts	lbs.	8, 16, 158
v, w	Deflections of a point on the meridian of the true conical frustum taken tangential and normal to the undeflected meridian, respectively (Refer to Figure 6)	in.	60, 63
W	A simplifying substitution		158
X	A simplifying substitution		158
x, y	Coordinates of a point on the meridian taken parallel and normal to the axis of symmetry, respectively (Refer to Figures 6, 8, 11 through 14, 18 and 20)	in.	
Y	A simplifying substitution		158
y_L	The deflection at the tip of the cantilevered beam (Refer to Figure 8)	in.	101
Z	A simplifying substitution		158

LIST OF SYMBOLS (CONT)

Symbol		Units	Defined by Equation No.
α	A central angle measured from the radial bisector of the arc between supports to a radial line through a point on the ring (Refer to Figure 3). Also denotes the coefficient of linear thermal expansion	Degrees In/In/F°	49
β	A central angle measured from a radial line from the support point to a radial line through a point on the ring (Refer to Figure 3)	Degrees	
γ	Angle of twist of a cross-section of the ring with respect to the cross-section at a support point	Degrees	30
δ	Deflection of the ring	in.	
ε	Strain	in/in.	
ζ	An angle measured the same as, but never exceeding the angle β (Refer to Figure 4)	Degrees	
η_s, η_θ	The angular deflections of the meridian and of the side of the regular polygon cut by a plane normal to the axis of symmetry, respectively (Refer to Figures 7 and 18)	Degrees	
θ	Half of the central angle between support points on the ring (Refer to Figure 3)	Degrees	
λ	Ratio of the seam to gore stiffness		144
μ	Poisson's ratio		
ν	A simplifying substitution	$in.^{-1}$	95
ρ_m	The minimum allowable bend radius	in.	37
ρ_1, ρ_2	The principal radii of curvature of the meridian in the plane of the meridian and in the plane perpendicular to the meridian, respectively.	in.	

LIST OF SYMBOLS (CONT)

Symbol		Units	Defined by Equation No.
σ	Stress	psi	
τ	Torsional shear stress	psi	48
φ	The slope of the meridian (Refer to Figure 2)	Degrees	
ψ	The slope at the tip of the deflected cantilevered beam (Refer to Figure 8)	Degrees	
ω	Angle between the meridian of the conical surface formed by the supporting cables and the plane normal to the axis of symmetry (Refer to Figure 2)	Degrees	

Subscripts

a, b Denote location at the small and large bases of the "conical" frustum respectively

c Denotes the circumferential direction in the ring

cr Denotes the critical value

g Denotes gore

H, o Also denotes the large and small bases of the "conical" frustum respectively

h, p Denotes the direction that is in the plane of the ring

M Dnotes the part due to bending moment

n, v Denotes direction normal to the plane of the ring

r Denotes the radial direction

s Denotes seam

LIST OF SYMBOLS (CONT)

Subscripts

T	Denotes the part due to torque
t	Denotes transverse direction in a gore
θ, φ	Denote circumferential and meridian directions, respectively

ANALYSIS

I. Analysis of the Ring

A. General

A thorough treatment of the foldable base ring is documented in Reference 1. This analysis is summarized herein and is applied to the 60 ft. diameter, diamond cross-section ring. The three loading conditions considered in the design of the ring and the corresponding analyses conducted for each are summarized below.

1. The Static Loading Due to the Applied Axial Load on the Cone

This is reflected to the ring as (1) uniformly distributed and concentrated radial compressive loads from the cone and cables respectively and (2) uniformly distributed loads normal to the plane of the ring from the cone that are reacted by the normal components of the concentrated cable loads. For these loadings the ring is analyzed for:

a. Strength
b. Buckling in the plane of the ring
c. Buckling out of the plane of the ring
d. Local buckling

2. Packaging Loads

For the specified packaging requirements, the maximum bending stresses are determined from the smallest bend radii involved.

3. Folding Loads

Folding is defined as the first step in the packaging of the ring whereby the diamond cross-section is collapsed (folded) into a line. The resulting maximum circumferential stresses are determined.

4. Energy Required to Fold or Open the Diamond Cross-Section

For the folding condition, a calculation is made to show the energy required to open or fold the diamond cross-section ring. This is the energy that must be supplied by internal springs.

B. Detailed Ring Analysis

1. The Static Loading Condition

A schematic diagram of the configuration is shown in Figure 1. The cone is loaded by mechanically extending the column to produce the load, Q, shown in Figure 2. This load is balanced by the forces in the cone, ring and cables as also shown in Figure 2. The applied ring loads may be resolved into the three loading conditions shown in Figure 3 and each may then be analyzed separately and the results combined according to the principle of superposition.

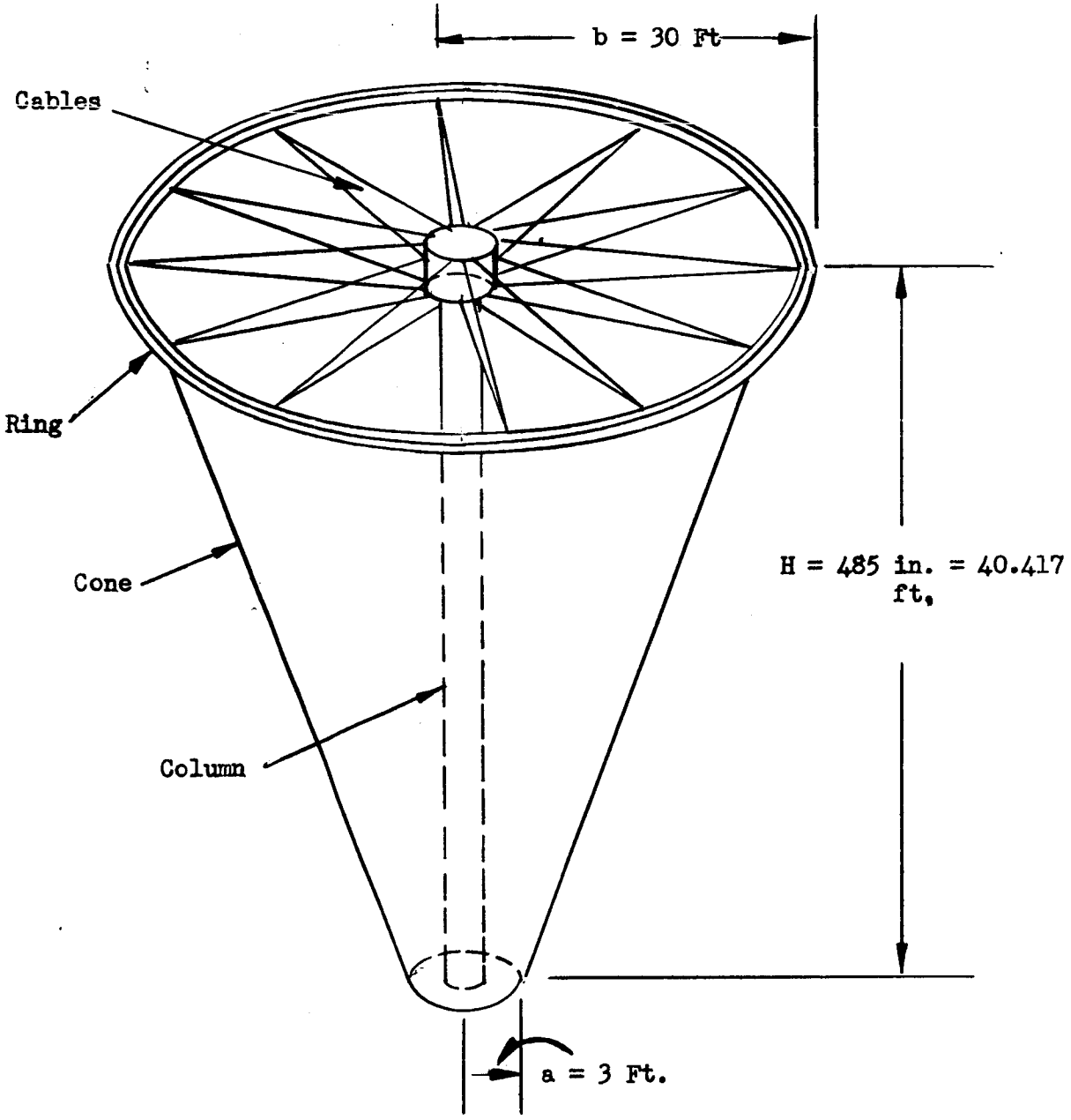

FIGURE 1 - Schematic Diagram of the Cone and Column Reflector

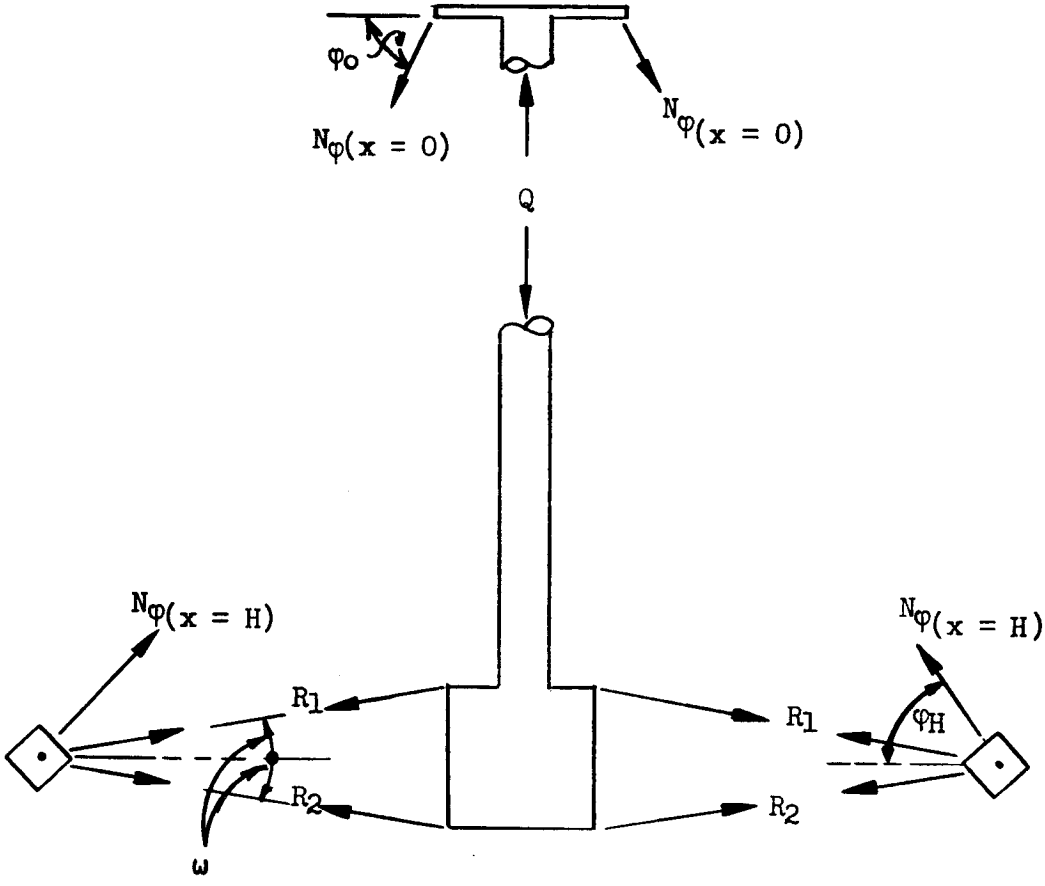

FIGURE 2 - Free-Body Forces on Cone, Column, Ring and Cables

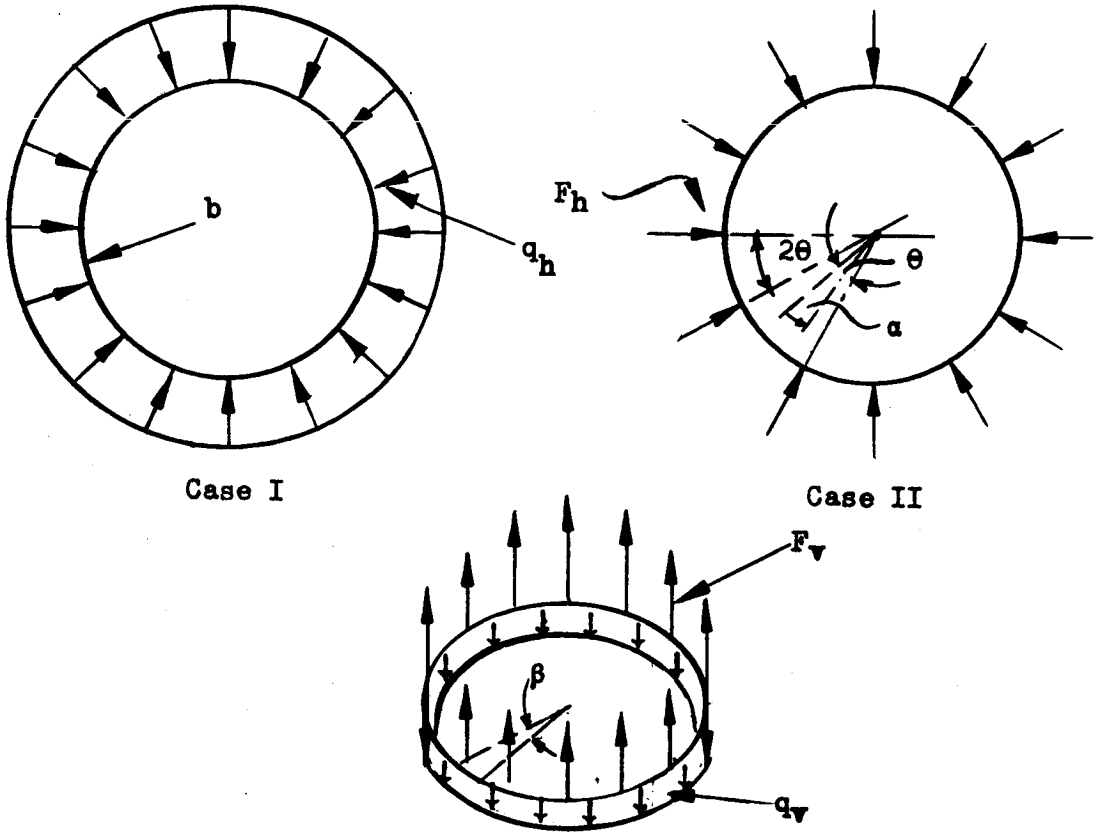

FIGURE 3 - Ring Load Cases

Equations of statics relating the loading components of Figure 2 and 3 with the applied column load, Q, are

$$q_h = N_{\varphi(x = H)} \cos \varphi_H = \frac{Q}{2 \pi b} \cot \varphi_H \quad (1)$$

$$q_v = N_{\varphi(x = H)} \sin \varphi_H = \frac{Q}{2 \pi b} \quad (2)$$

$$F_v = \frac{Q}{n} \quad (3)$$

$$F_h = (R_1 + R_2) \cos \omega = 2 R_p \cos \omega \quad \left[R_p \geq \frac{Q}{2n \sin \omega} \right] \qquad (4)$$

Where:

n = the number of cable attachments on the ring

R_p = the resultant of cable pretensions at each point, n, in either conical surface 1 or 2

a. Strength Requirements

CASE I

The uniform radial loading of Case I, Figure 3, causes only compression in the ring. This compression force is easily seen from statics to be,

$$C = q_h b \qquad (5)$$

CASE II

The compressive force, C, in-plane bending moment, M_p, shear force, V_p, and radial bending deflection, δ_r, may be readily determined from Case 9, Page 158 of Reference 2 as,

$$C = \tfrac{1}{2} F_h \left[\frac{\cos \alpha}{\sin \theta} \right] \qquad (6)$$

$$M_p = \tfrac{1}{2} F_h b \left[\frac{\cos \alpha}{\sin \theta} - \frac{1}{\theta} \right] \qquad (7)$$

$$V_p = \tfrac{1}{2} F_h \left[\frac{\sin \alpha}{\sin \theta} \right] \qquad (8)$$

$$\text{at } \alpha = 0,\ \delta_{r_o} = -\frac{F_h\, b^3}{4\,(EI)_p}\left[\frac{2}{\theta} - \frac{1}{\sin\theta} - \theta\,\frac{\cos\theta}{\sin^2\theta}\right] \tag{9}$$

$$\text{at } \alpha = \theta,\ \delta_{r_o} = \frac{F_h\, b^3}{2\,(EI)_p}\left[\frac{1}{2\sin^2\theta}(\theta + \sin\theta\cos\theta) - \frac{1}{\theta}\right] \tag{10}$$

where: (Refer to Figure 3)

$$\theta = \frac{\pi}{n} \tag{11}$$

$(EI)_p$ = the in-plane bending stiffness of the ring. Positive deflections are inward

CASE III

Expressions for the out-of-plane moments, M_n, shears, V_n, and torques were derived in Reference 1. However, the independent derivations given below revealed errors in the moment and torque equations. The derivations herein are therefore used along with additional expressions for the out-of-plane deflections.

First, consider the static equilibrium of Case III in Figure 3. Then, rather than using Equations 3 for F_v, we may write,

$$F_v = 2\,b\,\theta\,q_v \tag{12}$$

or in general, if q_v were not constant but some smooth function of the angle β, symmetrical about the plane that bisects the angle 2θ (Refer to Figure 4)

$$F_v = b \int_0^{2\theta} q_v \, d\beta \tag{13}$$

Because of symmetry, a segment of the ring subtended by the angle 2θ may be considered separately in Figure 4. Also, by symmetry, the torque at the support is zero, i.e., $T_o = 0$.

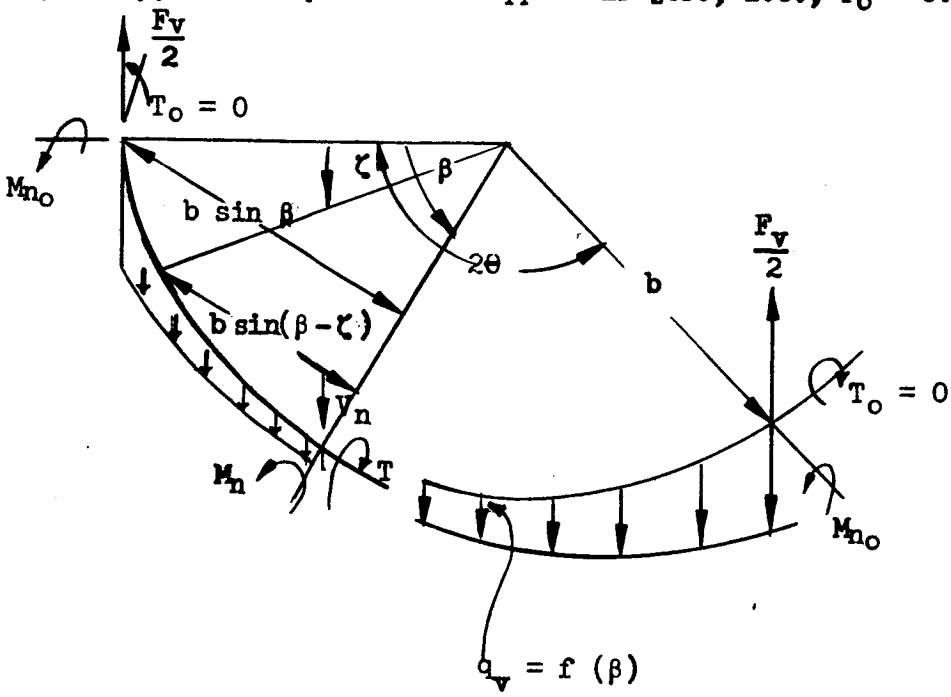

FIGURE 4 - Free Body of a Ring Segment Between Supports

From the Statics of Figure 4,

$$T = \frac{F_v}{2} \, b \, (1 - \cos \beta) + M_{n_o} \sin \beta - b^2 \int_0^{\beta} q_v \, [1 - \cos (\beta - \zeta)] \, d\zeta \tag{14}$$

$$M_n = \frac{F_v}{2} b \sin \beta + M_{n_o} \cos \beta - b^2 \int_o^\beta q_v \sin (\beta - \zeta) \, d\zeta \tag{15}$$

$$V_v = \frac{F_v}{2} - b \int_o^\beta q_v \, d\zeta \tag{16}$$

Substituting for F_v from Equation 13 into Equations 14, 15 and 16 gives,

$$T = M_{n_o} \sin \beta + b^2 \left\{ \frac{1 - \cos \beta}{2} \int_o^{2\theta} q_v \, d\beta - \int_o^\beta q_v \left[1 - \cos (\beta - \zeta) \right] d\zeta \right\} \tag{17}$$

$$M_n = M_{n_o} \cos \beta + b^2 \left\{ \frac{\sin \beta}{2} \int_o^{2\theta} q_v \, d\beta - \int_o^\beta q_v \sin (\beta - \zeta) \, d\zeta \right\} \tag{18}$$

$$V_n = b \left[\tfrac{1}{2} \int_o^{2\theta} q_v \, d\beta - \int_o^\beta q_v \, d\zeta \right] = b \int_\beta^\theta q_v \, d\zeta \tag{19}$$

In the above equations, M_{n_o} is determined by summing up moments on a 2θ arc about the tangent at one of its ends. Thus,

$$M_{n_o} = \frac{b^2}{\sin 2\theta} \int_o^{2\theta} \left[\frac{1 + \cos 2\theta}{2} - \cos (2\theta - \beta) \right] q_v \, d\beta \tag{20}$$

For the particular case of q_v constant, the above equations become:

$$M_{n_o} = q_v b^2 (\theta \cot \theta - 1) \tag{21}$$

$$M_n = M_{n_o} \cos \beta + q_v b^2 [\, \theta \sin \beta - 1 + \cos \beta \,]$$

$$= q_v b^2 \left[\frac{\theta \cos (\theta - \beta)}{\sin \theta} - 1 \right] \tag{22}$$

$$T = M_{n_o} \sin \beta + q_v b^2 [\, \theta (1 - \cos \beta) - \beta + \sin \beta \,]$$

$$= q_v b^2 \left[(\theta - \beta) - \frac{\theta \sin (\theta - \beta)}{\sin \theta} \right] \tag{23}$$

$$V_n = q_v b (\theta - \beta) \tag{24}$$

Deflections

Transverse deflection, δ, due to bending moment M_n and Torque T can be found from equations (Reference 7)

$$\frac{M_n}{EI} = \frac{\zeta}{b} - \frac{1}{b^2} \frac{d^2 \delta}{d \beta^2} \tag{25}$$

$$\frac{T}{GJ} = \frac{1}{b} \cdot \frac{d\zeta}{d\beta} + \frac{1}{b^2} \frac{d\delta}{d\beta} \tag{26}$$

where ζ is the angle of twist of the ring cross section. Differentiating Equation (25) with respect to β and combining the resulting equation and Equation (26) yields

$$\frac{d^3 \delta}{d \beta^3} + \frac{d\delta}{d\beta} = - b^2 \left[\frac{1}{EI} \frac{d M_n}{d\beta} - \frac{T}{GJ} \right] \tag{27}$$

This is a third order linear differential equation, and its solution contains three constants of integration which can be determined from the boundary condition

$$\left.\begin{aligned} \delta &= 0 \quad \text{at } \beta = 0 \\ \frac{d\delta}{d\beta} &= 0 \quad \text{at } \beta = 0 \\ \frac{d\delta}{d\beta} &= 0 \quad \text{at } \beta = \theta. \end{aligned}\right\} \tag{28}$$

Noting that $\frac{d M_n}{d\beta} = + q_v b^2 \frac{\theta}{\sin \theta} \sin (\theta - \beta)$ (from Equation 22) the general solution of Equation (27) is

$$\delta = C_1 \cos \beta + C_2 \sin \beta + C_3 + \frac{q_v b^4}{2} \left\{ \left[\frac{1}{EI} + \frac{1}{GJ} \right] \frac{\theta}{\sin \theta} \beta \sin (\theta - \beta) - \frac{(\theta - \beta)^2}{GJ} \right\} \tag{29}$$

Taking into account the boundary conditions (28), the constants C_1, C_2 and C_3 are

$$C_1 = -\frac{q_v b^4 \theta^2}{2 \sin^2 \theta} \left\{ \frac{1}{EI} + \frac{1}{GJ} + \frac{\sin 2\theta}{2\theta} \left[\frac{1}{EI} + \frac{3}{GJ} \right] \right\} \tag{30}$$

$$C_2 = -\frac{q_v b^4 \theta}{2}\left[\frac{1}{EI} + \frac{3}{GJ}\right] \quad (31)$$

$$C_3 = \frac{q_v b^4 \theta}{2}\left[\frac{1}{EI} + \frac{3+\theta}{GJ}\right] \quad (32)$$

Then the deflection equation can be found from Equation (29) (for $0 \leq \beta \leq \theta$) upon substituting Equations (30) to (33) for C_1, C_2 and C_3.

b. Buckling in the Plane of the Ring

The critical circumferential buckling stress is taken directly from Reference 1.

$$f_{cr} = \frac{C_{cr}}{4\,pt_r} = \frac{3\,(EI)_p}{4\,pt_r\,b^2} \quad (33)$$

where:

p = the length of one side of the diamond cross-section

t_r = The wall thickness of the diamond cross-section

c. Buckling Out-of-the-Plane of the Ring

The out-of-plane buckling criteria for the critical circumferential stress due to uniform radial load, q_h, and for the critical in-plane bending moment, respectively, are (References 1 and 8)

$$f_{cr} = \frac{q_{hcr}\, b}{4\, pt_r} = \frac{3\,(EI)_n}{pt_r\, b^2}\left[\frac{1}{4 + \frac{(EI)_n}{GJ}}\right] \tag{34}$$

$$M_{cr} = \frac{(EI)_n + GJ}{2b} - \sqrt{\left[\frac{(EI)_n - GJ}{2b}\right]^2 + \frac{4(EI)_n\, GJ}{b^2}} \tag{35}$$

d. Local Buckling

In checking the local buckling of the wall of the ring, the criterion used in Reference 1 is again applied.

$$f_{cr} = 3.6\, E\left[\frac{t_r}{p}\right]^2 \tag{36}$$

2. Packaging Stresses

The diamond cross-section is first folded as shown in Figure 5. The folded cross-section (of thickness 2 t_r) is then looped successively and packaged around a central hub. This looping is done normal to the conical surface defined by the sides of the folded cross-section so that bending stresses are induced. Applying the flexural formula to this problem, the bending stress corresponding to any given minimum bend radius, ρ_m, incurred during packaging may be determined as (where the wall is conservatively assumed to act as one plate of thickness 2 t_r),

$$f_b = \frac{E\, t_r}{\rho_m} \tag{37}$$

3. Folding Stresses

In folding the diamond cross-section, the maximum strains occur when the section is half open as can easily be seen in Figure 5.

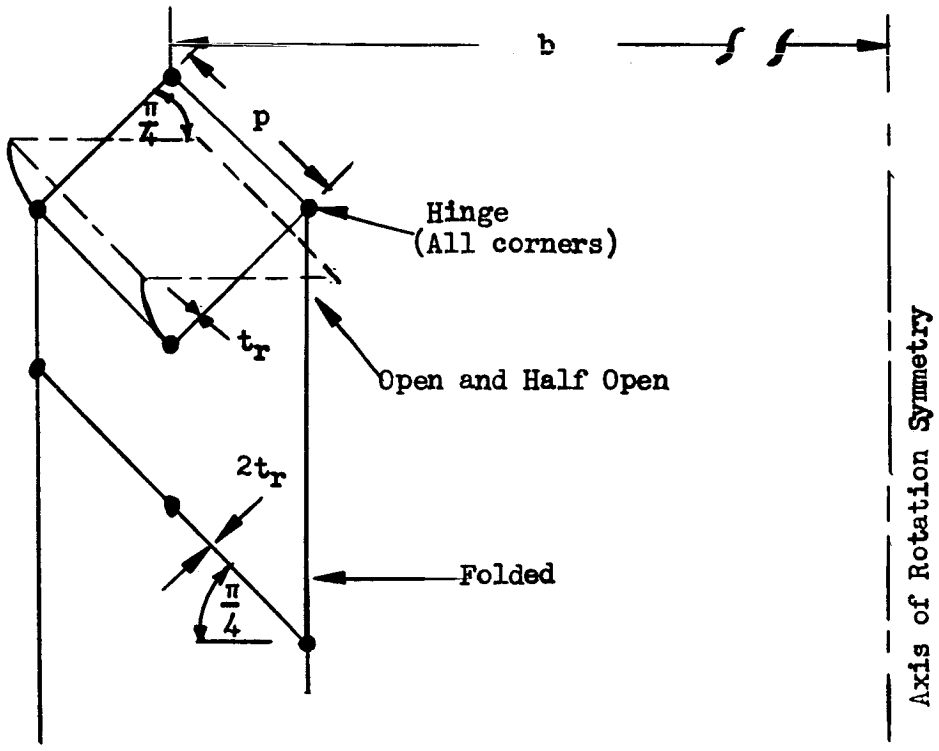

FIGURE 5 - Folding of the Diamond Cross-Section Ring

This maximum circumferential strain may be derived from the geometry of Figure 5 as,

$$\varepsilon_\theta = \pm \frac{p}{2b}\left[1 - \cos\frac{\pi}{4}\right] = \pm \frac{p}{4b}\left[2 - \sqrt{2}\right] \tag{38}$$

and, by Hooke's law the corresponding stress is,

$$f_\theta = \pm \frac{pE}{4b}\left[2 - \sqrt{2}\right] \tag{39}$$

4. Energy Required to Fold or Open the Diamond Cross-Section

From Reference 1, this energy is given by,

$$U = \frac{\pi E p^3 t_r}{3b}\left[3 - 2\sqrt{2}\right] \tag{40}$$

C. A Design Example

Having presented the necessary equations for the structural analysis of a large foldable ring of a diamond cross-section, such an analysis is now conducted for a typical example. The given data are:

$H = 485$ in.
$a = 36$ in.
$b = 360$ in.
$\rho_m = 4$ in.
$p = 3.5$ in.
$t_r = 0.020$ in.

$\varphi_o \approx \varphi_H \approx 56.25$ degs.
$\omega = 13$ degs.
$\theta = 3$ degs.

Titanium 6AL - 4V
$F_{ty} = 120$ ksi
$E = 16 \times 10^3$ ksi

$Q = 60$ lbs.
$n = 60$
$\mu = 0.29$
$G = 6.2 \times 10^3$ ksi

The above data is compatible with the preliminary design of a cone-and column solar concentrator of Reference 1 except for the wall thickness which is taken as 0.020 in. rather than 0.014 in. in order to obtain a minimum factor of safety on buckling of 1.5. The angles φ_o and φ_H have been taken equal and equal to the complement of the half angle of the theoretically true cone. Actually these angles will be unequal to conform with the cone design which is a membrane of revolution having anticlastic curvature. The resulting differences between the true and assumed angles will be sufficiently small to be negligible for the analysis of the ring.

The applied axial column load, Q, has been arbitrarily taken as 60 lbs. As yet, there is no basis for this number other than Reference 1 where this value ($N_{\varphi R}$ = 0.032 lbs/in) was used but also arbitrarily. It appears that the required axial column load must be determined experimentally for a cone design that is basically different than that proposed to date. This conclusion is based on the analytical work presented in Section II of this report.

The analysis of the example ring is now continued.

1. <u>Section Properties, Stiffnesses and Stress Equations</u>

$$I_p = I_n = \frac{4}{3} p^2 t_r \left[\frac{p}{2} + t_r \right] = \left[\frac{4}{3} \right] (12.25)(0.020) \left[\frac{3.5}{2} + 0.020 \right] = 0.58 \text{ in.}^4 \qquad (41)$$

$$J = 4 \frac{p^4 t_r}{4p} = p^3 t_r = (42.875)(0.02) = 0.8575 \text{ in.}^4 \qquad (42)$$

$$(EI)_p = (EI)_n = (16)(0.58) \times 10^6 = 9.28 \times 10^6 \text{ lbs-in}^2 \qquad (43)$$

$$GJ = (6.2)(0.8575) \times 10^6 = 5.32 \times 10^6 \text{ lbs-in}^2 \qquad (44)$$

a. Circumferential Ring Stress

$$f_c = \frac{C}{4p\ t_r} = \frac{C}{4\ (3.5)\ (0.020)} = 3.57\ C \qquad (45)$$

b. Circumferential Bending Stress

$$f_b = \frac{M\ p}{I\sqrt{2}} = \frac{3.5\ M}{0.58\sqrt{2}} = 4.26\ M \qquad (46)$$

c. Direct Shear Stress

$$f_s = \frac{3V\sqrt{2}}{8p\ t_r} = \frac{3V\sqrt{2}}{8\ (3.5)\ (0.020)} = 7.58\ V \qquad (47)$$

d. Torsional Shear Stress

$$\tau = \frac{T}{2p^2\ t_r} = \frac{T}{2\ (12.25)\ (0.020)} = 2.04\ T \qquad (48)$$

2. Applied Loads

In determining F_H by Equation 4, the pretension in the cables must be known. The lower limit, $R_p = Q/n \sin \omega$, will first be used and the additional allowable pretension will then be determined based on the strength of the ring.

From Equations 1 through 4,

$$q_v = \frac{60}{2\ (360)\ \pi} = 0.0265\ \text{lbs/in.}$$

$$q_h = q_v \cot \varphi_H = (0.0265)\ (0.6682) = 0.0177\ \text{lbs/in.}$$

$$F_V = \frac{60}{60} = 1.0 \text{ lbs.}$$

$$F_h = \frac{2\,(60)}{(60)} \cot \omega = 2\,(4.331) = 8.662 \text{ lbs.}$$

3. Design Loads

a. Case I

$$C = (0.0177)\,(360) = 6.38 \text{ lbs.}$$

b. Case II

$$C_{max} = \tfrac{1}{2}\,(8.662)\,(19.11) = 82.9 \text{ lbs} \quad \text{at } \alpha = 0$$

$$Mp_{max} = (4.331)\,(360)\left[19.11 - \frac{180}{3\pi}\right] \approx 0$$

$$Vp_{max} = 4.331 \text{ lbs} \quad \text{at } \alpha = 0$$

c. Case III

$$Vn_{max} = (0.0265)\,(360)\,(0.0525) = 0.5 \text{ lbs} \quad \text{at } \beta = 0$$

$$Mn_{max} = (0.0265)\,(360)^2\left\{\left[\frac{3\pi}{180}\right](19.081) - 1\right\} \approx 0, \text{ at } \beta = 0$$

$$T_{max} \approx 0$$

d. Combined Loads

$$C = 89.3 \text{ lbs}, \quad M_{max} \approx 0$$

$$V_{max} = 4.331 \text{ lbs.} \quad T_{max} \approx 0$$

4. Deflections

a. In-Plane Bending Deflections

From Equations 9 and 10,

$$\text{at } \alpha = 0, \quad \delta_{r_o} = -\frac{(8.662)\,(360)^3}{4\,(9.28 \times 10^6)} \left[\frac{2}{0.0525} - \frac{1}{0.0525} - \frac{1}{0.0525} \right] = 0$$

$$\text{at } \alpha = \theta, \quad \delta_{r_o} = 0$$

5. Design Stresses

Substituting the combined loads in Equations 45 through 48,

$$f_c = (3.57)\,(89.3) = 319$$

$$f_b = (4.26)\,(0) = 0$$

$$\text{Total} = f = 319 \text{ lbs/in.}^2$$

$$f_s = (7.58)\,(4.331) = 32.8 \text{ psi}$$

$$\tau = 0$$

6. Allowable Stresses and Factors of Safety

a. Buckling in the Plane of the Ring (Equation 33)

$$f_{cr} = \frac{3\,(9.28 \times 10^6)}{4\,(3.5)\,(0.020)\,(360)^2} = 768 \text{ lbs/in}^2$$

Comparing this allowable to the applied stress of 319 lbs/in^2 shows the ring has an adequate factor of safety of F.S. = 2.40

b. Buckling Out of the Plane of the Ring (Equations 34 and 35)

Since the in-plane moment is zero, only Equation 34 is of interest

$$f_{cr} = \frac{4\,(768)}{4 + \frac{9.28}{5.32}} = 535 \text{ lbs/in}^2$$

$$\text{F.S.} = \frac{535}{319} = 1.68$$

c. Local Buckling (Equation 36)

$$f_{cr} = (3.6)\,(16 \times 10^6)\left[\frac{0.020}{3.5}\right]^2 = 1880 \text{ lbs/in}^2$$

Comparing this allowable to the combined applied stress of 359.3 lb/in^2 shows the ring has an adequate factor of safety of F.S. = 5.22.

7. Packaging Stresses (Equation 37)

$$f_b = (16 \times 10^6)\left[\frac{0.020}{4}\right] = 80{,}000 \text{ lbs/in}^2$$

$$\text{F.S.} = \frac{120}{80} = 1.5$$

8. Folding Stresses (Equation 39)

$$f_\theta = \frac{(3.5)\,(16 \times 10^6)}{4\,(360)} \left[2 - \sqrt{2} \right] = 22{,}800 \text{ lbs/in}^2$$

$$\text{F.S.} = \frac{120}{22.8} = 5.25$$

9. Energy Required to Fold or Open the Cross-Section (Equation 40)

$$U = \frac{\pi\,(16 \times 10^6)\,(3.5)^3\,(0.020)}{3\,(360)} \left[3 - 2\sqrt{2} \right] = 6{,}860 \text{ in-lbs}$$

10. The Allowable Additional Pretension in the Cables

For a factor of safety of F.S. = 1.5 on the ring stability, the allowable additional resultant of the cable pretensions, R_{pa}, greater than $Q/n \sin \omega$ (refer to Equation 4) is next determined.

This calculation is dictated by the out-of-plane buckling analysis ($f_{cr} = 535$ lbs/in^2). Then,

$$f_a = \frac{f_{cr}}{\text{F.S.}} - f_c = \frac{535}{1.5} - 319 = 38 \text{ lbs/in}^2$$

By Equation (45)

$$C_a = 4\,p\,t_r\,f_a = 4\,(3.5)\,(0.020)\,(38) = 10.6 \text{ lbs.}$$

By Equation (6)

$$F_{ha} = 2\,C_a \sin\theta = 2\,(10.6)\,(0.05234) = 1.11 \text{ lbs.}$$

and, finally, from Equation (4)

$$R_{pa} = \frac{F_{ha}}{2 \cos \omega} = \frac{1.11}{2\,(0.9744)} = 0.57 \text{ lbs.}$$

II. ANALYSIS OF THE CONE

A. General

Since deployment of the cone is accomplished by applying only axial load (the base ring provides circumferential forces but only locally near the ring), the primary problem is the development of adequate circumferential tensile stresses to reduce residual creases and wrinkles to a satisfactory reflectivity level. Unfortunately, the primary circumferential stresses are zero everywhere in an axially loaded cone. Secondary, higher-order, circumferential tensile stresses are induced due to the deflections, but these are insignificant. The analysis of these stresses and corresponding deflections is presented herein.

In order to obtain an analytical estimate of the circumferential stresses required to minimize meridian wrinkles, an apparently conservative approach was taken. A unit width strip of the Mylar film with transverse creases was considered and a solution for the large, nonlinear, deflections of cantilevered beams was adapted. Force-deflection relationships that yielded infinite slope at the tip of the cantilevered beams were generated and the results plotted. These curves may be used to determine the required membrane force to minimize the wrinkles for a given allowable reduction in the developed length due to these creases and for a given spacing between creases.

In order to obtain the required circumferential stresses, 1) the true cone must be subjected to distributed loads over the entire surface such as provided by internal pressurization or, 2) under only applied uniaxial meridian forces, it is necessary to deviate from a true cone by fabricating a membrane of revolution with anticlastic (negative) curvature. From both a fabrication and structural viewpoint, the first approach is preferred. However, because the basic concept proposed in Reference 3 depends on axial load alone, it is necessary to take the second approach. Various curves may be considered for the meridian that defines

the anticlastic surface of revolution. Two are considered herein; 1) meridians which yield constant circumferential stresses everywhere and 2) parabolic meridians. Families of these curves for various ratios of the applied axial load, Q, to the circumferential stress, f_θ, are generated along with the corresponding meridian and circumferential stresses at various locations on the surface. A "cone" design may thus be selected for given required circumferential stresses, axial loads and meridian curves.

As a consequence of the anticlastic surface approach, the fabrication problem of making a surface of double curvature arises. In pressurized bodies that are fabricated from gores of single curvature, the desired shape is controlled by the pressure, i.e. as the pressure is increased the originally flat gores develop curvature, pass through the desired body of revolution and then take a lobed shape such as observed in a parachute, for example. The question is, will a similar approach work in the problem at hand whereby the axial load now replaces the pressure in forcing the flat gores to take double curvature? The analysis contained herein considers a gored body with meridian seams. Although certain simplifying assumptions are necessary, the results are considered adequate for the feasibility determination. It is concluded that although circumferential curvature occurs upon application of axial load, a true body of revolution cannot be obtained. In fact, for the restraints imposed on the geometry and axial force of the example problem, only small deviations from the undeformed polygon cut by a plane normal to the axis of symmetry are possible. Results of experiments on preliminary models indicate the above conclusion is correct. However, it has by no means been experimentally verified.

B. Detailed Analysis of a True Cone

The approach of Chapter 14 of Reference 4 is taken. In general, the same nomenclature is also used.

1. General Deflection Equations for Uniform Meridian Tension and Axisymmetrical Temperature Gradients

Consider the frustum of a conical shell without bending stiffness and subjected to an axial force, Q, and a smooth temperature gradient along the meridian as shown in Figure 6. The symbol T represents the temperature change from the datum.

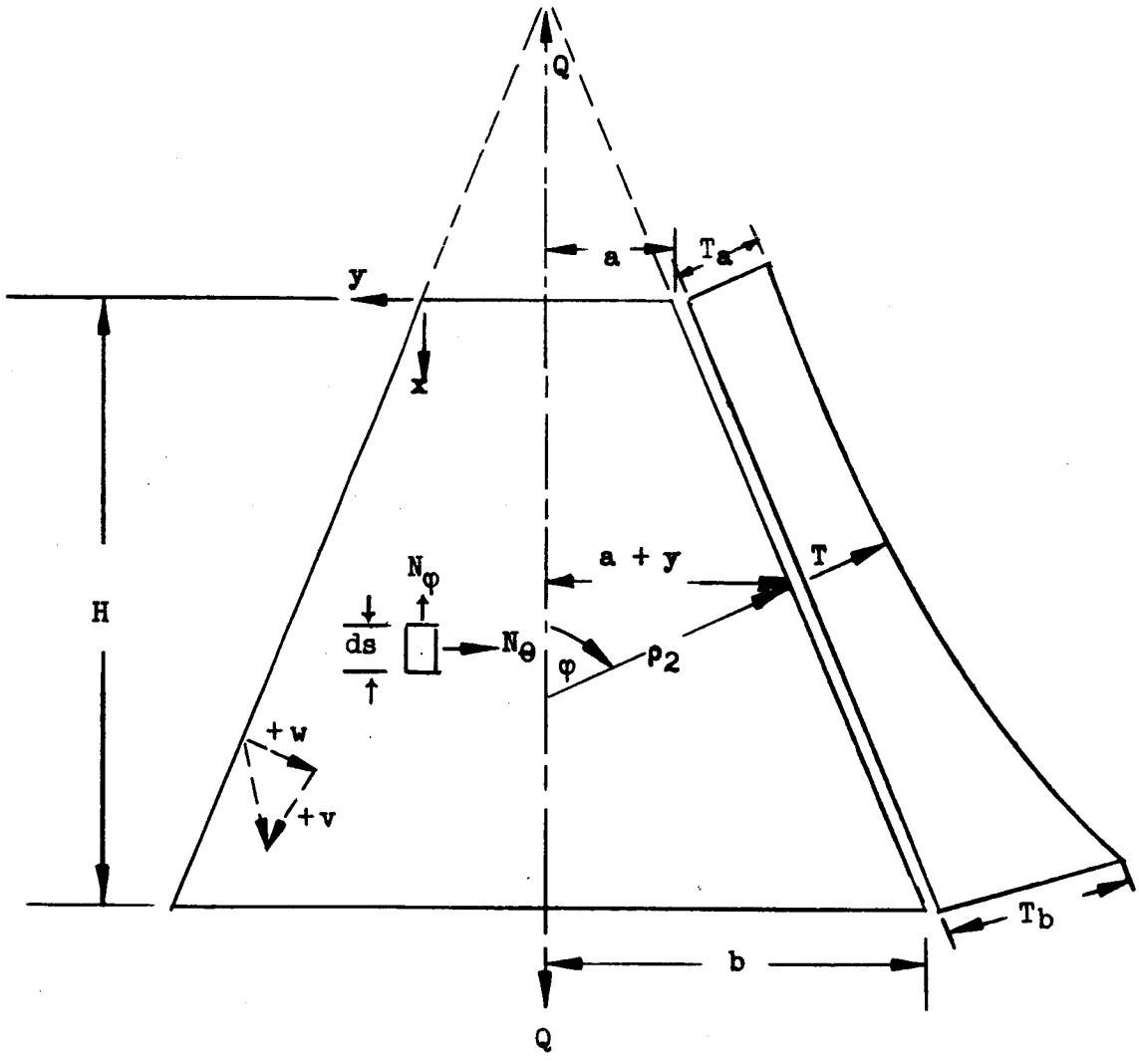

FIGURE 6 - Frustum of a Cone

The strain components in an elastic body undergoing thermal expansion are related to the stresses by the well known Duhamel-Neumann law (Reference 5),

$$\left.\begin{aligned} \varepsilon_\varphi &= \frac{\sigma_\varphi}{E_\varphi} - \frac{\mu_{\theta\varphi}}{E_\theta}\ \sigma_\theta + \alpha_\varphi T \\ \varepsilon_\theta &= \frac{\sigma_\theta}{E_\theta} - \frac{\mu_{\varphi\theta}}{E_\varphi}\ \sigma_\varphi + \alpha_\theta T \end{aligned}\right\} \tag{49}$$

For an isotropic film of thickness, h, Equations (49) may be reduced and written in terms of the membrane forces as,

$$\left.\begin{aligned} \varepsilon_\varphi &= \frac{1}{Eh}\ (N_\varphi - \mu\ N_\theta) + \alpha\ T \\ \varepsilon_\theta &= \frac{1}{Eh}\ (N_\theta - \mu\ N_\varphi) + \alpha\ T \end{aligned}\right\} \tag{50}$$

From the statics of Figure 6,

$$N_\varphi = \frac{Q}{2\pi\ (a + y) \sin \varphi} \tag{51}$$

or, defining

$$q = N_{\varphi(y\,=\,0)} = \frac{Q}{2\pi\ a \sin \varphi} \tag{52}$$

$$a + y = r_o \tag{53}$$

Equation 51 becomes,

$$N_\varphi = \frac{a}{r_o} q \tag{54}$$

Because there is no external load applied normal to the surface of the cone and because the meridian radius of curvature for a cone is infinite, it may be shown from the well known membrane equation (256) of Reference 4 that,

$$N_\theta = 0 \tag{55}$$

Consider the displacements of an element of meridian length, ds, and take its normal and tangential components of deflection, w and v respectively, to be positive as shown in Figure 6. The strain-displacement equations of Reference 3 then become,

$$\left.\begin{aligned} \varepsilon_\varphi &= \frac{dv}{ds} \\ \varepsilon_\theta &= \frac{1}{\rho_2} (v \cot \varphi - w) \end{aligned}\right\} \tag{56}$$

Considering the first of Equations 50 along with Equations 54 and 55 and substituting into the first of Equation 56 yields,

$$\frac{dv}{ds} = \frac{aq}{Eh\, r_o} + \alpha T \tag{57}$$

But, from Figure 6

$$ds = \frac{d\, r_o}{\cos \varphi} \tag{58}$$

$$\therefore \frac{dv}{ds} = \frac{dv}{d r_o} \cos \varphi = \frac{a q}{Eh r_o} + \alpha T \qquad (59)$$

Integrate Equation 59,

$$v \Big|_{v_a}^{v} = \frac{a q}{Eh \cos \varphi} \ell n \, r_o \Big|_a^{r_o} + \frac{\alpha}{\cos \varphi} \int_a^{r_o} T \, dr_o$$

and

$$v = \frac{a q}{Eh \cos \varphi} \ell n \frac{r_o}{a} + \frac{\alpha}{\cos \varphi} \int_a^{r_o} T \, dr_o \qquad (60)$$

where, $v_a = 0$ at $r_o = a$

Similarly, the normal deflection is determined by substituting the second of Equations 50 along with Equations 54, 55 and 60 into the second of Equations 56. Also Equation 61 is used.

From Figure 6 and Equation 53,

$$\rho_2 = \frac{r_o}{\sin \varphi} \qquad (61)$$

Then,

$$v \cot \varphi - w = \left[- \frac{\mu a q}{Eh r_o} + \alpha T \right] \rho_2 = - \frac{\mu a q}{Eh \sin \varphi} + \frac{r_o \alpha T}{\sin \varphi}$$

(62)

and,

$$w = \frac{\mu\, a\, q}{Eh \sin\varphi} - \frac{r_o\, a\, T}{\sin\varphi} + \frac{a\, q}{Eh \sin\varphi} \ell n \frac{r_o}{a} + \frac{a}{\sin\varphi} \int_a^{r_o} T\, dr_o$$

$$= \frac{a\, q}{Eh \sin\varphi} \left[\ell n \frac{r_o}{a} + \mu \right] - \frac{a}{\sin\varphi} \left[T\, r_o - \int_a^{r_o} T\, dr_o \right] \qquad (63)$$

It is interesting to note that if the v and w components are resolved to the radial displacement, the part of this radial displacement due to the axial load is constant everywhere,

$$\text{Radial displacement} = \varepsilon_\theta\, r_o = w \sin\varphi - v \cos\varphi \qquad (64)$$

Substituting for v and w from Equations 60 and 63 into 64 yields

$$\varepsilon_\theta\, r_o = \frac{\mu\, a\, q}{Eh} - a\, T\, r_o \qquad (65)$$

Since one basis of evaluating the accuracy of a solar concentrator is the angular error (or deviation of the slope of the deflected meridian from that of the perfect one), the angular deflections that correspond to the linear v and w displacements are next determined. The equation of the displaced meridian is first determined by adapting a new coordinate system based on the undisplaced meridian as shown in Figure 7.

From Figure 7 and Equations 60 and 63, the u and z coordinates of the deflected meridian are

$$u = \frac{r_o}{\cos\varphi} + v = \frac{r_o}{\cos\varphi} + \frac{a\, q}{Eh \cos\varphi} \ell n \frac{r_o}{a} + \frac{a}{\cos\varphi} \int_a^{r_o} T\, dr_o \qquad (66)$$

$$z = -w = \frac{a}{\sin\varphi} \left[T\, r_o - \int_a^{r_o} T\, dr_o \right] - \frac{a\, q}{Eh \sin\varphi} \left[\ell n \frac{r_o}{a} + \mu \right] \qquad (67)$$

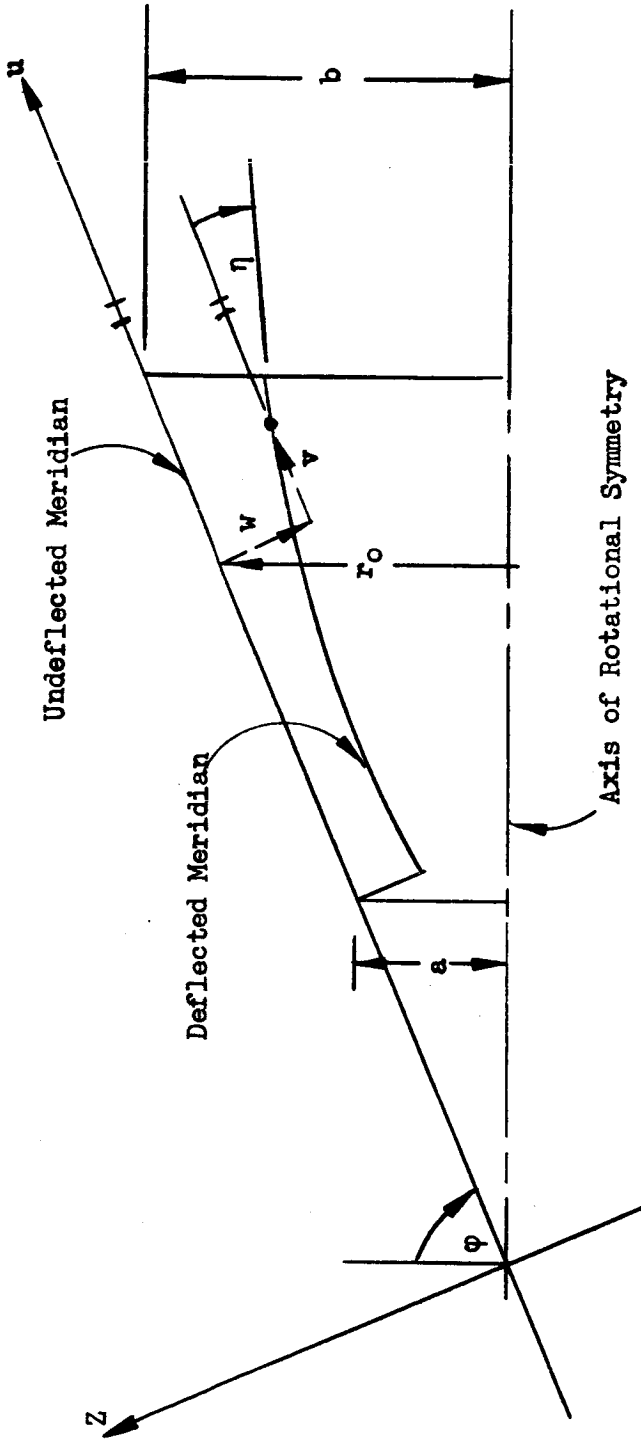

FIGURE 7 - Coordinate System for the Deflected Meridian

The tangent of the desired angular deflection is the slope of the deflected meridian,

$$\tan \eta = \frac{dz}{du} = \frac{\frac{dz}{d r_o}}{\frac{du}{d r_o}}$$

$$= \frac{\frac{\alpha}{\sin \varphi}\left[T + r_o \frac{dT}{d r_o} - T \right] - \frac{a q}{r_o Eh \sin \varphi}}{\frac{1}{\cos \varphi} + \frac{a q}{r_o Eh \cos \varphi} + \frac{\alpha T}{\cos \varphi}}$$

$$\frac{r_o \alpha \frac{dT}{d r_o} - \frac{a q}{r_o Eh}}{1 + \frac{a q}{r_o Eh} + \alpha T} \cot \varphi$$

and,

$$\tan \eta = \frac{\frac{r_o^2}{a} \alpha \frac{dT}{d r_o} - \frac{q}{Eh}}{\frac{r_o}{a}(1 + \alpha T) + \frac{q}{Eh}} \cot \varphi \qquad (68)$$

2. Deflection of the Cone Under Uniform Meridional Tension

The general equations of the preceding section are now applied to the example problem considered in Section I - "Analysis of the Ring". No temperature gradient is considered so that the terms containing T in the equations drop out.

The film considered is 1 mil Mylar having E = 735,000 psi and $\mu = 0.3$.

Substituting the proper values into Equations 52, 60, 63 and 68 yields,

$$q = \frac{60}{2\pi\,(36)\,(0.8315)} = 0.319 \text{ lbs/in.} \tag{69}$$

$$v = \frac{(36)\,(0.319)}{(735000)\,(0.001)\,(0.5556)}\ \ell n\left[\frac{r_o}{36}\right]$$

$$= 0.0281\ \ell n\left[\frac{r_o}{36}\right] \text{ in.} \tag{70}$$

$$w = \frac{(36)\,(0.319)}{(735)\,(0.8315)}\left\{\ell n\left[\frac{r_o}{36}\right] + 0.3\right\}$$

$$= 0.0188\left\{\ell n\left[\frac{r_o}{36}\right] + 0.3\right\} \text{ in.} \tag{71}$$

$$\tan\eta = -\frac{\left[\frac{0.319}{735}\right](0.668)}{\frac{r_o}{36} + \frac{0.319}{735}} = -\frac{2.13}{204\,r_o + 3.19} \tag{72}$$

From Equation (72), the angular deflections are seen to be very small. They vary from about 0.0166 degrees to 0.00166 degrees from r_o = a to r_o = b respectively.

3. The Secondary Circumferential Stresses Due to the Cone Deflections

Let

$$m = \frac{aq}{Eh} \tag{73}$$

Then, Equations 66 and 67 may be written, (for T = 0)

$$u = \frac{r_o}{\cos \varphi} + \frac{m}{\cos \varphi} \ell n \frac{r_o}{a} \tag{74}$$

$$z = -\frac{m}{\sin \varphi} \left[\ell n \frac{r_o}{a} + \mu \right] \tag{75}$$

The first and second derivatives of u and z with respect to r_o become,

$$\left.\begin{aligned} u' &= \frac{1}{\cos \varphi} \left[1 + \frac{m}{r_o} \right] \\ u'' &= -\frac{m}{r_o^2 \cos \varphi} \\ z' &= -\frac{m}{r_o \sin \varphi} \\ z'' &= \frac{m}{r_o^2 \sin \varphi} \end{aligned}\right\} \tag{76}$$

The radius of curvature of the meridian is given on page 200 of Reference 6 as

$$\rho_1 = \frac{\left[(u')^2 + (z')^2 \right]^{3/2}}{u' z'' - z' u''} \tag{77}$$

Substituting Equations 76 into 77 and simplying yields,

$$\rho_1 = \frac{r_o^2 \sin \varphi}{m \cos^2 \varphi} \left\{ \left[1 + \frac{m}{r_o} \right]^2 + \left[\frac{m \cot \varphi}{r_o} \right]^2 \right\}^{3/2} \qquad (78)$$

The corresponding principal radius of curvature normal to the meridian plane may be determined from the geometry of the deflected meridian in Figure 7. Then,

$$\begin{aligned} \rho_2 \sin (\varphi + \eta) &= r_o - w \sin \varphi + v \cos \varphi \\ &= r_o - m \left[\ell n \frac{r_o}{a} + \mu \right] + m \ell n \frac{r_o}{a} \\ &= r_o - m \mu \end{aligned} \qquad (79)$$

Since η is small, the approximations, $\sin \eta \approx \tan \eta \approx \eta$ and $\cos \eta \approx 1$ are made and substituted into Equation 79 so that,

$$\rho_2 \approx \frac{r_o - m \mu}{\sin \varphi + \eta \cos \varphi} \qquad (80)$$

Substituting for $\eta \approx \tan \eta$ from Equation 68 into Equation 80 and simplifying gives

$$\rho_2 \approx \frac{(r_o + m)(r_o - m \mu) \sin \varphi}{(r_o + m) \sin^2 \varphi - m \cos^2 \varphi} \qquad (81)$$

The in-plane meridian membrane forces may again be determined from statics, but this is now done by considering the deformed geometry to yield,

$$N_\varphi = \left[\frac{a - m\mu}{r_o - m\mu} \right] \frac{\sin(\varphi + \eta_o)}{\sin(\varphi + \bar{\eta})} q \qquad (82)$$

where η_o is the angular deflection at $r_o = a$

The well-known membrane equation (Reference 4) when the force normal to the surface is zero and when ρ_1 is opposite in direction to ρ_2 becomes

$$\frac{N_\varphi}{\rho_1} - \frac{N_\theta}{\rho_2} = 0 \qquad (83)$$

Substituting Equations 78, 81 and 82 into Equation 83, solving for N_θ and simplifying gives,

$$N_\theta = (a - m\mu) \frac{\sin(\varphi + \eta_o)}{\sin^2(\varphi + \eta)} \frac{m \cos^2 \varphi}{r_o^2 \sin \varphi} \left\{ \left[1 + \frac{m}{r_o} \right]^2 \right.$$

$$\left. + \left[\frac{m \cot \varphi}{r_o} \right]^2 \right\}^{-3/2} q \qquad (84)$$

Again, making the small angle approximation,

$$\sin(\varphi + \eta_o) \approx \sin \varphi + \eta_o \cos \varphi \approx \sin \varphi - \frac{m \cot \varphi}{a + m} \cos \varphi$$

$$\approx \frac{(a + m) \sin^2 \varphi - m \cos^2 \varphi}{(a + m) \sin \varphi}$$

and,

$$\sin^2(\varphi + \eta)$$

$$\approx \frac{(r_o + m)^2 \sin^4\varphi - 2m(r_o + m)\sin^2\varphi\cos^2\varphi + m^2\cos^4\varphi}{(r_o + m)^2 \sin^2\varphi}$$

$\therefore$

$$\frac{\sin(\varphi + \eta_o)}{\sin^2(\varphi + \eta)}$$

$$= \frac{(a + m)\sin^2\varphi - m\cos^2\varphi}{(r_o + m)^2 \sin^4\varphi - 2m(r_o + m)\sin^2\varphi\cos^2\varphi + m^4\cos^4\varphi}$$

$$\times \frac{(r_o + m)^2}{a + m} \sin\varphi \qquad (85)$$

Substituting Equation 85 into Equation 84 and simplifying gives

$$N_\theta = \frac{m(a - m\mu)(r_o + m)^2}{(a + m)r_o^2} \frac{(a + m)\sin^2\varphi - m\cos^2\varphi}{[(r_o + m)\sin^2\varphi - m\cos^2\varphi]^2}$$

$$\times \left\{ \left[1 + \frac{m}{r_o} \right]^2 + \left[\frac{m\cot\varphi}{r_o} \right]^2 \right\}^{-3/2} q\cos^2\varphi \qquad (86)$$

Substituting for m from Equation 73 into 85 and simplifying yields

$$N_\theta = \left[\frac{r_o}{a}\right]\left[\frac{q^2}{Eh}\right] \tan\varphi \sin^2\varphi \left[\frac{1 - \frac{\mu q}{Eh}}{1 + \frac{q}{Eh}}\right]\left\{\left[1 + \frac{q}{Eh}\right]\sin^2\varphi - \frac{q}{Eh}\cos^2\varphi\right\}$$

$$\times \left[\frac{r_o + \frac{aq}{Eh}}{\left[r_o + \frac{aq}{Eh}\right]\sin^2\varphi - \frac{aq}{Eh}\cos^2\varphi}\right]^2$$

$$\times \left\{\left[1 + \frac{a\,q}{Eh\,r_o}\right]^2\left[\frac{r_o \tan\varphi}{a}\right]^2 + \left[\frac{q}{Eh}\right]^2\right\}^{-3/2} \qquad (87)$$

In the example problem, q/Eh is very small. Equation 87 greatly simplifies for this case to yield the approximate equation,

$$N_\theta \approx \frac{q^2}{Eh}\left[\frac{a}{r_o}\cot\varphi\right]^2 \qquad (88)$$

Substitution of the example problem values into Equation 88 shows that even the maximum secondary circumferential membrane force (at $r_o = a$) is negligible.

$$N_{\theta_{max}} = \frac{(0.319)^2}{735}(0.668)^2 = 62 \times 10^{-6} \text{ lbs/in.}$$

or, the corresponding stress is only,

$$f_{\theta_{max}} = 0.062 \text{ lbs/in.}^2$$

C. Estimated Circumferential Stress Required to Minimize Residual Meridian Wrinkles

In order to achieve a perfectly smooth surface free of wrinkles and waves, the thin film must be subjected to biaxial stresses. This is predicated on observations of simple uniaxial strip tensile tests, for example. Here, even narrow, uncreased Mylar strips are observed to take transverse curvature at relatively small longitudinal stress levels. For wider strips, the edges first curl and then a series of waves develop across the section.

Unfortunately, the above phenomenon occurs in the uniaxially loaded cone-column reflector. In addition, the necessary meridian seams that are stiffer than the basic film cause wrinkles [at least, locally near the seams] and since the cone must be packaged, some creasing will occur necessitating the application of circumferential as well as meridian stresses to remove them.

The approach taken in the following analysis of the stress required to minimize wrinkling is based on the premise that a conservative solution for the more easily defined problem of wrinkling due to packaging will yield results that govern over the other two problems mentioned above.

Consider only meridian creases. Then for N creases, the length between them at any radius, r_o, is

$$2S = \frac{2\pi r_o}{N} \qquad (89)$$

The circumferential stress required to pull out these creases can be determined as follows:

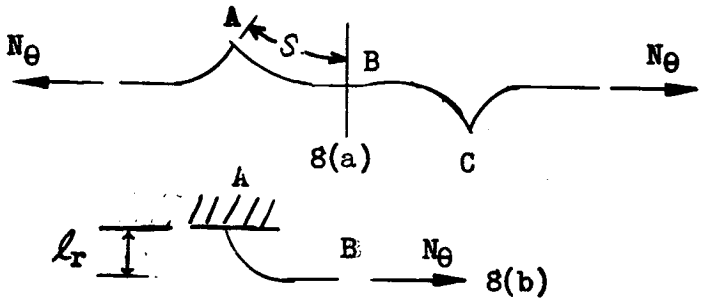

FIGURE 8 - A Creased Unit Width of Film Under Axial Tension N_θ

Preliminary investigation indicated that with the film thickness under consideration the axial load N_θ that produces plastic joints at the creases A and C is negligibly small. This was done by considering the non-linear elastic deflection of a cantilever beam with a tip concentrated load. This indicates that the problem is an inelastic one, and for this reason it must be restated as follows: Determine the circumferential stress N_θ which would bring the height of the creases, ℓ_r, (See Figure 8b) to a predetermined value, dictated by the desired smoothness of the surface.

The moment at the point A (Figure 8b) is

$$M_A = N_\theta \ \ell_r \tag{90}$$

Since the cross section at A is assumed fully plastic, the value of M_A is

$\frac{\sigma_y h^2}{4}$, where σ_y is the yield strength of the film and h the film thickness. Then Equation (90) becomes:

$$N_\theta \ell_r = \frac{\sigma_y h^2}{4}$$

For 1.0 mil Mylar (σ_y = 10,000; h = 0.001) the above equation becomes

$$N_\theta \ell_r = 0.0025 \text{ in-lb/in} \qquad (91)$$

With a fully plastic hinge at A the crease tends to disappear; this, of course, would require a small increase in the tension N_θ, which is accompanied by a subsequent decrease in ℓ_r. The process of complete elimination of the creases is rather complex, because it would require the knowledge of a precise stress-strain diagram for the Mylar film. However such a diagram, with the desired accuracy, is not available. As the section at A becomes fully plastic the tension N_θ assumes first its lowest possible value, and the respective ℓ_r assumes its highest value. In this sense Equation (91) is a conservative one, because it can be used with confidence to determine the lowest tension N_θ that leaves surface irregularities described by the parameter ℓ_r. Figure 9 offers a plot of the tension N_θ in terms of ℓ_r.

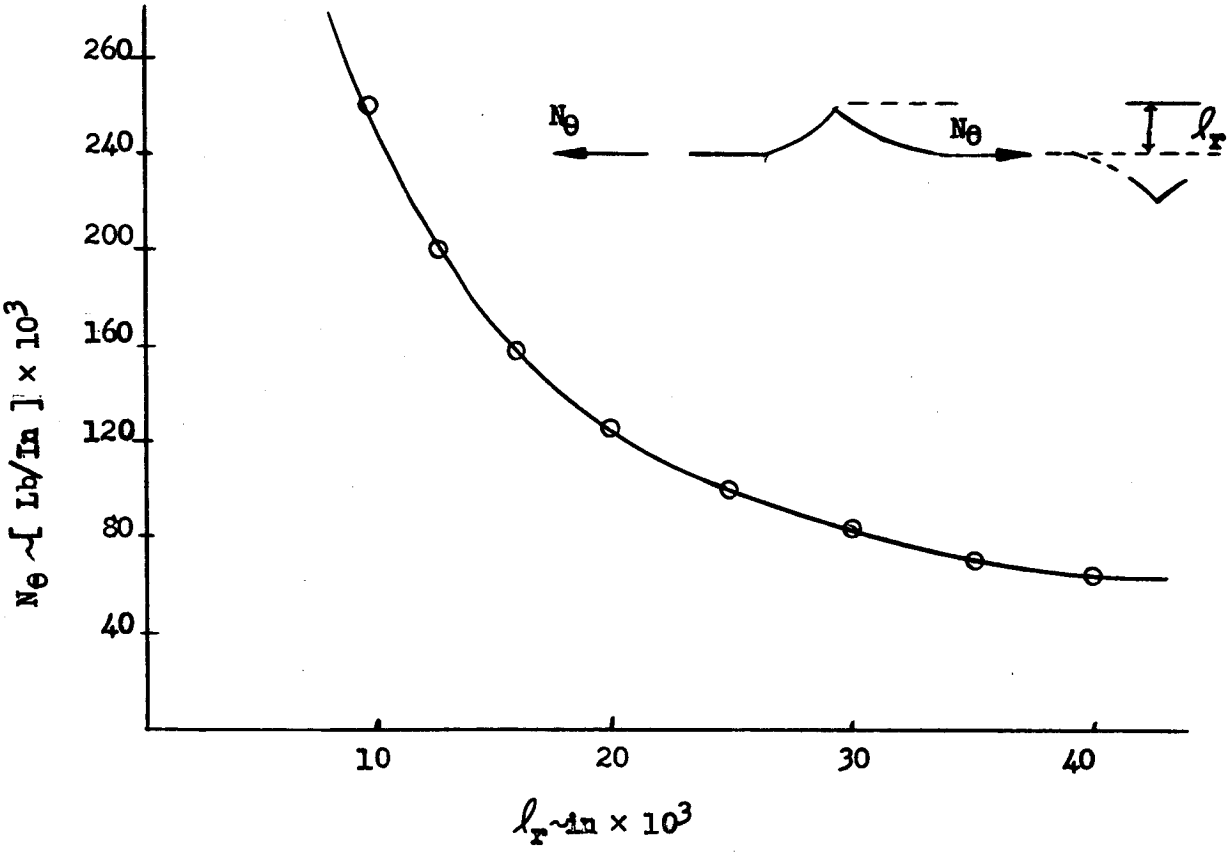

FIGURE 9 - Force-Deflection Relationship for Unit Width 1-Mil Mylar Strip

If surface irregularities in the order of 15 mil, for example, could be tolerated, the required tension N_θ would be 0.167 lb/in, which corresponds to a stress of 167 psi.

D. Surfaces of Revolution Having Anticlastic Curvature

Although many curves may be considered for the meridian that defines the anticlastic surface, only two types are analyzed herein; 1) meridians that yield constant circumferential stresses everywhere and 2) parabolic meridians.

Consider a general meridian curve that forms a surface of revolution as shown with its coordinate axes in Figure 10.

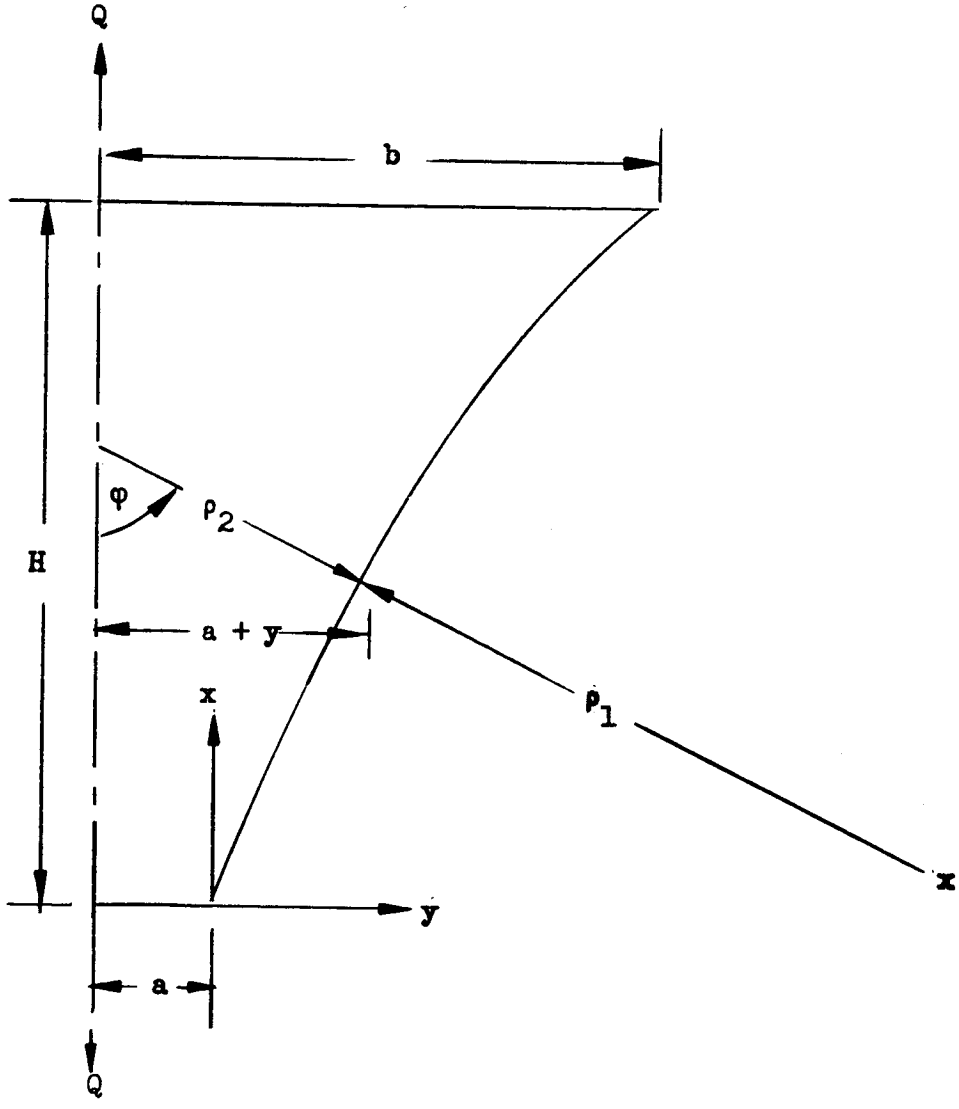

FIGURE 10 - The Anticlastic Meridian Curve

Again consider Equation 83,

$$\frac{N_\varphi}{\rho_1} - \frac{N_\theta}{\rho_2} = 0 \qquad (83)$$

The meridional radius of curvature is given in any calculus text as

$$\rho_1 = \frac{(1 + y'^2)^{3/2}}{y''} \qquad (108)$$

where the primes denote differentiation with respect to x.

From Figure 10,

$$\rho_2 = \frac{a + y}{\sin \varphi} \qquad (109)$$

But, since the slope of the curve is $y' = \cot \varphi$, it follows that,

$$\sin \varphi = (1 + y'^2)^{-\frac{1}{2}} \qquad (110)$$

Substituting Equation 110 into 109 and the result (along with Equation 108) into Equation 83 yields,

$$\frac{y'' N_\varphi}{(1 + y'^2)^{3/2}} - \frac{N_\theta}{(a + y)(1 + y'^2)^{\frac{1}{2}}} = 0$$

and, simplifying gives

$$N_\theta = (a + y) \frac{y''}{(1 + y'^2)} N_\varphi \qquad (111)$$

The meridian force is given from the statics of Figure 10 and by use of Equation 110,

$$2 \pi (a + y) N_\varphi \sin \varphi = Q$$

or

$$N_\varphi = \frac{Q}{2 \pi (a + y) \sin \varphi} = \frac{Q (1 + y'^2)^{\frac{1}{2}}}{2 \pi (a + y)} \qquad (112)$$

Substituting Equation 112 into Equation 111

$$N_\theta = \frac{Q}{2 \pi} y'' (1 + y'^2)^{-\frac{1}{2}} \qquad (113)$$

1. <u>The Constant Circumferential Stress, Anticlastic Surface</u>

The equation of the meridian that gives constant circumferential stress everywhere is determined by setting N_θ equal to a constant in Equation 113 and then solving the resulting differential equation.

Let

$$K = 2 \pi \frac{N_\theta}{Q} \qquad (114)$$

Then, Equation 113 becomes

$$y'' \left(1 + y'^2\right)^{-\frac{1}{2}} = K \tag{115}$$

But note that this equation is the same as,

$$\tfrac{1}{2} \left(1 + y'^2\right)^{-\frac{1}{2}} \frac{d\left(1 + y'^2\right)}{dy} = K \tag{116}$$

Integrating Equation 116,

$$\left(1 + y'^2\right)^{\frac{1}{2}} = K y + C_1$$

and,

$$y' = \frac{dy}{dx} = \sqrt{(K y + C_1)^2 - 1} \tag{117}$$

The equation of the meridian curve is given by performing the integration of Equation 117, e.g.

$$x = \int \frac{dy}{\sqrt{(K y + C_1)^2 - 1}} + C_2 \tag{118}$$

Let,

$$K y + C_1 = \cosh t, \qquad t = \cosh^{-1} (K y + C_1)$$

$$K\, dy = \sinh t\, dt, \qquad dy = 1/K \sinh t\, dt$$

Making these substitutions in Equation 118 and simplifying gives,

$$x = \int \frac{1}{K} \frac{\sin t \, dt}{\sqrt{\cosh^2 t - 1}} + C_2 = \int \frac{dt}{K} + C_2 \qquad (119)$$

The integral of Equation 119 simply gives

$$x = \frac{t}{K} + C_2 \qquad (120)$$

The desired equation of the meridian is finally given by substituting for t into Equation 120 and evaluating the two constants of integration from the two boundary conditions,

$$\left.\begin{aligned} &x = 0 \text{ at } y = 0 \\ \text{and,} \quad &x = H \text{ at } y = b - a \end{aligned}\right\} \qquad (121)$$

Then,

$$\left.\begin{aligned} x &= \frac{1}{K} \cosh^{-1} (K y + C_1) + C_2 \\ \text{or,} \quad y &= \frac{1}{K} \cosh [\, K (x - C_2) \,] - \frac{C_1}{K} \end{aligned}\right\} \qquad (122)$$

where,

$$\left.\begin{aligned} C_1 &= \cosh (-K C_2) = \cos h (K C_2) \\ C_2 &= \frac{H}{2} - \frac{1}{K} \sinh^{-1} \left[\frac{K (b - a)}{2 \sinh \left[\frac{K H}{2} \right]} \right] \end{aligned}\right\} \qquad (123)$$

$$K = 2\pi \frac{N_\theta}{Q} = 2\pi h \frac{f_\theta}{Q} \qquad (114)$$

The resulting meridian (or generating) curves are plotted in Figure 11 for various ratios of the axial load to circumferential (or hoop) stress. Figure 12 presents the corresponding meridian stresses (as determined from Equation 112).

2. <u>The Anticlastic Surface Formed by a Parabolic Meridian</u>

The general equation of a parabola is

$$y = A x^2 + B x + C \qquad (124)$$

Three boundary conditions are required. Since the curve must pass through the points $x = 0$, $y = 0$ and $x = H$, $y = b - a$, one easily obtains,

$$\text{and,} \quad \left.\begin{aligned} C &= 0 \\ AH + B &= \frac{b - a}{H} \end{aligned}\right\} \qquad (125)$$

The third condition is based upon a given required circumferential stress at the small base of the "conical frustum". That is, N_{θ_o} will be given.

Then, from Equation 113, this third boundary condition may be stated,

$$y'' (1 + y'^2)^{-\frac{1}{2}} = 2\pi \frac{N_{\theta_o}}{Q} = 2\pi h \frac{f_{\theta_o}}{Q} = K_o \qquad (126)$$

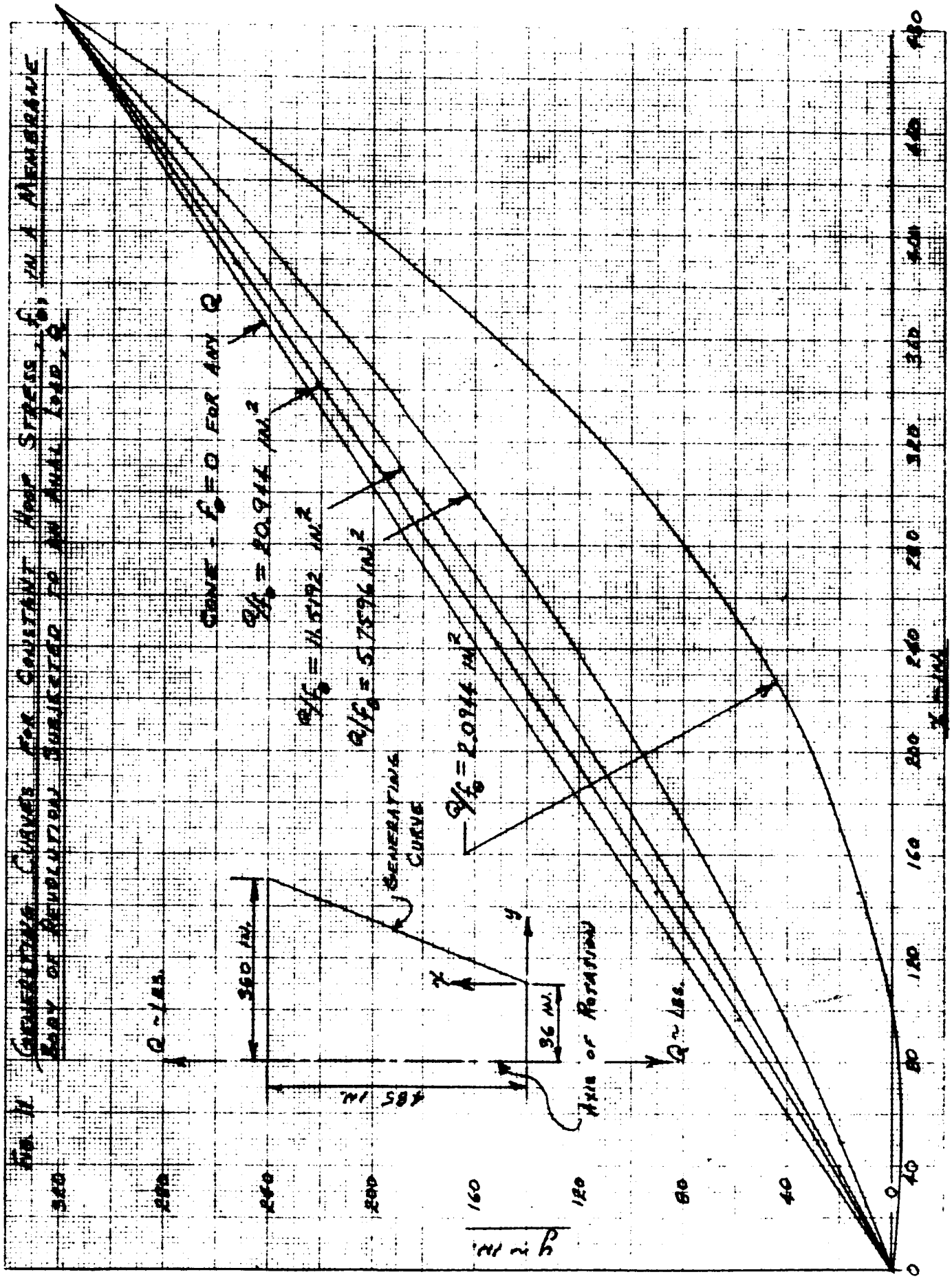
Fig. 11
Generating Curves for Constant Hoop Stress f_θ in a Membrane
Body of Revolution Subjected to an Axial Load Q
Curve - $f_\theta = 0$ for Any Q
$Q/f_\theta = 20.944$ in.^{2}
$Q/f_\theta = 14.5192$ in.^{2}
$Q/f_\theta = 5.75796$ in.^{2}
$Q/f_\theta = 2.0944$ in.^{2}
Generating Curve
Q ~ Lbs.
360 in.
58° in.
36 in.
Axis of Rotation
y in in.
x in in.

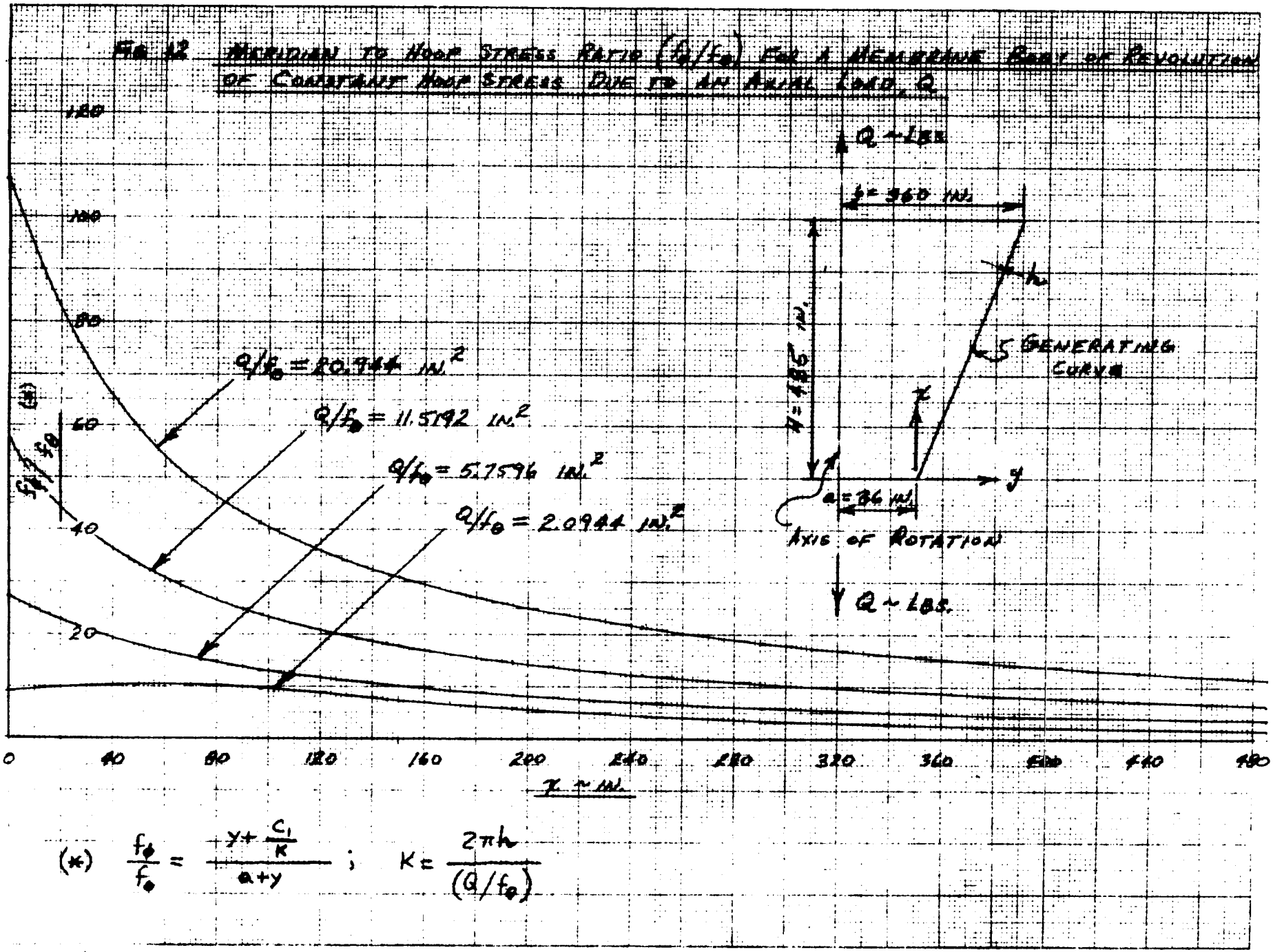

(*) $\frac{f_\phi}{f_\theta} = \frac{y + \frac{C_1}{K}}{a+y}$; $K = \frac{2\pi h}{(Q/f_\theta)}$

3ER-12114

The first and second derivatives of Equation 124 are

$$\left.\begin{aligned} y' &= 2A\,x + B \\ y'' &= 2A \end{aligned}\right\} \qquad (127)$$

Evaluating Equations 127 at $x = 0$ and substituting the result into Equation 126 yields

$$2A\,(1 + B^2)^{-\frac{1}{2}} = K_o \qquad (128)$$

When solving Equation 125 and 128 simultaneously for A and B, the following quadratic arises,

$$\left\{\left[\frac{2}{K_o}\right]^2 - H^2\right\} A^2 + 2\,(b - a)\,A - \left[\frac{b - a}{H}\right]^2 - 1 = 0 \qquad (129)$$

At this point, it is necessary to resort to numerical calculations. The geometric values for the example problem considered throughout this report were substituted into Equation 129 along with two different K_o values. Solution of Equation 129 revealed one positive and one negative root. Since the A coefficient corresponds to the slope of the meridian, it is easily seen from Figure 10 that the positive root is the only one of interest. Having thus determined A, B and C were then calculated from Equation 125 and substituted into Equation 124 to give the desired equations for the parabolic meridians. These are plotted in Figure 13. Figure 14 and 15 present the corresponding meridian and circumferential stresses as determined from Equations 127, 113 and 112.

FIG. 13 PARABOLIC GENERATING CURVES FOR MEMBRANE BODIES OF REVOLUTION SUBJECTED TO AXIAL LOAD, Q, FOR VARIOUS RATIOS OF Q TO THE HOOP STRESS AT THE ORIGIN, f_{θ_0}

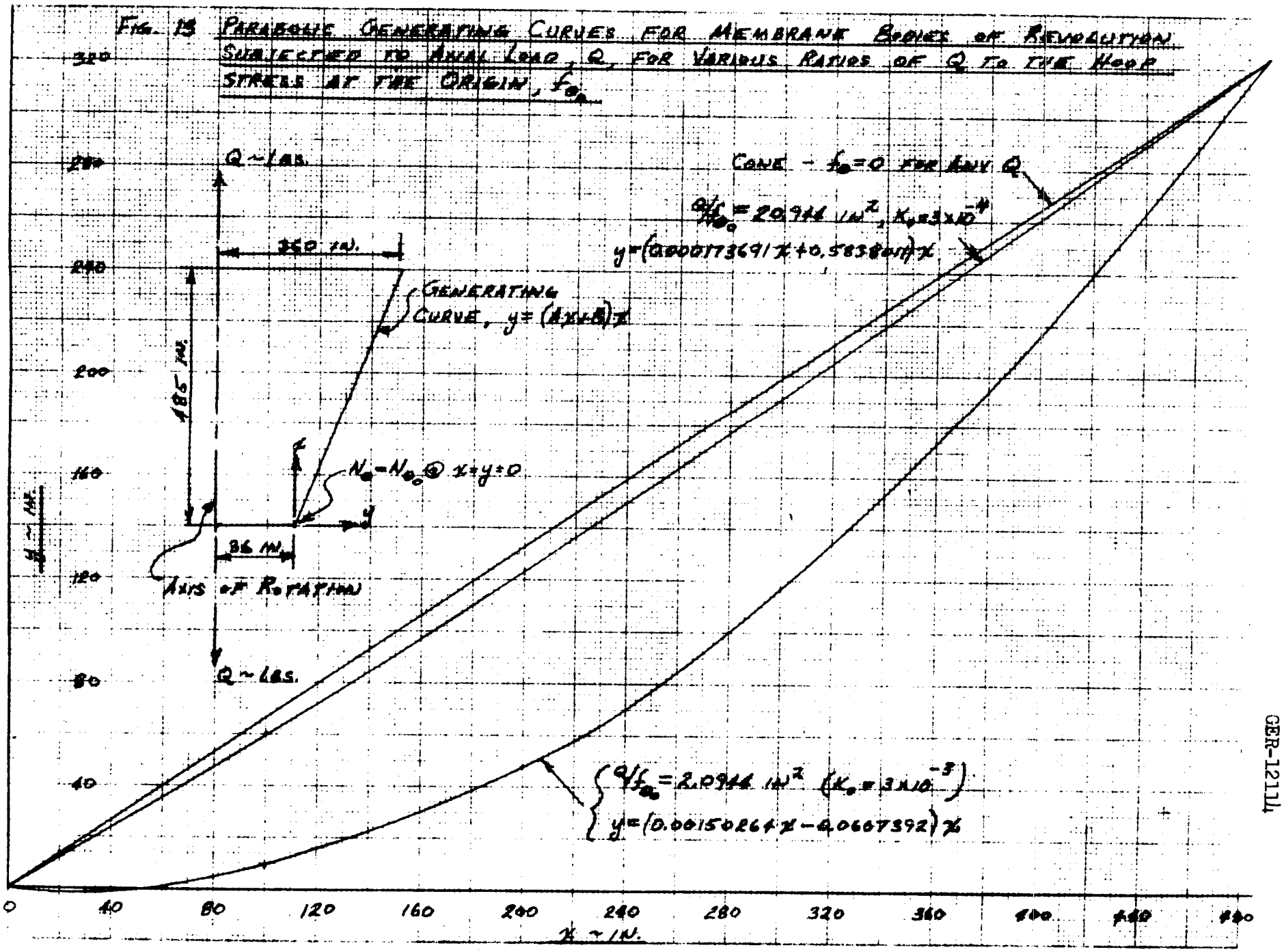

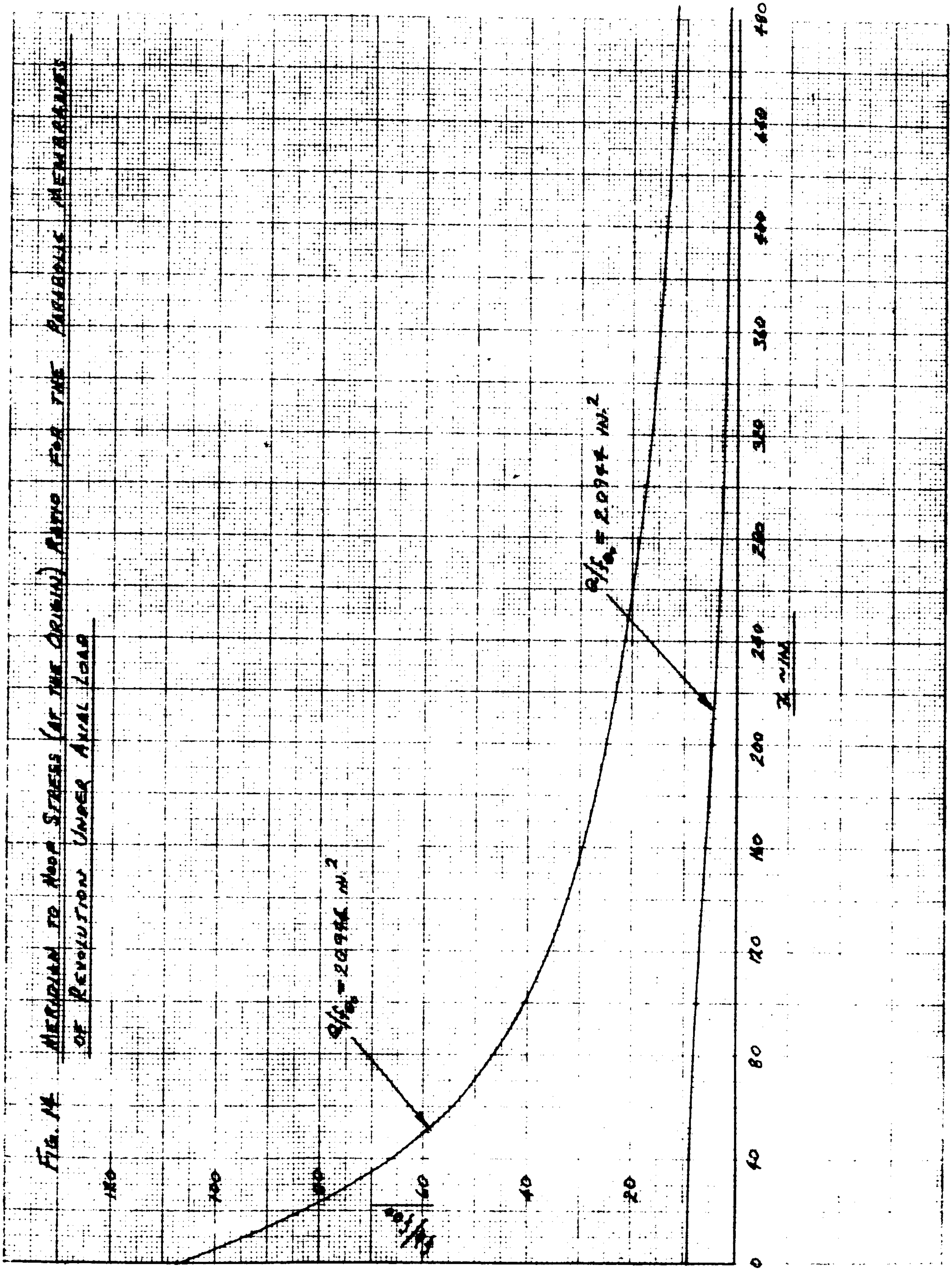

FIG. 14 MERIDIAN TO HOOP STRESS (AT THE ORIGIN) RATIO FOR THE PARABOLIC MEMBRANES OF REVOLUTION UNDER AXIAL LOAD

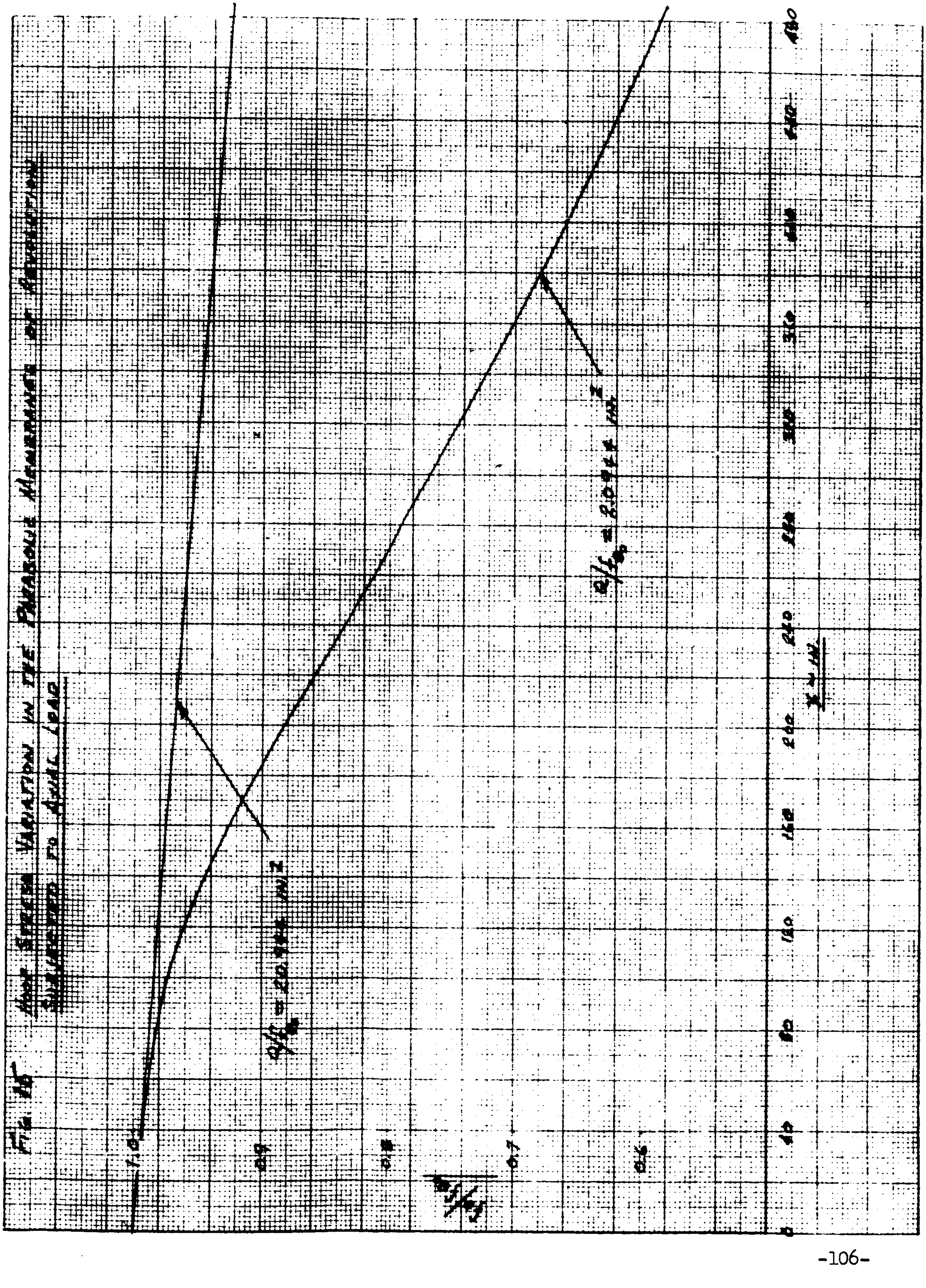
FIG.
HOOP STRESS VARIATION IN THE PARABOLIC MEMBRANES OF REVOLUTION
SUBJECTED TO AXIAL LOAD
1.0
0.9
0.8
0.7
0.6
0
40
80
120
240
Y ~ IN.

3. Design Examples

Comparisons of Figure 12 and 14 show there exist no large differences between the general shapes of the constant hoop stress and the parabolic meridian curves. They diverge with decreasing axial load to hoop stress ratios, but even for the lowest ratios considered, the meridians are very similar, the parabolic curve being slightly closer to the true cone. The meridian curves corresponding to a range of one order of magnitude in the axial load to hoop stress ratio have been presented in both figures. Although the lower boundary is unreasonably remote from the true cone, it has been included to show the shape that would be required for a combination of a 60 lb. axial load [as used in Reference 1] and a required circumferential stress of about 28 psi which corresponds to a surface irregularity of 0.09 inches as can be determined from Equation (91) for 1 mil Mylar film.

From optical considerations, an anticlastic surface that closely approximates a true cone is desired; one that is defined by the upper boundary [$Q/f_\theta = 20.944$] of Figures 12 and 14. However, to obtain a hoop stress of 28 psi, an excessive axial load of 600 lbs. would be required. This high load combined with the practical consideration of manufacturing a surface to the resulting close tolerances indicates only larger deviations from the cone are feasible.

As an example, consider the curve for $Q/f_\theta = 5.7597$ in.^{2} in Figure 12. For $f_\theta = 28$ psi, an axial load of approximately 162 lbs. or 2.7 times the originally proposed load of 60 lbs. is required. From a structural viewpoint this design would be feasible since the corresponding maximum meridian stress from Figure 13 is only 770 psi as compared to the Mylar yield strength of 11,000 psi. However, the strength of the ring as discussed in Section I-C would have to be increased.

E. Development of a Body of Revolution from an Initially Fabricated Body Having Bases that are Regular Polygons

The feasibility of generating a body of revolution of negative meridian curvature from an initially fabricated regular "pyramid-type" body by applying only axial force must be determined. This problem arises because the desired anticlastic surface is nondevelopable whereas the originally proposed cone was.

Consider the gored body with meridian seams of Figure 16. Any section cut by a plane normal to the axis of symmetry is a regular polygon of r sides. Feasibility is substantiated by proving that the polygon deforms to a circle under the application of axial load.

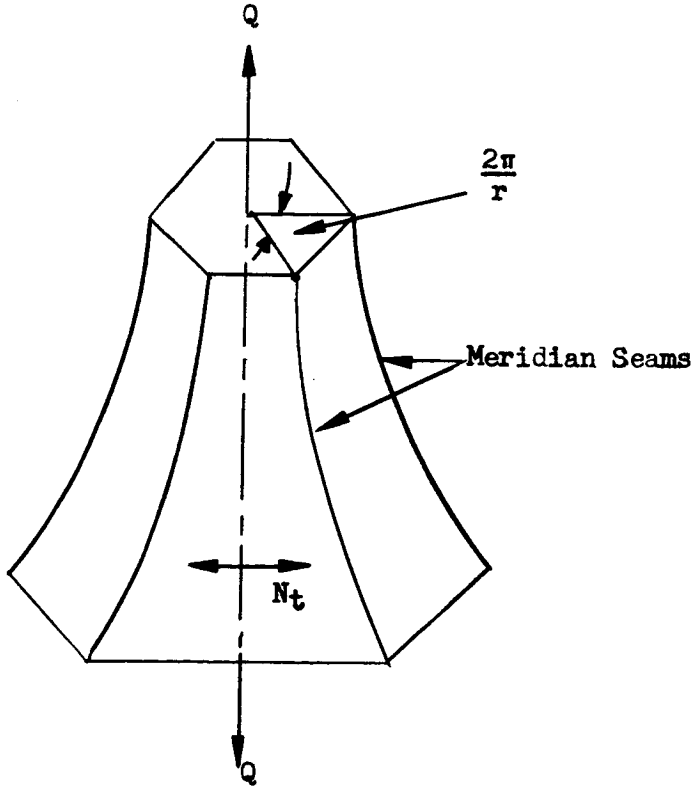

FIGURE 16 - Undeformed, Gored Body with Meridian Seams

The total axial load is resisted partly by the seams and partly by the gores,

$$Q = Q_s + Q_g \tag{130}$$

The tension force in any one seam at a point defined by the angle φ (see Figure 17 for example) is

$$T = \frac{Q_s}{r \sin \varphi} \tag{131}$$

Two simplifying assumptions are now made, 1) the meridian seam is closely approximated by a circular arc and 2) the membrane stress in the gore and normal to its centerline is assumed to be constant. The variation of this stress (denoted by N_t in Figure 16) is actually unknown but the assumption should be adequate for this feasibility study since it has been shown in Figure 15 that the hoop stress variation is small in the body of parabolic meridian that is "near" the cone.

A free body of a seam may now be described as shown in Figure 17. The x and y coordinates of a point on the seam are (from Figure 17),

$$\left.\begin{aligned} x &= \rho_{1_s} (\cos \varphi - \cos \varphi_a) \\ y &= \rho_{1_s} (\sin \varphi_a - \sin \varphi) \end{aligned}\right\} \tag{132}$$

From the static equilibrium in the horizontal direction of Figure 17,

$$T_b \cos \varphi_b - T_a \cos \varphi_a = 2 N_t \sin \frac{\pi}{r} \rho_{1_s} \int_{\varphi_b}^{\varphi_a} \sin \varphi \, d\varphi \tag{133}$$

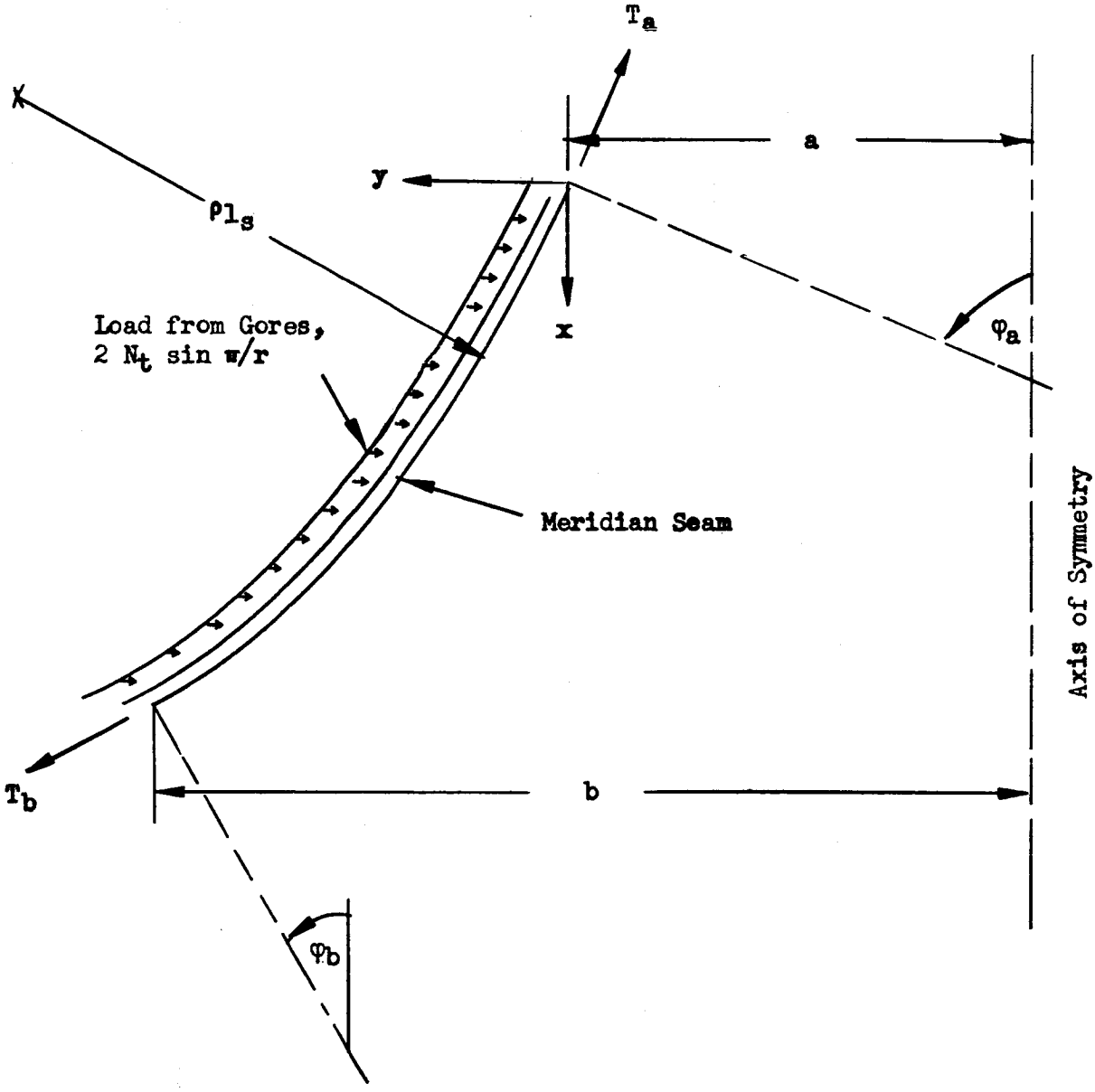

FIGURE 17 - Free Body of a Meridian Seam

Substituting for T_a and T_b from Equation 131 and integrating Equation 133 yields

$$\frac{Q_s}{r} (\cot \varphi_b - \cot \varphi_a) = 2 N_t \rho_{l_s} \sin \frac{\pi}{r} (\cos \varphi_b - \cos \varphi_a) \tag{134}$$

or,

$$N_t = \frac{Q_s j}{2 r \rho_{l_s} \sin \frac{\pi}{r}} \tag{135}$$

where,

$$j = \frac{\cot \varphi_b - \cot \varphi_a}{\cos \varphi_b - \cos \varphi_a} \tag{136}$$

The analysis is now limited to cases where the number of gores is sufficiently large so that the small angle approximation is valid, e.g.,

$$\sin \frac{\pi}{r} \approx \tan \frac{\pi}{r} \approx \frac{\pi}{r} \text{ and } \cos \frac{\pi}{r} \approx 1$$

Equation 135 then becomes

$$N_t = \frac{Q_s j}{2 \pi \rho_{l_s}} \tag{137}$$

Next, consider the stress-strain equations. Conservatively assume a uniaxial stress condition exists and the meridian strain in the seam is then

$$\varepsilon_{\varphi_s} = \frac{T}{(AE)_s} = \frac{Q_s}{r\,(AE)_s \sin\varphi} \tag{138}$$

The gore is subjected to biaxial stresses so that the stress-strain equations are given by dropping the terms containing T in Equations 50,

$$\left.\begin{aligned} \varepsilon_{\varphi_g} &= \frac{1}{(Eh)_g}\,(N_\varphi - \mu\, N_t) \\ \varepsilon_{t_g} &= \frac{1}{(Eh)_g}\,(N_t - \mu\, N_\varphi) \end{aligned}\right\} \tag{139}$$

Solving Equations 139 simultaneously for N_φ gives

$$N_\varphi = \frac{(Eh)_g}{1-\mu^2}\,(\varepsilon_{\varphi g} + \mu\,\varepsilon t_g) \tag{140}$$

Since the gores and seams are connected to rigid bases and must elongate the same amount, strain compatibility between gore and seam is assumed,

$$\varepsilon_{\varphi_s} = \varepsilon_{\varphi g} \tag{141}$$

This facilitates substituting Equation 138 into Equation 140 to yield

$$N_\varphi = \frac{1}{1-\mu^2}\left[\frac{Q_s\,(Eh)_g}{r\,(AE)_s \sin\varphi} + \mu\,N_t - \mu^2\,N_\varphi\right] \qquad (142)$$

and, solving for N_φ

$$N_\varphi = \left[\frac{Q_s}{\lambda\, r \sin\varphi} + \mu\,N_t\right] \qquad (143)$$

where

$$\lambda = \frac{(AE)_s}{(Eh)_g} \qquad (144)$$

Substituting for N_t from Equation 135 into Equation 143,

$$N_\varphi \approx \left[\frac{1}{\lambda\, r \sin\varphi} + \frac{\mu\, i}{2\,\pi\,\rho_{l_s}}\right] Q_s \qquad (145)$$

Another equation for N_φ is available from the static equilibrium of a gore in the direction parallel to the axis of symmetry.

$$N_\varphi = \frac{Q_g}{2\,\pi\,(a+y)\sin\varphi} \qquad (146)$$

Equating Equations 145 and 146,

$$Q_g = \left[\frac{2\,\pi\,(a+y)}{\lambda\, r} + \frac{\mu\, i}{\rho_{l_s}}(a+y)\sin\varphi\right] Q_s \qquad (147)$$

Substitute Equation 147 into Equation 130,

$$\frac{Q}{Q_s} = 1 + \left[\frac{2\pi}{\lambda r} + \frac{\mu j}{\rho l_s} \sin \varphi \right] (a + y)$$

and,

$$Q_s = \frac{\lambda r \rho l_s Q}{\lambda r \rho l_s + (2\pi \rho l_s + \mu j \lambda r \sin \varphi)(a + y)} \qquad (148)$$

Substituting Equation 148 into Equations 145 and 135

$$N_\varphi = \frac{(2\pi \rho l_s + \mu j \lambda r \sin \varphi) Q}{2\pi \lambda r \rho l_s \sin \varphi + (2\pi \rho l_s + \mu j \lambda r \sin \varphi)(2\pi)(a + y) \sin \varphi} \qquad (149)$$

$$N_t = \frac{j \lambda r Q}{2\pi \lambda r \rho l_s + (2\pi \rho l_s + \mu j \lambda r \sin \varphi)(2\pi)(a + y)} \qquad (150)$$

The membrane equation (Equation 83) may once again be applied; this time, to the gore.

$$\frac{N_\varphi}{\rho l_g} - \frac{N_t}{\rho 2_g} = 0 \qquad (151)$$

Substituting for N_φ and N_t from Equations 149 and 150 and simplifying

$$\rho_{2_g} = \frac{j\lambda r \sin\varphi}{2\pi \rho_{1_s} + \mu j \lambda r \sin\varphi} \rho_{1_g} \tag{152}$$

Next consider the deformation of one side of an original polygon on a plane normal to the axis of symmetry of the body (Figure 18). If this side (along with the others) is assumed to always be an arc of a circle during deformation, a strain displacement equation based on the original length plus the transverse strain and the arc length of the deformed side may be written, (see Figure 18)

$$(a + y)(1 + \varepsilon_t) \sin\frac{\pi}{r} = \left[\frac{\pi}{r} - \eta_\theta\right] R_\theta \tag{153}$$

If the parameter angle, φ, that defines the cut section is assumed to be essentially constant, the radius of the deformed circle, R_θ, may be related to the principal radius of curvature that is normal to the meridian plane (refer to Figure 10) by,

$$R_\theta = \rho_{2_g} \sin\varphi \tag{154}$$

Substituting Equation 152 into 154, the result into Equation 153 and solving for ε_t yields,

$$\varepsilon_t = \frac{j\lambda r \sin^2\varphi}{(a + y)(2\pi \rho_{1_s} + \mu j \lambda r \sin\varphi)} \left[1 - \frac{r\eta_\theta}{\pi}\right] \rho_{1_g} - 1 \tag{155}$$

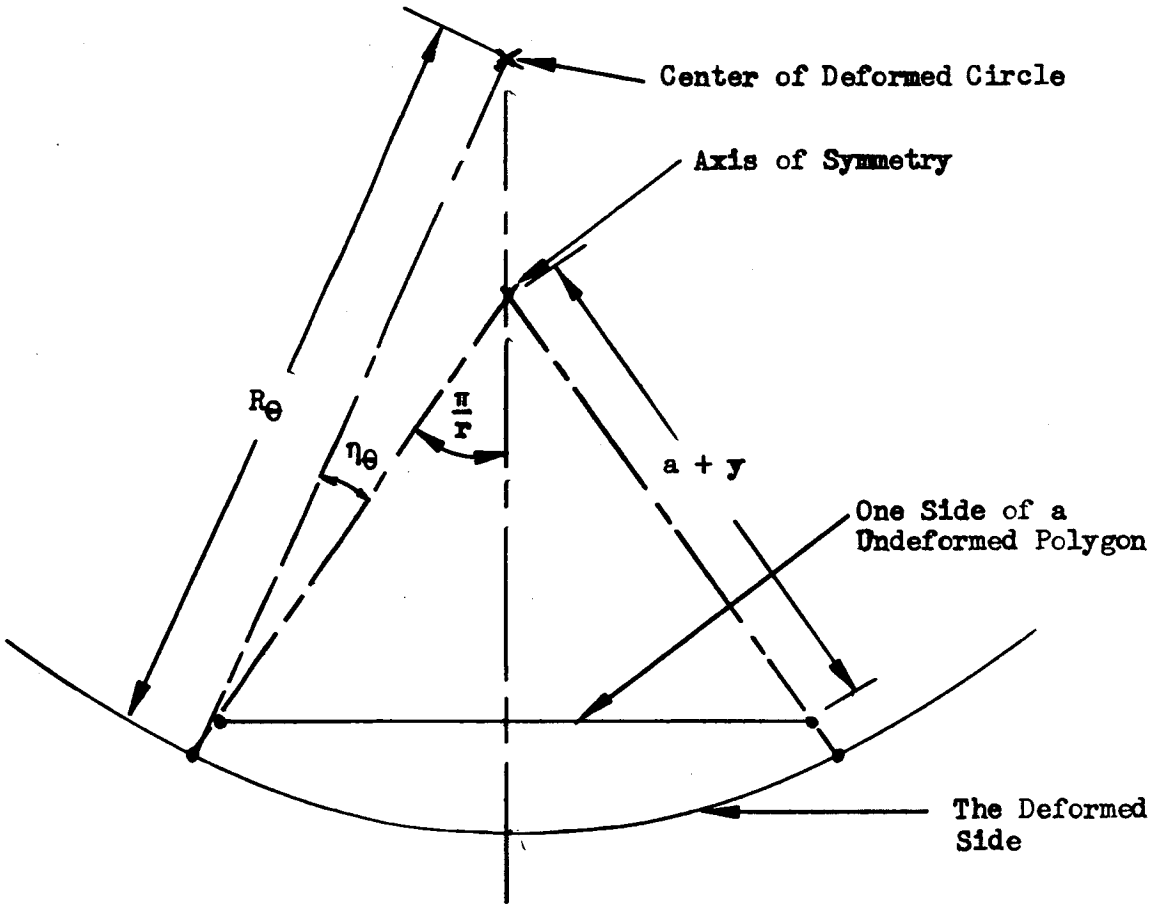

FIGURE 18 - Undeformed and Deformed Side of a Regular Polygon Cut by a Plane Normal to the Axis of Symmetry

The meridian radius of curvature of the gore cannot be constant, as implied above, even for the undeformed geometry since the seams have been chosen to be circular arcs. Therefore, an undeformed meridian through the gore lies on an ellipse. However, for the large number of gores that have already been specified, the differences between meridian radii of curvature at various locations on the gore and seams will be negligible. Considering the large meridian radii of curvature for these anticlastic surfaces that are "close" to a true cone and in keeping with the previously employed simplifying assumptions, discriminations between the gore and seam meridian radii of curvature in Equation 155 is considered to be unnecessary for purposes of this feasibility study.

Dropping the s and g subscripts in Equation 155 and setting this equal to the second of Equations 139 gives,

$$N_t - \mu N_\varphi = \frac{(Eh)_g \, j \lambda \, r \sin^2 \varphi}{(a + y)(2\pi \rho_1 + \mu \, j \lambda \, r \sin \varphi)} \left[1 - \frac{r \eta_\theta}{\pi} \right] \rho_1 - (Eh)_g \qquad (156)$$

But, N_t and N_φ are given by Equations 149 and 150, where the subscripts s and g are now dropped. If the substitutions for N_t and N_φ are made and the result simplified, the following cubic equation in r is obtained.

$$\frac{Q}{2\pi (Eh)_g \sin \varphi} = \frac{-\frac{\eta_\theta}{\pi} R r^3 + (R - S + T) r^2 + (U - V) r - W}{X r^2 + Y r - Z} \qquad (157)$$

where

$$
\left.
\begin{aligned}
R &= j\,\rho_{l_s}\,(\lambda \sin\varphi)^2\,[\,\rho_{l_s} + \mu\, j\,(a+y)\sin\varphi\,] \\
S &= \mu\, j\,\rho_l\,\lambda^2\,(a+y)\sin\varphi \\
T &= j\,\lambda\,(a+y)\,[2\,\eta_\theta\,\rho_{l_s}^2 - \mu^2\, j\,\lambda\,(a+y)]\sin^2\varphi \\
U &= 2\pi\,\lambda\,\rho_{l_s}{}^2\,(j\sin^2\varphi - 1)\,(a+y) \\
V &= (a+y)^2\,4\pi\,\mu\, j\,\lambda\,\rho_{l_s}\sin\varphi \\
W &= (a+y)^2\,(2\pi\,\rho_{l_s})^2 \\
X &= (a+y)\,\mu\,(1-\mu^2)\,(j\,\lambda\sin\varphi)^2 \\
Y &= (a+y)\,(1-2\,\mu^2)\,(2\pi\, j\,\lambda\,\rho_{l_s}\sin\varphi) \\
Z &= 4\,\mu\,(a+y)\,\pi^2\,\rho_{l_s}{}^2
\end{aligned}
\right\} \quad (158)
$$

For given values of Poisson's ratio, the gore and seam stiffness, the allowable reflective angle, η_θ, and the meridian radius of curvature, the required axial force to the number of gores relation at a particular cross-section may be determined from Equations 157 and 158.

1. A Design Example

Again consider the sample "cone" used throughout this report. However, to show the maximum effect of the axial load, the extreme case of the minimum radius of the circular meridian is considered. This minimum radius is taken as that of a circle that has its center in the plane of the small base of the "conical" frustum. It then follows that,

$$\rho_{1_s} = 679.323 \text{ in.}$$

$$\varphi_a = \frac{\pi}{2} \text{ and } j = \frac{1}{\sin \varphi_b} \text{ (See Equation 136)}$$

Since, the reflective angle, η_θ, is critical at the large base, the section $a + y = b$ is considered. Then,

$$a + y = 360 \text{ in. and } \varphi = \varphi_b = 51^\circ, 26.43 \text{ min.}$$

Furthermore, 1 mil Mylar gores with $\frac{1}{2}$ in. wide, 1 mil Mylar seams are taken so that,

$$\left.\begin{aligned} (Eh)_g &= 735 \text{ lbs/in} \\ (EA)_s &= 368 \text{ lbs} \end{aligned}\right\} \quad \lambda = \tfrac{1}{2} \text{ in.}$$

Substituting the above values along with $\mu = 0.3$ into Equations 158 gives

$$R = (0.782)(679.32)(0.25)[679.32 + (0.3)(360)] = 104.5 \times 10^3$$

$$S = (0.3)(679.32)\left[\frac{360}{4}\right] = 18.33 \times 10^3$$

$$T = (0.782)\left[\frac{360}{2}\right]\left\{2(679.32)^2 \eta_\theta - \left[\frac{0.09}{0.782}\right]\left[\frac{360}{2}\right]\right\}$$

$$= \left[407 \times 10^3 \frac{\eta_\theta}{\pi} - 2.915\right] 10^3$$

$$U = \pi (679.32)^2 [(0.782) - 1](360) = -113.7 \times 10^6$$

$$V = (360)^2 4\pi (0.3)\left(\tfrac{1}{2}\right)(679.32) = 166 \times 10^6$$

$$W = [2\pi (679.32)(360)]^2 = 2.36 \times 10^{12}$$

$$X = (360)(0.3)(0.91)\left(\tfrac{1}{4}\right) = 24.6$$

$$Y = (360)(0.82)\pi (679.32) = 630 \times 10^3$$

$$Z = 4(0.3)(360)\pi^2 (679.32)^2 = 1.96 \times 10^9$$

Substituting the above values into Equation 157, rearranging and simplifying, yields the cubic,

$$r^3 - \left[0.796 \frac{\pi}{\eta_\theta} + 3900 - 65.1 \times 10^{-9} Q \frac{\pi}{\eta_\theta}\right] r^2 + \frac{\pi}{\eta_\theta}\left[2680 + \right.$$

$$\left. + 1.67 \times 10^{-3} Q\right] r + \frac{\pi}{\eta_\theta}\left[22.6 \times 10^6 - 5.19 Q\right] = 0 \quad (159)$$

It is now obvious that only unreasonably high axial loads, Q, have any effects upon Equation 159. Even axial loads as high as a ton or more may be neglected. This analysis of the deformations of polygonal bodies under axial load has therefore been carried far enough to show that it is not feasible to generate the desired body of revolution by applying axial load to a shape made from flat gores.

The alternatives are then: (1) making an anticlastic surface of pre-formed double curvature gores, and (2) inducing circumferential stress by the application of circumferential stiffeners to the surface. The second approach is now being investigated experimentally.

CONCLUSIONS

The 60 foot diameter foldable ring of diamond cross-section as described in the design example of Section I is structurally adequate for a 60 lb axial load and the packaging and deployment loadings. The minimum factor of safety is 1.5 which occurs under the packaging loads and also under the out-of-plane buckling consideration if the maximum allowable pretensions in the cables are applied.

The results of Section II indicate the following conclusions:

1. The secondary circumferential stresses induced by the deflections of a membrane cone under axial load alone are far less than those required to reduce the residual wrinkles and creases to a satisfactory reflectivity level.

2. A smooth surface may be obtained by deviating from a true cone to a membrane of revolution of anticlastic curvature.

3. An anticlastic membrane of revolution cannot be obtained by applying only axial load to an initially fabricated body having bases that are regular polygons.

4. A solution to the problem of cone construction will be found only by using designs more complex than those considered in Section II.

Another method of fabricating a true cone that will have the required smooth surface under axial load only is presently being investigated experimentally. The concept is based upon the application of collapsible circumferential structural members distributed over the external surface of the cone. These members will provide the circumferential compressive and flexural stiffnesses required to restrain the compressive strains that induce wrinkles in an unstiffened membrane cone. The results of these investigations will be included in another report.

REFERENCES

1. Mandel, J. A. - "Structural Analysis of the Cone and Column Reflector Solar Concentrator", GER 11283, Goodyear Aerospace Corporation, Akron, Ohio, October 15, 1963.

2. Roark, R. J. - "Formulas for Stress and Strain", Third Edition, McGraw-Hill Book Company, Inc., New York, New York, 1954.

3. GAP 2687 - "Proposal for Development of Supporting Structure and the Design and Fabrication of a Five Foot Diameter Cone and Column Solar Concentrator Model", Goodyear Aerospace Corporation, Akron, Ohio, June 15, 1964.

4. Timoshenko, S. and Woinowsky, S. - "Theory of Plates and Shells", Second Edition, McGraw-Hill Book Co., New York, New York, 1959.

5. Sokolnikoff, I. S. - "Mathematical Theory of Elasticity", McGraw-Hill Book Co., New York, New York, 1956.

6. Clements, G. R. & Wilson, L. T. - "Manual of Mathematics and Mechanics", Second Edition, Second Impression, McGraw-Hill Book Co., Inc., New York, New York, 1947.

7. Tabakman, H. D. and Valentijn, H. P. - "Distortion of Circular Rings", Machine Design, October 22, 1964.

8. Timoshenko, S. and Gere, J. - "Theory of Elastici Stability", Second Edition, McGraw-Hill Book Co., New York, New York, 1961.

APPENDIX B

CONE AND COLUMN SOLAR CONCENTRATOR

THERMAL ANALYSIS PROGRAM

TABLE OF CONTENTS

LIST OF FIGURES

LIST OF TABLES

INTRODUCTION

The cone and column solar concentrator is thermally represented as shown in Figure 1. The basic dimensions those of a 60 foot diameter concentrator while the cone node locations are established primarily by the solar reflections from the column. Solar reflections from column node 14 strikes cone nodes 2 and 3, from column node 15 strikes cone nodes 4 and 5, from column node 16 strikes cone nodes 6, 7 and 8, while cone nodes 9, 10, 11, and 12 receive no specular solar reflections from the column. A temperature discontinuity may exist between nodes 8 and 9; the node sizes are adjusted in this area to better define this discontinuity. The concentrator may also be positioned with respect to a planet (Earth) as shown in Figure 2, so that the planet effects cause a circumferential variation in temperature in addition to the basic radial variation.

In order to reduce thermal deformations, it may be desirable to vary the thermal coatings over the cone external surface. These variations may occur radially but not circumferentially, since the concentrator is solar oriented but not planet oriented. For this reason the cone external thermal properties are included as input data for each node. Other input data (system variables) are the cone internal properties, the column properties, the properties of the base (internal and external),

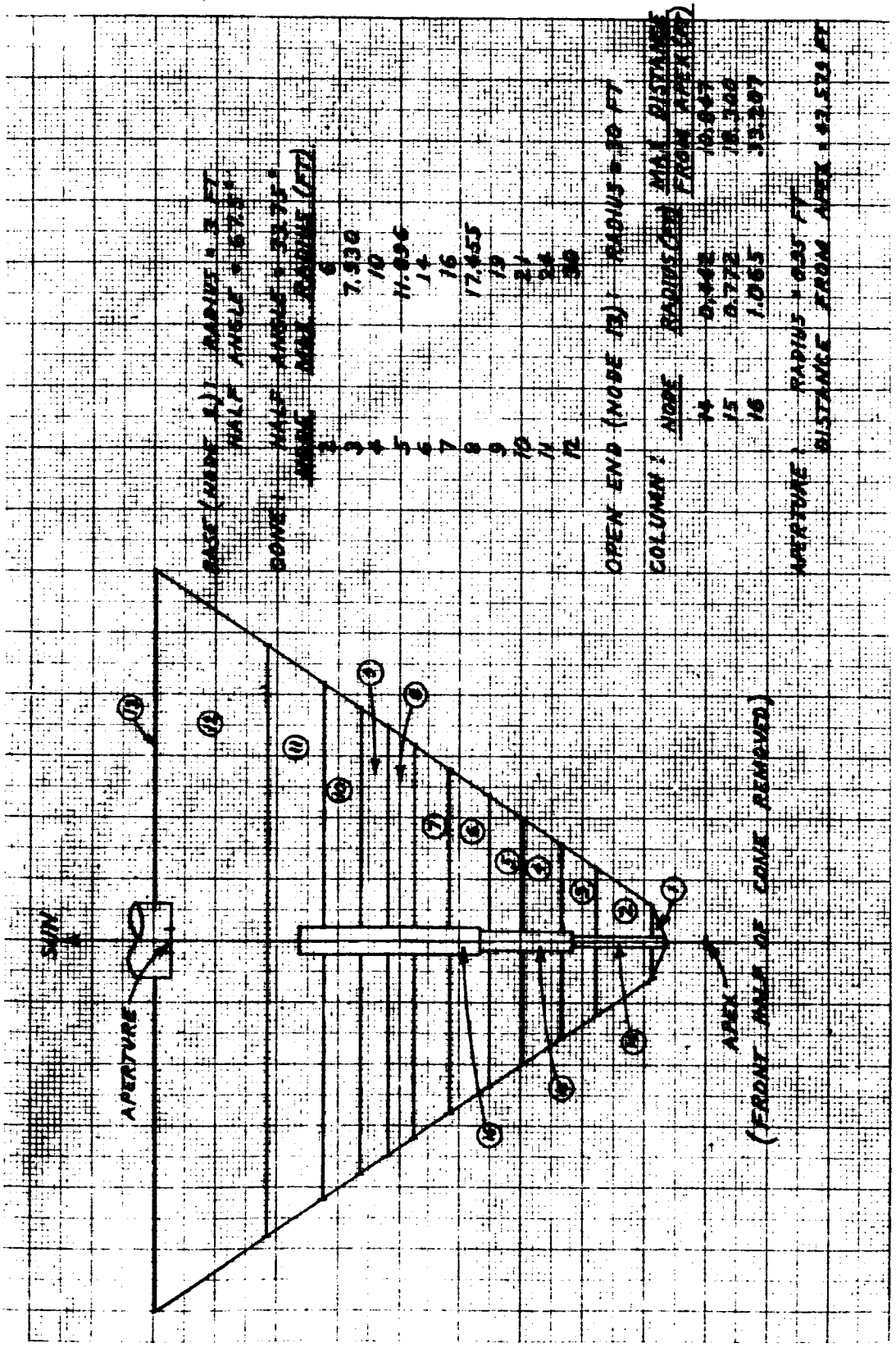

FIGURE 1. CONE AND COLUMN THERMAL SCHEMATIC

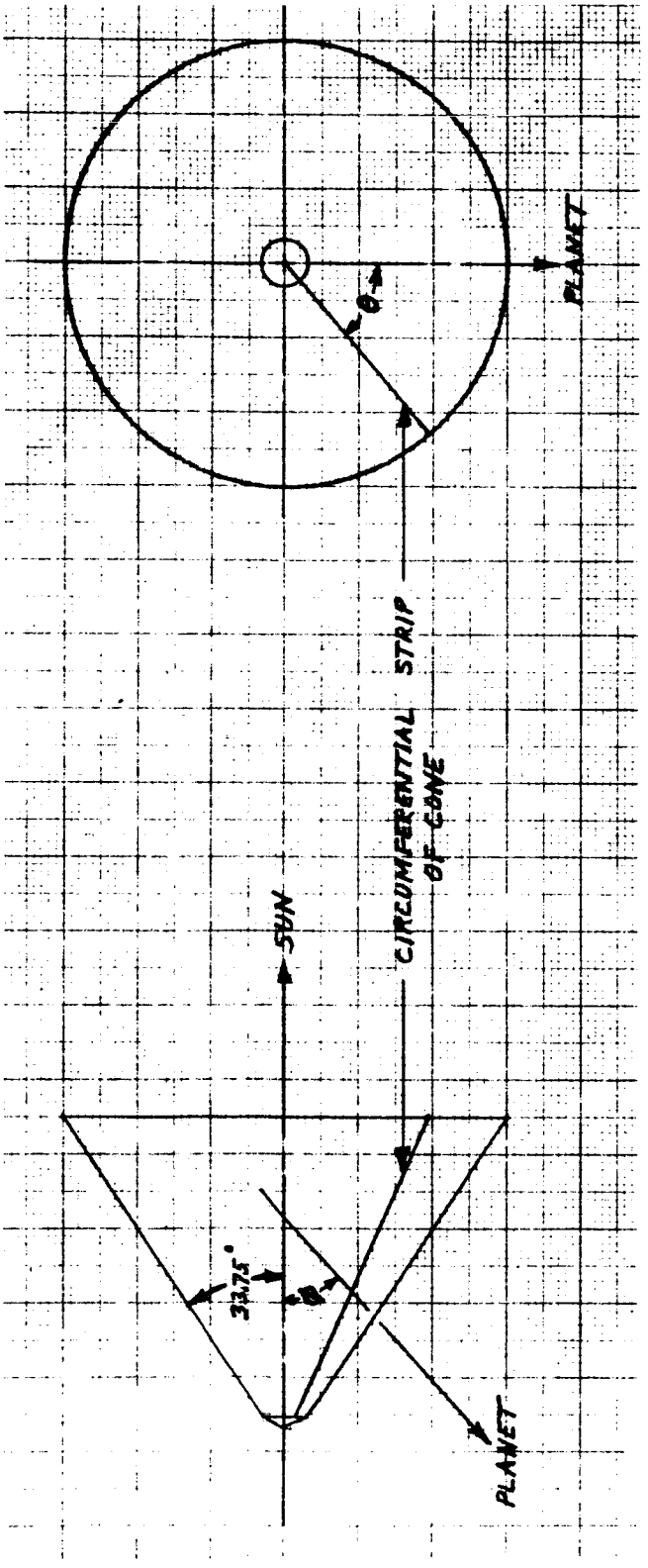

FIGURE 2. CONE AND COLUMN ORBITAL SCHEMATIC

the orbital altitude, and the position with respect to the earth-sun line. Planetary effects may be neglected if desired.

The method of attack is to compute the cone node temperatures neglecting circumferential variations, then refine each node temperature to account for circumferential variations. No transient effects will be included since the thermal response time of the cone is considerably smaller than the orbital period. Neglecting the transient effects of the column and other hard structure should result in a slightly conservative analysis.

The primary purpose of this report is to analyze cone temperatures. Column effects are therefore neglected wherever possible. An estimate of column temperatures is included, but does not attain the accuracy of the cone temperatures.

SYMBOLS

Symbol	Description	Units
A_n	Area of subscripted node or disk	ft^2
C	Solar constant (442.4)	$BTU/hr\text{-}ft^2$
F_{n-m}	Radiation view factor from first subscript node, disk, or point to second subscript node or disk	--
H_{n-m}	Distance between planes or points denoted by subscripts	ft
h	Dimensionless distance parameter	--
$\overline{h}$	Orbital altitude	miles
i,j,m,m',n,n'	Node, disk, or point numbers	--
K	Dimensionless orbital altitude parameter	--
P_n	Planetary view factor from subscripted node	--
P_θ	Planetary view factor at cone location θ	--
Q	Heat flux	BTU/hr
Q_n	Incident heat flux on subscripted node	BTU/hr
$\overline{Q}_n$	Diffusely reflected heat flux from subscripted node	BTU/hr
q_n	Absorbed heat flux of subscripted node	BTU/hr
R_a	Location solar ray initially strikes cone	ft
R_b	Location solar ray double reflected strikes cone	ft
R_c	Column radius	ft

SYMBOLS (Continued)

Symbol	Description	Units
R_n	Radius of subscripted circle	ft
R_p	Planet radius	miles
r	Dimensionless radius parameter	—
r_{cd}	Diffuse solar reflectance of cone internal surface	—
r_{cs}	Specular solar reflectance of cone internal surface	—
r_{pd}	Diffuse solar reflectance of column	—
r_{ps}	Specular solar reflectance of column	—
T_n	Temperature of subscripted node	°R
$T_{n\theta}$	Temperature of subscripted node at location θ	°R
X	Distance along axis from apex of cone	ft
α_i	Solar absorptance of cone internal surface	—
α_{li}	Solar absorptance of base internal surface	—
α_n	Solar absorptance of cone node n external surface	—
α_p	Solar absorptance of column	—
β	Angle between surface normal vector and surface-planet line	radians
ϵ_i	Emittance of cone internal surface	—

SYMBOLS (Continued)

Symbol	Description	Units
ϵ_{li}	Emittance of base internal surface	—
ϵ_n	Emittance of cone node n external surface	—
ϵ_p	Emittance of column	—
θ	Angle around cone from planet side	radians
λ	Rim angle of disk with respect to point	radians
σ	Stefan-Boltzmann constant (0.1714×10^{-8})	$BTU/hr\text{-}ft^2\text{-}°R^4$
ϕ	Angle of satellite from earth-sun line	radians

Subscripts

Symbol	Description
ap	Aperture
i,j,m,m',n,n'	Node, disk, or point number (general)
1 to 13	Node, disk, or point number as indicated
ma,mb,na,nb,nc	Location on node or corresponding disk
ne	External surface of node n
ni	Internal surface of node n
nr	Node n from all cone nodes
θ	Angle around cone from planet (general)
0°,15°,30°, ... 180°	Angle around cone from planet (general)

RADIATION VIEW FACTORS

A. System

Since heat transfer in the system occurs almost exclusively by radiation, the view factors within the system are required. A small portion of the cone diffuse radiation will strike the column, and this portion will be reflected or reemitted diffusely. For simplicity this column effect is neglected by presuming the view factor from the cone to the column node is zero. The column will, however, receive specular reflections from the cone of which a portion may be scattered diffusely, or absorbed and reemitted. To place this diffuse radiation back within the cone node system the view factors from the column to the cone nodes are required. Figure 1 is used throughout this section.

To evaluate the view factors between nodes 1 to 13, it is convenient to consider the plane areas bounded by the node boundaries. The symbol n' or m' will be used to denote the circular disk at the larger end of node n or m. These circular discs are opposed, so that the view factor between any two may be obtained from the Reference 1 expression:

$$F_{n'-m'} = \frac{1}{2}\left[\frac{h^2+1}{r^2} + 1 - \sqrt{\left(\frac{h^2+1}{r^2}+1\right)^2 - \frac{4}{r^2}}\right] \quad (1)$$

where:

$$r = R_{n'} / R_{m'}$$

$$h = H_{n'-m'} / R_{m'} \qquad (1a)$$

The view factor from any circular disk to any node is then:

$$F_{n'-m'} = F_{n'-m'} - F_{n'-(m-1)'} \qquad (m \leq n)$$

$$F_{n'-m} = F_{n'-(m-1)'} - F_{n'-m'} \qquad (m > n) \qquad (2)$$

The view factor from any node to any circular disk is:

$$F_{n-m'} = F_{m'-n} A_{m'} / A_n \qquad (3)$$

The view factor between any two nodes is then:

$$F_{n-m} = F_{n-(m-1)'} - F_{n-m'} \qquad (m > n)$$

$$F_{n-m} = 1 - F_{n-(m-1)'} - F_{n-m'} \qquad (m = n)$$

$$F_{n-m} = F_{n-m'} - F_{n-(m-1)'} \qquad (m < n) \qquad (4)$$

Table I presents the values of these view factors.

TABLE I

SYSTEM RADIATION VIEW FACTORS

m	1	2	3	4	5	6	7	8	9	10	11	12	13
A_m (ft^2)	30.76	152.68	152.03	209.88	234.75	308.10	339.28	275.25	318.49	452.38	763.39	1832.1	2827.4
n	F_{n-m}												
1	0.0808	0.3652	0.0789	0.0467	0.0267	0.0202	0.0138	0.0078	0.0068	0.0073	0.0084	0.0115	0.3259
2	0.0736	0.2973	0.1301	0.0828	0.0483	0.0363	0.0244	0.0137	0.0119	0.0125	0.0143	0.0190	0.2358
3	0.0160	0.1307	0.1512	0.1252	0.0783	0.0610	0.0416	0.0235	0.0204	0.0213	0.0243	0.0320	0.2745
4	0.0068	0.0602	0.0910	0.1288	0.0972	0.0796	0.0562	0.0323	0.0283	0.0297	0.0340	0.0448	0.3111
5	0.0035	0.0314	0.0507	0.0869	0.0994	0.0932	0.0684	0.0402	0.0358	0.0380	0.0440	0.0584	0.3501
6	0.0020	0.0180	0.0301	0.0543	0.0710	0.0937	0.0774	0.0467	0.0424	0.0457	0.0538	0.0726	0.3923
7	0.0012	0.0110	0.0187	0.0348	0.0473	0.0703	0.0780	0.0515	0.0476	0.0524	0.0629	0.0867	0.4376
8	0.0009	0.0076	0.0130	0.0246	0.0343	0.0523	0.0635	0.0520	0.0508	0.0569	0.0695	0.0978	0.4768
9	0.0007	0.0057	0.0098	0.0187	0.0264	0.0410	0.0507	0.0439	0.0507	0.0598	0.0742	0.1067	0.5117
10	0.0005	0.0042	0.0072	0.0138	0.0197	0.0311	0.0393	0.0346	0.0421	0.0594	0.0787	0.1160	0.5534
11	0.0003	0.0029	0.0048	0.0094	0.0135	0.0217	0.0279	0.0250	0.0310	0.0467	0.0780	0.1266	0.6122
12	0.0002	0.0016	0.0027	0.0051	0.0075	0.0122	0.0161	0.0147	0.0186	0.0286	0.0527	0.1245	0.7155
13	0.0036	0.0127	0.0148	0.0231	0.0291	0.0428	0.0525	0.0464	0.0576	0.0885	0.1653	0.4636	0.0000
14	0.1973	0.4616	0.1325	0.0640	0.0293	0.0186	0.0110	0.0057	0.0047	0.0047	0.0051	0.0064	0.0591
15	0.0066	0.1201	0.1901	0.2063	0.1336	0.0921	0.0533	0.0262	0.0206	0.0194	0.0196	0.0222	0.0899
16	0.0008	0.0115	0.0292	0.0659	0.0910	0.1216	0.1163	0.0759	0.0694	0.0724	0.0780	0.0872	0.1808

$A_{14} = 20.70\ ft^2$, $A_{15} = 36.15\ ft^2$, $A_{16} = 99.75\ ft^2$

To evaluate the view factors from the column nodes to the cone nodes, the column radius is neglected and the circular disk concept defined above is again used. Three points on each column node n will be considered, i.e. the ends of the node and the center denoted as n a, n b, and n c respectively. The view factor from any column point i to any circular disk m' is:

$$F_{i-m'} = (\lambda - \sin\lambda \cos\lambda) / \pi \qquad (5)$$

where:

$$\tan\lambda = R_m / H_{i-m'} \qquad (5a)$$

The view factor from any column point i to any cone node m is then:

$$F_{i-m} = F_{i-(m-1)'} - F_{i-m'} \qquad \text{(pt on apex side of disks)}$$

$$F_{i-m} = 1 - F_{i-m'} - F_{i-(m-1)'} \qquad \text{(pt bracketed by disks)}$$

$$F_{i-m} = F_{i-m'} - F_{i-(m-1)'} \qquad \text{(disks on apex side of pt)} \qquad (6)$$

The view factor from a column node n to a cone node m is taken as a weighted average of the view factors from points n a, n b, and n c to the cone node m:

$$F_{n-m} = \frac{1}{6} F_{na-m} + \frac{1}{6} F_{nb-m} + \frac{4}{6} F_{nc-m} \qquad (7)$$

Table I also presents the values of these view factors.

B. Planetary

The view factor of the planet will be required to evaluate planet effects on the system temperatures. Figure 2 is used for this analysis. Let θ be the circumferential angle of a cone strip or line from the side of the cone facing the planet, and let ϕ be the angle of the satellite about the planet from the planet-sun line. An angle β may then be defined as the angle between the normal vector to the external surface of the cone strip and the concentrator-planet vector. Then:

$$\cos\beta = \cos 33.75^\circ \sin\phi \cos\theta + \sin 33.75^\circ \cos\phi \qquad (0 \leq \beta \leq \pi) \qquad (8)$$

A dimensionless altitude factor K is defined as:

$$K = R_p / (R_p + \bar{h}) \qquad (9)$$

The planetary view factor is then:

$$P_\theta = K^2 \cos\beta \qquad (0 \leq \beta \leq \cos^{-1} K)$$

$$P_\theta = K^2 \cos\beta \left[1 - \pi^{-1} \sin^{-1}\left(\sqrt{K^2 - \cos^2\beta} \,/\, K \sin\beta\right)\right] + \pi^{-1} \sin^{-1}\left(\sqrt{K^2 - \cos^2\beta} \,/\, \sin\beta\right) - \pi^{-1}\sqrt{(K^2 - \cos^2\beta)(1 - K^2)} \qquad (\cos^{-1} K \leq \beta \leq \pi/2)$$

$$P_\theta = K^2 \cos\beta \; \pi^{-1} \sin^{-1}\left(\sqrt{K^2 - \cos^2\beta} \; / \; K \sin\beta\right)$$

$$+ \pi^{-1} \sin^{-1}\left(\sqrt{K^2 - \cos^2\beta} \; / \; \sin\beta\right)$$

$$- \pi^{-1} \sqrt{(K^2 - \cos^2\beta)(1 - K^2)} \qquad (\pi/2 \leq \beta \leq \cos^{-1}(-K))$$

$$P_\theta = 0 \qquad (\cos^{-1}(-K) \leq \beta \leq \pi) \qquad (10)$$

P_θ is evaluated for values of θ of 0° to 180° at 15° increments. The view factor from any cone node (nodes 2 to 12) to the planet is taken as a weighted average of the 13 values of P_θ:

$$P_n = (3/8\, P_{0°} + 7/6\, P_{15°} + 23/24\, P_{30°} + P_{45°} + P_{60°}$$

$$+ P_{75°} + P_{90°} + P_{105°} + P_{120°} + P_{135°} + 23/24\, P_{150°}$$

$$+ 7/6\, P_{165°} + 3/8\, P_{180°}) / 12 \qquad (11)$$

The view factor from the base (node 1) to the planet is similarly computed, utilizing the half angle 67.5° in lieu of 33.75° in equation (8). The view factor from the open end (node 13) to the planet may also be computed from equation (10) using the expression:

$$\beta = \pi - \phi \qquad (12)$$

Planetary view factors from all system external node surfaces have now been obtained. These factors are a function of the orbital altitude $\bar{h}$ and the angle about the planet ϕ. Local values about the cone have also been obtained.

RADIATION FLUXES

A. Solar

Solar radiation will enter the open end of the cone, strike and be reflected from the cone, column, and cone before entering the aperture. This sequence is shown graphically in Figure 3. The direct solar flux which strikes the open end (node 13) is denoted as Q:

$$Q = C A_{13} \tag{13}$$

The direct solar flux Q_n which strikes each cone node n may be expressed in terms of its maximum radius R_n and minimum radius R_m:

$$Q_n = Q (R_n^2 - R_m^2) / R_{13}^2 \qquad (2 \leq n \leq 12) \tag{14}$$

The receiver structure is presumed to have a radius of 3 ft and shadow node 1 so that $Q_1 = 0$. The portion of this flux absorbed by each node is:

$$q_n = Q_n \alpha_i \qquad (2 \leq n \leq 12) \tag{15}$$

A portion of the flux Q_n will be reflected diffusely:

$$\overline{Q}_n = Q_n r_{cd} \qquad (2 \leq n \leq 12) \tag{16}$$

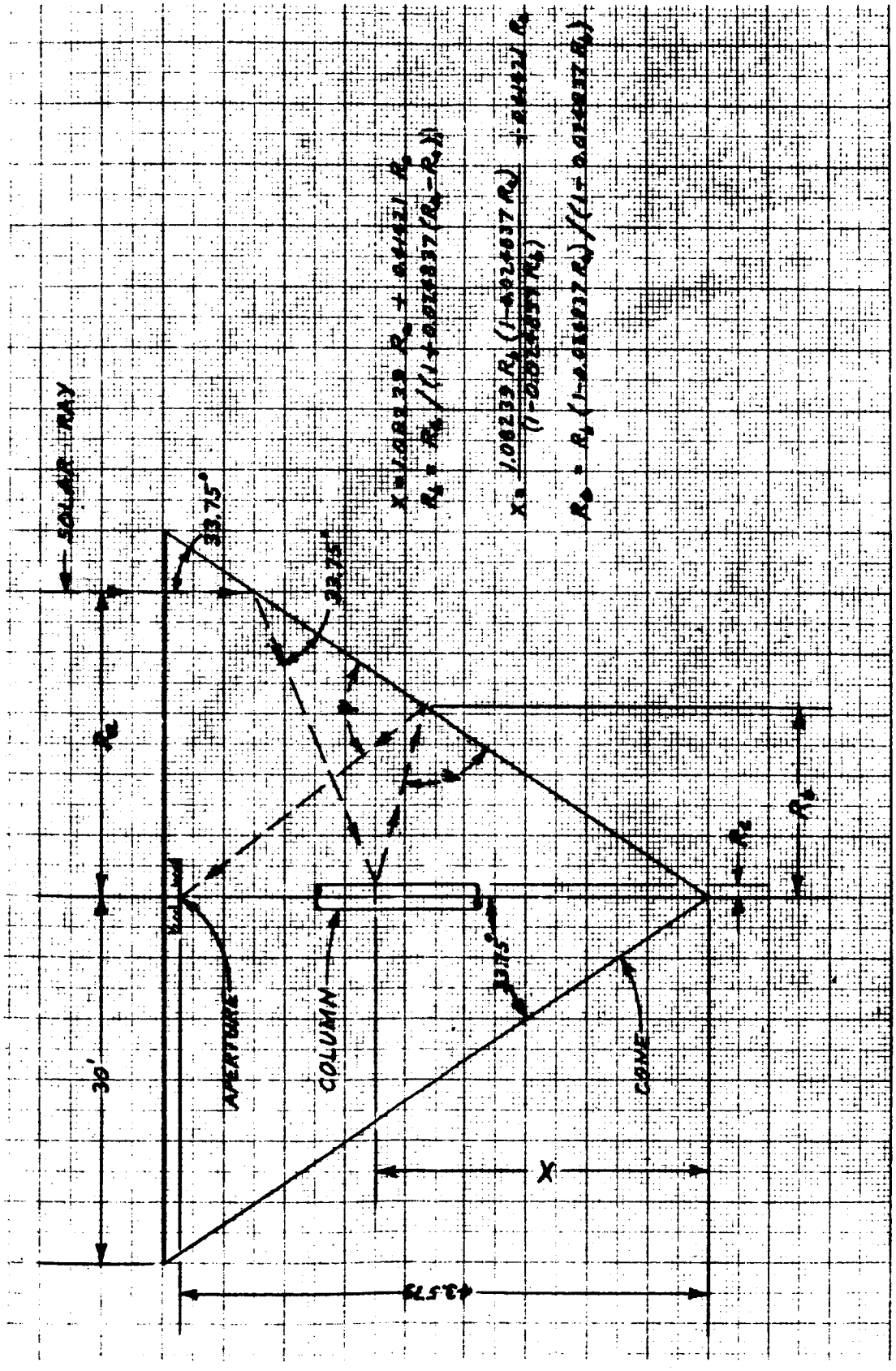

FIGURE 3. SPECULAR REFLECTION SCHEMATIC

These diffuse reflections will bounce around the cone and eventually be absorbed by nodes 1 to 12 or pass through the open end (node 13). Presuming that further reflections of these diffuse reflections are also diffuse, the Reference 2 technique may be used to determine the value of these absorbed fluxes for each node.

The specular reflections from nodes 2 to 12 will strike the column nodes 14 to 16. A column node has a maximum and minimum value of x which corresponds to values of R_a per Figure 3 and denoted as R_{na} and R_{ma} respectively. The reflected solar flux which strikes each node n is:

$$Q_n = Q\, r_{cs} \left(R_{na}^2 - R_{ma}^2\right) / R_{13}^2 \qquad (14 \leq n \leq 16) \qquad (17)$$

The portion of this flux absorbed by each node is:

$$q_n = Q_n \alpha_p \qquad (14 \leq n \leq 16) \qquad (18)$$

The portion reflected diffusely is:

$$\bar{Q}_n = Q_n\, r_{pd} \qquad (14 \leq n \leq 16) \qquad (19)$$

A portion of these diffuse reflections will strike the cone nodes (nodes 1 to 12). The quantity of this flux which strikes each node is:

$$Q_n = \sum_{j=14}^{16} \bar{Q}_j\, F_{j-n} \qquad (1 \leq n \leq 12) \qquad (20)$$

The portion of this flux absorbed by each node is:

$$q_n = Q_n \alpha_i \qquad (2 \leq n \leq 12)$$

$$q_1 = Q_1 \alpha_{1i} \qquad (21)$$

Presuming all reflections of diffuse incident radiation are diffuse, the reflected values are:

$$\overline{Q}_n = Q_n (1 - \alpha_i) \qquad (2 \leq n \leq 12)$$

$$\overline{Q}_1 = Q_1 (1 - \alpha_{1i}) \qquad (22)$$

The reference 2 technique is again used to evaluate these reflections.

The specular reflections from nodes 14 to 16 will strike the cone nodes 1 to 8. Each of these nodes has a maximum and minimum radius (R_b of Figure 3) which corresponds to values of R_a per Figure 3, the latter denoted as R_{na} and R_{ma} respectively (for node 1, R_{ma} is 3 due to shadowing). The double reflected solar flux which strikes each node n is:

$$Q_n = Q\, r_{cs}\, r_{ps}\, (R_{na}^2 - R_{ma}^2) / R_{13}^2 \qquad (1 \leq n \leq 8)$$

$$Q_n = 0 \qquad (9 \leq n \leq 12) \qquad (23)$$

The absorbed portions are again:

$$q_n = Q_n \alpha_i \qquad (2 \leq n \leq 8)$$

$$q_1 = Q_1 \alpha_{1i} \qquad (24)$$

The diffusely reflected portions, presuming node 1 to be a diffuse reflector, are:

$$\overline{Q}_n = Q_n r_{cd} \qquad (2 \leq n \leq 8)$$

$$\overline{Q}_1 = Q_1 (1 - \alpha_{1i}) \qquad (25)$$

The Reference 2 technique is again used to handle these reflections.

The triple specular reflections from nodes 2 to 8 then proceed to the aperture.

B. Aperture Reradiation

A portion of the solar energy which enters the aperture is reradiated. Presuming 20% reradiation and 10% shadow losses, the flux from the aperture to the cone is:

$$Q = 0.2 \times 0.9\ C\ A_{13}\ r_{cs}\ r_{ps}\ r_{cs} \tag{26}$$

The distribution of this radiation on the cone nodes may be obtained from the radiation view factors from the aperture to the cone nodes. Let R_n and R_m denote the maximum and minimum radius of node n, and H_{ap-n} and H_{ap-m} denote the axial distance between the aperture and the node boundaries while considering the aperture as a relatively small disk. Then:

$$Q_n = Q \left[1 / (1 + H_{ap-n}^2/R_n^2) - 1 / (1 + H_{ap-m}^2/R_m^2) \right]$$

$$(2 \leq n \leq 11)$$

$$Q_{12} = Q \left[1 - 1/ (1 + H_{ap-m}^2/R_m^2) \right] \tag{27}$$

Due to the high aperture temperature, the wavelengths of this radiation is between that of solar radiation and the infrared radiation emitted by the cone, column, and planet. For simplicity, this radiation is presumed to be 50% solar and 50% infrared. The absorbed portion of this flux is:

$$q_n = Q_n (\alpha_i + \epsilon_i) /2 \qquad (2 \leq n \leq 12) \qquad (28)$$

All infrared radiation is presumed to be reflected diffusely, so that the diffuse reflections are:

$$\bar{Q}_n = Q_n (r_{cd} + (1 - \epsilon_i))/2 \qquad (2 \leq n \leq 12) \qquad (29)$$

The Reference 2 techniques is used on these reflections.

The specular reflections from nodes 2 to 8 will strike the column nodes 14 to 16, while the specular reflections from nodes 9 to 12 escape out the open end. Each column node has a maximum and minimum value of X which corresponds to values of R_b per Figure 3 denoted as R_{nb} and R_{mb} respectively. The reflected aperture flux which strikes each node n is:

$$Q_n = Q\, r_{cs} \left[1/(1 + H_{ap-nb}^2/R_{nb}^2) - 1/(1 + H_{ap-mb}^2/R_{mb}^2)\right] / 2$$

$$(14 \leq n \leq 16) \qquad (30)$$

The absorbed portion of this flux is:

$$q_n = Q_n \alpha_p \qquad (14 \leq n \leq 16) \qquad (31)$$

The diffusely reflected portion of this flux is:

$$\bar{Q}_n = Q_n r_{pd} \qquad (14 \leq n \leq 16) \qquad (32)$$

The value of this diffusely reflected radiation which strikes each cone node is:

$$Q_n = \sum_{j=14}^{16} \overline{Q}_j F_{j-n} \qquad (1 \leq n \leq 12) \qquad (33)$$

The absorbed value of this flux is:

$$q_n = Q_n \alpha_i \qquad (2 \leq n \leq 12)$$

$$q_1 = Q_1 \alpha_{1i} \qquad (34)$$

Presuming all reflections of diffuse incident radiation are diffuse, the reflected values are:

$$\overline{Q}_n = Q_n (1 - \alpha_i) \qquad (2 \leq n \leq 12)$$

$$\overline{Q}_1 = Q_1 (1 - \alpha_{1i}) \qquad (35)$$

The Reference 2 technique is then used on these reflections.

The specular reflections from nodes 14 to 16 will strike the cone nodes 2 to 12. Each of these nodes has a maximum and minimum radius (R_a of Figure 3) which corresponds to values of R_b of Figure 3, the latter denoted as R_{nb} and R_{mb} respectively. The double reflected aperture radiation which strikes each node n is:

$$Q_n = Q\, r_{cs}\, r_{ps} \left[1/(1 + H_{ap\text{-}nb}{}^2/R_{nb}{}^2) - 1/(1 + H_{ap\text{-}mb}{}^2/R_{mb}{}^2) \right] /2 \qquad (2 \leq n \leq 12) \qquad (36)$$

The absorbed portion of this flux is:

$$q_n = Q_n\, \alpha_i \qquad (2 \leq n \leq 12) \qquad (37)$$

The diffusely reflected portion of this flux is:

$$\bar{Q}_n = Q_n\, r_{cd} \qquad (2 \leq n \leq 12) \qquad (38)$$

which is again handled by the Reference 2 technique. The specular reflections escape through the open end.

C. Planetary

Planetary emitted infrared radiation may strike the external node surfaces and enter the open end to strike the internal node surfaces. The absorbed radiation on the external surfaces is:

$$q_n = 0.16\ C\ A_n\ P_n\ \epsilon_n \qquad (1 \leq n \leq 12) \qquad (39)$$

The radiation which enters the open end (node 13) is presumed to be distributed internally according to the view factors from node 13 to the individual nodes. The direct planetary flux striking each node is then:

$$Q_n = 0.16\ C\ A_{13}\ P_{13}\ F_{13-n} \qquad (1 \leq n \leq 12) \qquad (40)$$

The absorbed portion is:

$$q_n = Q_n\ \epsilon_i \qquad (2 \leq n \leq 12)$$

$$Q_1 = Q_1\ \epsilon_{1i} \qquad (41)$$

The reflected portion is:

$$\bar{Q}_n = Q_n\ (1 - \epsilon_i) \qquad (2 \leq n \leq 12)$$

$$\bar{Q}_1 = Q_1\ (1 - \epsilon_{1i}) \qquad (42)$$

The reference 2 technique is used on these reflections.

D. Albedo

The albedo (planet reflected solar) radiation analysis is very similar to the planetary radiation analysis. This flux varies around the planet as a function of the angle ϕ. For low orbits, which are the most severe case, the angle dependence approaches a cosine relationship; the absorbed radiation on the external surfaces becomes:

$$q_n = 0.36\ C\ A_n\ P_n\ \alpha_n \cos\phi \qquad (0 \leq \phi \leq \pi/2)\ (1 \leq n \leq 12)$$

$$q_n = 0 \qquad (\pi/2 \leq \phi \leq \pi) \qquad (43)$$

The direct albedo flux striking the internal surfaces becomes:

$$Q_n = 0.36\ C\ A_{13}\ P_{13}\ F_{13-n} \cos\phi \qquad (0 \leq \phi \leq \pi/2)\ (1 \leq n \leq 12)$$

$$Q_n = 0 \qquad (\pi/2 \leq \phi \leq \pi) \qquad (44)$$

The absorbed portion is:

$$q_n = Q_n\ \alpha_i \qquad (2 \leq n \leq 12)$$

$$q_1 = Q_1\ \alpha_{1i} \qquad (45)$$

The reflected portion is:

$$\overline{Q}_n = Q_n\ (1 - \alpha_i) \qquad (2 \leq n \leq 12)$$

$$\overline{Q}_1 = Q_1\ (1 - \alpha_{1i}) \qquad (46)$$

The Reference 2 technique is used on these reflections.

E. Column Reradiation

The column nodes (14 to 16) are noted to have partially absorbed solar radiation and aperture reradiation. This radiation will be reemitted as infrared radiation. Let $\overline{Q}_j$ be the flux emitted by the column nodes. The quantity of the flux which strikes each cone node is:

$$Q_n = \sum_{j=14}^{16} \overline{Q}_j F_{j-n} \qquad (1 \leq n \leq 12) \qquad (47)$$

The absorbed portion is:

$$q_n = Q_n \epsilon_i \qquad (2 \leq n \leq 12)$$

$$q_1 = Q_1 \epsilon_{1i} \qquad (48)$$

The reflected portion is:

$$\overline{Q}_n = Q_n (1 - \epsilon_i) \qquad (2 \leq n \leq 12)$$

$$\overline{Q}_1 = Q_1 (1 - \epsilon_{1i}) \qquad (49)$$

The Reference 2 technique is used on these reflections.

TEMPERATURES

A. Cone

In the preceding sections, the absorbed fluxes for cone nodes 1 to 12 were computed, and include solar, aperture reradiation, planetary, albedo, and column reradiation. Let q_{ni} represent these absorbed fluxes for node n on the internal surface and q_{ne} on the external surface. Each cone node will reemit these absorbed fluxes plus any radiation it receives from the other cone nodes. The Reference 2 technique may be used to solve for the node temperatures taking into account internal reflections, and is represented as follows.

Let n' represent a dummy position corresponding to node n. An energy balance on node n then becomes:

$$\epsilon_n A_n \sigma T_n^4 + \frac{\epsilon_i A_n}{(1-\epsilon_i)} (\sigma T_n^4 - \sigma T_{n'}^4) = q_{ni} + q_{ne} \qquad (2 \leq n \leq 12)$$

$$\epsilon_1 A_1 \sigma T_1^4 + \frac{\epsilon_{1i} A_1}{(1-\epsilon_{1i})} (\sigma T_1^4 - \sigma T_{1'}^4) = q_{1i} + q_{1e} \qquad (50)$$

On the dummy positions, defining $T_{13'}$ as 0:

$$\frac{\epsilon_i A_n}{(1-\epsilon_i)} (\sigma T_n^4 - \sigma T_{n'}^4) = \sum_{m=1}^{13} A_n F_{n-m} (\sigma T_{n'}^4 - \sigma T_{m'}^4) \qquad (2 \leq n \leq 12)$$

$$\frac{\epsilon_{1i} A_1}{(1-\epsilon_{1i})} (\sigma T_1^4 - \sigma T_{1'}^4) = \sum_{m=1}^{13} A_1 F_{1-m} (\sigma T_{1'}^4 - \sigma T_{m'}^4) \qquad (51)$$

Equations (50) and (51) are seen to describe 24 linear equations with the unknowns being T_n^4 and $T_{n'}^4$ $(1 \leq n \leq 12)$. Simultaneous solution of these equations yields the values of T_n^4 and $T_{n'}^4$, and hence T_n.

In order to refine the node temperatures to account for circumferential variations, equation (50) is rewritten as:

$$(\epsilon_n + \epsilon_i) . A_n \sigma T_n^4 = q_{ni} + q_{ne} + q_{nr} \qquad (2 \leq n \leq 12) \qquad (52)$$

where q_{nr} is the cone emitted fluxes absorbed by node n; this term q_{nr} may be computed from equation (52). Since the cone interior is highly reflective, the internal fluxes Q_{ni} and Q_{nr} will have only slight circumferential variations. Circumferential temperature variations will therefore be caused primarily by variations in the q_{ne} term, which includes planetary and albedo radiation. Equation (52) may therefore be rewritten as:

$$(\epsilon_n + \epsilon_i)\sigma T_{n\theta}^4 = (q_{ni} + q_{nr})/A_n + 0.16\ C\ P_\theta \epsilon_n + 0.36\ C\ P_\theta \alpha_n \cos\phi \qquad (0 \leq \phi \leq \pi/2)$$

$$(\epsilon_n + \epsilon_i)\ T_{n\theta}^4 = (q_{ni} + q_{nr})/A_n + 0.16\ C\ P_\theta \epsilon_n \qquad (\pi/2 \leq \phi \leq \pi) \qquad (53)$$

Equation (53) may be used to compute circumferential temperatures on nodes 2 to 12. It is noted that neglecting circumferential variation of internal fluxes should result in a slightly conservative analysis, since the flux intensity will be slightly higher on the cool side (away from planet) than the warm side.

B. Column

The column temperatures may be estimated using the fluxes and cone temperatures derived throughout this report. The column nodes were previously noted to have absorbed solar and aperture reradiation fluxes reflected specularly from the cone. The column nodes may also absorb some planetary and albedo flux entering through the open end (node 13), the value of this flux being:

$$q_n = C\, P_{13}\, A_n\, F_{n-13}\, (0.16\, \epsilon_p + 0.36\, \alpha_p \cos \phi) \qquad (0 \leq \phi \leq \pi/2)(14 \leq n \leq 16)$$

$$q_n = C\, P_{13}\, A_n\, F_{n-13}\, (0.16\, \epsilon_p) \qquad (\pi/2 \leq \phi \leq \pi)(14 \leq n \leq 16) \quad (54)$$

A number of diffuse reflections, i.e. solar, aperture reradiation, planetary, and albedo, were noted to be bouncing around the cone. The column nodes will intercept a portion of these reflections which is evaluated with the Reference 2 technique. The effect of the cone temperatures on the column temperatures, and the column temperatures, may then be evaluated by again using Reference 2 .

LIST OF REFERENCES

1. ERG Eckert and RM Drake, Jr., "Heat and Mass Transfer," 2nd Edition, 1959.

2. AK Oppenheim, "Radiation Analysis by the Network Method," ASME Transaction, May, 1956. Pgs. 725-728.

APPENDIX C

THERMAL ANALYSIS

COMPUTER OUTPUT DATA SHEETS

GOODYEAR AEROSPACE CORPORATION

DEPARTMENT 462 - G

CONE AND COLUMN SOLAR CONCENTRATOR THERMAL ANALYSIS

CONTRACT NAS1 - 4341

CONE GEOMETRY

CONE HALF ANGLE IS 33.75 DEGREES RIM RADIUS OF CONE IS 30.0 FEET

NODE 1 IS BASE OF CONE NODES 2 TO 12 ARE CIRCULAR STRIPS OF CONE NODE 13 IS OPEN END OF CONE

NODE	1	2	3	4	5	6	7	8	9	10	11	12	13
MAXIMUM RADIUS - FEET	3.000	6.000	7.930	10.000	11.896	14.000	16.000	17.455	19.000	21.000	24.000	30.000	30.000
AREA - SQUARE FEET	30.76	152.68	152.03	209.88	234.75	308.10	339.28	275.23	318.49	452.38	763.39	1832.13	2827.43

COLUMN GEOMETRY

SECTION	RADIUS FEET	DISTANCE FROM APEX FEET	AREA SQUARE FEET
1	0.442	3.394 TO 10.847	20.70
2	0.772	10.847 TO 18.300	36.15
3	1.065	18.300 TO 33.207	99.75

APERTURE HAS A RADIUS OF 0.95 FEET AND IS LOCATED 43.579 FEET FROM APEX

CONE AND COLUMN THERMAL ANALYSIS

NO PLANET IN VICINITY OF CONCENTRATOR

RADIATION PROPERTIES

INTERIOR OF CONE

SOLAR ABSORPTANCE IS 0.120 SPECULAR REFLECTANCE IS 0.860 DIFFUSE REFLECTANCE IS 0.020 EMITTANCE IS 0.040

EXTERIOR OF CONE

NODE	2	3	4	5	6	7	8	9	10	11	12
SOLAR ABSORPTANCE	0.150	0.150	0.150	0.150	0.150	0.150	0.150	0.150	0.150	0.150	0.150
EMITTANCE	0.400	0.400	0.400	0.400	0.400	0.400	0.400	0.400	0.400	0.400	0.400

COLUMN

SOLAR ABSORPTANCE IS 0.100 SPECULAR REFLECTANCE IS 0.880 DIFFUSE REFLECTANCE IS 0.020 EMITTANCE IS 0.400

BASE PLATE

SOLAR ABSORPTANCE - EXTERNAL IS 0.900 INTERNAL IS 0.900 EMITTANCE - EXTERNAL IS 0.900 INTERNAL IS 0.900

CONE TEMPERATURES

NODE	2	3	4	5	6	7	8	9	10	11	12	AVERAGE
TEMPERATURE - F	101.9	113.9	125.5	139.3	156.8	180.7	203.7	16.2	11.9	5.2	-5.0	69.1

COLUMN TEMPERATURES

SECTION	1	2	3
TEMPERATURE - F	497.2	532.8	585.3

BASE TEMPERATURE IS 69.9 DEGREES FAHRENHEIT

CONE AND COLUMN THERMAL ANALYSIS

NO PLANET IN VICINITY OF CONCENTRATOR

RADIATION PROPERTIES

INTERIOR OF CONE

SOLAR ABSORPTANCE IS 0.120 SPECULAR REFLECTANCE IS 0.860 DIFFUSE REFLECTANCE IS 0.020 EMITTANCE IS 0.040

EXTERIOR OF CONE

NODE	2	3	4	5	6	7	8	9	10	11	12
SOLAR ABSORPTANCE	0.250	0.250	0.250	0.250	0.250	0.250	0.250	0.250	0.250	0.250	0.250
EMITTANCE	0.900	0.900	0.900	0.900	0.900	0.900	0.900	0.900	0.900	0.900	0.900

COLUMN

SOLAR ABSORPTANCE IS 0.100 SPECULAR REFLECTANCE IS 0.880 DIFFUSE REFLECTANCE IS 0.020 EMITTANCE IS 0.400

BASE PLATE

SOLAR ABSORPTANCE - EXTERNAL IS 0.900 INTERNAL IS 0.900 EMITTANCE - EXTERNAL IS 0.900 INTERNAL IS 0.900

CONE TEMPERATURES

NODE	2	3	4	5	6	7	8	9	10	11	12	AVERAGE
TEMPERATURE - F	4.4	14.3	24.1	35.5	50.0	69.8	88.9	-66.4	-69.9	-75.4	-83.8	-22.5

COLUMN TEMPERATURES

SECTION	1	2	3
TEMPERATURE - F	495.8	531.5	584.5

BASE TEMPERATURE IS 66.9 DEGREES FAHRENHEIT

CONE AND COLUMN THERMAL ANALYSIS

ORBITAL ALTITUDE IS 300.0 MILES ANGLE FROM PLANET - SUN LINE IS 0.0 DEGREES

RADIATION PROPERTIES

INTERIOR OF CONE

SOLAR ABSORPTANCE IS 0.120 SPECULAR REFLECTANCE IS 0.860 DIFFUSE REFLECTANCE IS 0.020 EMITTANCE IS 0.040

EXTERIOR OF CONE

NODE	2	3	4	5	6	7	8	9	10	11	12
SOLAR ABSORPTANCE	0.150	0.150	0.150	0.150	0.150	0.150	0.150	0.150	0.150	0.150	0.150
EMITTANCE	0.400	0.400	0.400	0.400	0.400	0.400	0.400	0.400	0.400	0.400	0.400

COLUMN

SOLAR ABSORPTANCE IS 0.100 SPECULAR REFLECTANCE IS 0.880 DIFFUSE REFLECTANCE IS 0.020 EMITTANCE IS 0.400

BASE PLATE

SOLAR ABSORPTANCE - EXTERNAL IS 0.900 INTERNAL IS 0.900 EMITTANCE - EXTERNAL IS 0.900 INTERNAL IS 0.900

CONE TEMPERATURES

NODE	2	3	4	5	6	7	8	9	10	11	12	AVERAGE
TEMPERATURE - F	150.0	159.0	168.3	179.5	193.9	214.2	234.1	87.0	84.2	79.8	73.3	124.2

COLUMN TEMPERATURES

SECTION	1	2	3
TEMPERATURE - F	501.9	534.1	586.0

BASE TEMPERATURE IS 148.1 DEGREES FAHRENHEIT

CONE AND COLUMN THERMAL ANALYSIS

ORBITAL ALTITUDE IS 300.0 MILES ANGLE FROM PLANET - SUN LINE IS 45.0 DEGREES

RADIATION PROPERTIES

INTERIOR OF CONE

SOLAR ABSORPTANCE IS 0.120 SPECULAR REFLECTANCE IS 0.860 DIFFUSE REFLECTANCE IS 0.020 EMITTANCE IS 0.040

EXTERIOR OF CONE

NODE	2	3	4	5	6	7	8	9	10	11	12
SOLAR ABSORPTANCE	0.150	0.150	0.150	0.150	0.150	0.150	0.150	0.150	0.150	0.150	0.150
EMITTANCE	0.400	0.400	0.400	0.400	0.400	0.400	0.400	0.400	0.400	0.400	0.400

COLUMN

SOLAR ABSORPTANCE IS 0.100 SPECULAR REFLECTANCE IS 0.880 DIFFUSE REFLECTANCE IS 0.020 EMITTANCE IS 0.400

BASE PLATE

SOLAR ABSORPTANCE - EXTERNAL IS 0.900 INTERNAL IS 0.900 EMITTANCE - EXTERNAL IS 0.900 INTERNAL IS 0.900

CONE TEMPERATURES IN DEGREES FAHRENHEIT

ANGLE AROUND CONE FROM PLANET - DEGREES	- NODE - 2	3	4	5	6	7	8	9	10	11	12	AVERAGE
0	164.0	172.6	181.3	191.9	205.6	224.9	244.0	106.5	103.9	100.0	94.3	140.4
15	162.9	171.6	180.4	191.0	204.7	224.1	243.2	105.1	102.5	98.6	92.8	139.2
30	159.7	168.5	177.5	188.2	202.1	221.7	241.1	100.8	98.2	94.2	88.2	135.7
45	155.2	164.2	173.3	184.2	198.4	218.3	237.9	94.6	91.9	87.7	81.6	130.5
60	149.8	159.1	168.4	179.6	194.1	214.3	234.3	87.3	84.5	80.1	73.7	124.5
75	144.1	153.6	163.2	174.6	189.5	210.1	230.4	79.3	76.4	71.8	65.1	117.9
90	138.4	148.1	157.9	169.7	184.8	205.9	226.6	71.2	68.1	63.3	56.2	111.4
105	132.9	142.9	153.0	165.0	180.5	202.0	223.0	63.3	60.0	55.1	47.6	105.1
120	128.1	138.3	148.6	160.9	176.7	198.5	219.8	56.2	52.8	47.6	39.8	99.4
135	124.1	134.5	145.0	157.5	173.5	195.7	217.3	50.2	46.7	41.3	33.2	94.8
150	121.1	131.7	142.3	155.0	171.2	193.6	215.4	45.8	42.2	36.6	28.3	91.3
165	119.3	130.0	140.7	153.5	169.8	192.3	214.2	43.0	39.4	33.7	25.2	89.2
180	118.7	129.4	140.2	153.0	169.3	191.9	213.9	42.1	38.4	32.7	24.2	88.5
AVERAGE	140.4	150.0	159.7	171.4	186.4	207.4	227.9	74.0	71.0	66.3	59.3	113.7

COLUMN TEMPERATURES

SECTION	1	2	3
TEMPERATURE - F	500.6	534.1	586.1

BASE TEMPERATURE IS 123.5 DEGREES FAHRENHEIT

CONE AND COLUMN THERMAL ANALYSIS

ORBITAL ALTITUDE IS 300.0 MILES ANGLE FROM PLANET - SUN LINE IS 90.0 DEGREES

RADIATION PROPERTIES

INTERIOR OF CONE

SOLAR ABSORPTANCE IS 0.120 SPECULAR REFLECTANCE IS 0.860 DIFFUSE REFLECTANCE IS 0.020 EMITTANCE IS 0.040

EXTERIOR OF CONE

NODE	2	3	4	5	6	7	8	9	10	11	12
SOLAR ABSORPTANCE	0.150	0.150	0.150	0.150	0.150	0.150	0.150	0.150	0.150	0.150	0.150
EMITTANCE	0.400	0.400	0.400	0.400	0.400	0.400	0.400	0.400	0.400	0.400	0.400

COLUMN

SOLAR ABSORPTANCE IS 0.100 SPECULAR REFLECTANCE IS 0.880 DIFFUSE REFLECTANCE IS 0.020 EMITTANCE IS 0.400

BASE PLATE

SOLAR ABSORPTANCE - EXTERNAL IS 0.900 INTERNAL IS 0.900 EMITTANCE - EXTERNAL IS 0.900 INTERNAL IS 0.900

CONE TEMPERATURES IN DEGREES FAHRENHEIT

ANGLE AROUND CONE FROM PLANET - DEGREES	- NODE - 2	3	4	5	6	7	8	9	10	11	12	AVERAGE
0	138.1	148.1	158.0	169.7	184.9	206.0	226.7	71.4	68.3	63.5	56.5	111.5
15	137.2	147.2	157.2	169.0	184.2	205.4	226.1	70.1	67.0	62.2	55.0	110.5
30	134.7	144.9	154.9	166.8	182.2	203.6	224.4	66.5	63.3	58.4	51.1	107.6
45	131.0	141.4	151.6	163.7	179.3	200.9	222.0	61.1	57.8	52.8	45.3	103.3
60	126.6	137.2	147.6	159.9	175.8	197.8	219.2	54.6	51.2	46.0	38.1	98.2
75	121.8	132.6	143.3	155.9	172.1	194.4	216.1	47.5	43.9	38.4	30.2	92.7
90	117.1	128.2	139.0	151.9	168.4	191.1	213.1	40.3	36.6	30.8	22.2	87.1
105	112.8	124.1	135.1	148.3	165.0	188.1	210.4	33.6	29.7	23.7	14.7	82.0
120	109.1	120.6	131.9	145.2	162.2	185.6	208.1	27.8	23.8	17.6	8.2	77.7
135	106.4	118.1	129.5	143.0	160.2	183.7	206.4	23.5	19.4	13.0	3.3	74.5
150	104.7	116.5	128.0	141.6	158.9	182.6	205.4	20.8	16.6	10.0	0.2	72.5
165	103.9	115.7	127.3	140.9	158.3	182.0	204.9	19.5	15.2	8.7	-1.3	71.5
180	103.7	115.5	127.1	140.8	158.1	181.9	204.8	19.1	14.9	8.3	-1.7	71.3
AVERAGE	119.3	130.2	141.0	153.7	170.1	192.6	214.5	43.6	39.9	34.3	25.9	89.6

COLUMN TEMPERATURES

SECTION	1	2	3
TEMPERATURE - F	500.4	535.7	587.8

BASE TEMPERATURE IS 88.2 DEGREES FAHRENHEIT

CONE AND COLUMN THERMAL ANALYSIS

ORBITAL ALTITUDE IS 300.0 MILES ANGLE FROM PLANET - SUN LINE IS 180.0 DEGREES

RADIATION PROPERTIES

INTERIOR OF CONE

SOLAR ABSORPTANCE IS 0.120 SPECULAR REFLECTANCE IS 0.860 DIFFUSE REFLECTANCE IS 0.020 EMITTANCE IS 0.040

EXTERIOR OF CONE

NODE	2	3	4	5	6	7	8	9	10	11	12
SOLAR ABSORPTANCE	0.150	0.150	0.150	0.150	0.150	0.150	0.150	0.150	0.150	0.150	0.150
EMITTANCE	0.400	0.400	0.400	0.400	0.400	0.400	0.400	0.400	0.400	0.400	0.400

COLUMN

SOLAR ABSORPTANCE IS 0.100 SPECULAR REFLECTANCE IS 0.880 DIFFUSE REFLECTANCE IS 0.020 EMITTANCE IS 0.400

BASE PLATE

SOLAR ABSORPTANCE - EXTERNAL IS 0.900 INTERNAL IS 0.900 EMITTANCE - EXTERNAL IS 0.900 INTERNAL IS 0.900

CONE TEMPERATURES

NODE	2	3	4	5	6	7	8	9	10	11	12	AVERAGE
TEMPERATURE - F	-188.7	-187.1	-186.6	-186.2	-185.9	-185.7	-185.5	-185.4	-185.2	-185.0	-184.8	-185.4

COLUMN TEMPERATURES

SECTION	1	2	3
TEMPERATURE - F	-48.0	-35.1	-31.7

BASE TEMPERATURE IS -105.2 DEGREES FAHRENHEIT

CONE AND COLUMN THERMAL ANALYSIS

ORBITAL ALTITUDE IS 300.0 MILES ANGLE FROM PLANET - SUN LINE IS 0.0 DEGREES

RADIATION PROPERTIES

INTERIOR OF CONE

SOLAR ABSORPTANCE IS 0.120 SPECULAR REFLECTANCE IS 0.860 DIFFUSE REFLECTANCE IS 0.020 EMITTANCE IS 0.040

EXTERIOR OF CONE

NODE	2	3	4	5	6	7	8	9	10	11	12
SOLAR ABSORPTANCE	0.250	0.250	0.250	0.250	0.250	0.250	0.250	0.250	0.250	0.250	0.250
EMITTANCE	0.900	0.900	0.900	0.900	0.900	0.900	0.900	0.900	0.900	0.900	0.900

COLUMN

SOLAR ABSORPTANCE IS 0.100 SPECULAR REFLECTANCE IS 0.880 DIFFUSE REFLECTANCE IS 0.020 EMITTANCE IS 0.400

BASE PLATE

SOLAR ABSORPTANCE - EXTERNAL IS 0.900 INTERNAL IS 0.900 EMITTANCE - EXTERNAL IS 0.900 INTERNAL IS 0.900

CONE TEMPERATURES

NODE	2	3	4	5	6	7	8	9	10	11	12	AVERAGE
TEMPERATURE - F	75.3	81.6	88.1	96.1	106.5	121.2	135.9	33.5	31.7	29.0	25.0	57.9

COLUMN TEMPERATURES

SECTION	1	2	3
TEMPERATURE - F	500.4	532.8	585.1

BASE TEMPERATURE IS 146.0 DEGREES FAHRENHEIT

CONE AND COLUMN THERMAL ANALYSIS

ORBITAL ALTITUDE IS 300.0 MILES ANGLE FROM PLANET - SUN LINE IS 45.0 DEGREES

RADIATION PROPERTIES

INTERIOR OF CONE

SOLAR ABSORPTANCE IS 0.120 SPECULAR REFLECTANCE IS 0.860 DIFFUSE REFLECTANCE IS 0.020 EMITTANCE IS 0.040

EXTERIOR OF CONE

NODE	2	3	4	5	6	7	8	9	10	11	12
SOLAR ABSORPTANCE	0.250	0.250	0.250	0.250	0.250	0.250	0.250	0.250	0.250	0.250	0.250
EMITTANCE	0.900	0.900	0.900	0.900	0.900	0.900	0.900	0.900	0.900	0.900	0.900

COLUMN

SOLAR ABSORPTANCE IS 0.100 SPECULAR REFLLCTANCE IS 0.880 DIFFUSE REFLECTANCE IS 0.020 EMITTANCE IS 0.400

BASE PLATE

SOLAR ABSORPTANCE - EXTERNAL IS 0.900 INTERNAL IS 0.900 EMITTANCE - EXTERNAL IS 0.900 INTERNAL IS 0.900

CONE TEMPERATURES IN DEGREES FAHRENHEIT

ANGLE AROUND CONE FROM PLANET - DEGREES	- NODE - 2	3	4	5	6	7	8	9	10	11	12	AVERAGE
0	95.7	101.5	107.4	114.6	124.1	137.6	151.1	59.3	57.8	55.5	52.1	80.5
15	94.3	100.1	106.0	113.3	122.8	136.4	150.1	57.6	56.0	53.7	50.2	79.0
30	90.0	96.0	102.0	109.4	119.2	133.0	146.9	52.3	50.7	48.3	44.7	74.3
45	83.8	89.9	96.2	103.8	113.8	128.0	142.2	44.5	42.8	40.3	36.6	67.5
60	76.4	82.8	89.3	97.2	107.5	122.2	136.8	35.2	33.4	30.7	26.7	59.3
75	68.3	75.0	81.8	90.0	100.8	115.9	131.0	24.8	22.9	20.1	15.8	50.4
90	60.0	67.0	74.1	82.7	93.9	109.6	125.2	14.0	12.0	8.9	4.4	41.2
105	52.1	59.4	66.8	75.7	87.3	103.6	119.6	3.4	1.2	-2.1	-7.0	32.3
120	44.8	52.4	60.2	69.4	81.4	98.2	114.7	-6.5	-8.8	-12.3	-17.6	24.1
135	38.8	46.7	54.6	64.2	76.5	93.7	110.6	-14.9	-17.4	-21.1	-26.7	17.2
150	34.2	42.3	50.5	60.3	72.9	90.4	107.6	-21.4	-24.0	-27.9	-33.7	12.0
165	31.4	39.7	48.0	57.9	70.7	88.4	105.7	-25.4	-28.1	-32.1	-38.1	8.8
180	30.5	38.8	47.1	57.1	69.9	87.7	105.1	-26.8	-29.5	-33.5	-39.6	7.7
AVERAGE	62.9	69.8	76.8	85.3	96.3	111.8	127.2	17.8	15.9	12.8	8.4	44.4

COLUMN TEMPERATURES

SECTION	1	2	3
TEMPERATURE - F	499.2	532.8	585.3

BASE TEMPERATURE IS 121.2 DEGREES FAHRENHEIT

CONE AND COLUMN THERMAL ANALYSIS

ORBITAL ALTITUDE IS 300.0 MILES ANGLE FROM PLANET - SUN LINE IS 90.0 DEGREES

RADIATION PROPERTIES

INTERIOR OF CONE

SOLAR ABSORPTANCE IS 0.120 SPECULAR REFLECTANCE IS 0.860 DIFFUSE REFLECTANCE IS 0.020 EMITTANCE IS 0.040

EXTERIOR OF CONE

NODE	2	3	4	5	6	7	8	9	10	11	12
SOLAR ABSORPTANCE	0.250	0.250	0.250	0.250	0.250	0.250	0.250	0.250	0.250	0.250	0.250
EMITTANCE	0.900	0.900	0.900	0.900	0.900	0.900	0.900	0.900	0.900	0.900	0.900

COLUMN

SOLAR ABSORPTANCE IS 0.100 SPECULAR REFLECTANCE IS 0.880 DIFFUSE REFLECTANCE IS 0.020 EMITTANCE IS 0.400

BASE PLATE

SOLAR ABSORPTANCE - EXTERNAL IS 0.900 INTERNAL IS 0.900 EMITTANCE - EXTERNAL IS 0.900 INTERNAL IS 0.900

CONE TEMPERATURES IN DEGREES FAHRENHEIT

ANGLE AROUND CONE FROM PLANET - DEGREES	- NODE - 2	3	4	5	6	7	8	9	10	11	12	AVERAGE
0	64.6	71.5	78.5	86.9	97.8	113.2	128.5	20.3	18.4	15.4	11.1	46.5
15	63.2	70.2	77.2	85.7	96.7	112.2	127.5	18.4	16.5	13.5	9.1	45.0
30	59.2	66.4	73.6	82.2	93.4	109.2	124.8	13.3	11.2	8.1	3.6	40.6
45	53.3	60.7	68.1	77.0	88.6	104.7	120.7	5.4	3.3	0.1	-4.8	34.0
60	46.1	53.9	61.6	70.8	82.7	99.4	115.7	-4.3	-6.6	-10.1	-15.2	25.9
75	38.2	46.3	54.4	64.0	76.3	93.5	110.4	-15.3	-17.7	-21.5	-27.1	16.9
90	30.2	38.7	47.1	57.1	69.9	87.7	105.1	-26.8	-29.4	-33.5	-39.6	7.7
105	22.6	31.5	40.3	50.7	64.0	82.4	100.2	-37.9	-40.8	-45.2	-51.8	-1.1
120	16.1	25.4	34.4	45.2	58.9	77.8	96.1	-47.7	-50.8	-55.6	-62.7	-8.6
135	11.2	20.7	30.1	41.1	55.2	74.4	93.1	-55.4	-58.7	-63.7	-71.3	-14.4
150	8.1	17.8	27.3	38.5	52.8	72.3	91.2	-60.4	-63.7	-69.0	-76.9	-18.1
165	6.6	16.4	26.0	37.3	51.7	71.3	90.3	-62.8	-66.2	-71.6	-79.7	-19.9
180	6.2	16.0	25.7	37.0	51.4	71.1	90.0	-63.4	-66.8	-72.2	-80.4	-20.3
AVERAGE	33.9	42.2	50.4	60.2	72.8	90.4	107.5	-21.5	-24.0	-27.9	-33.8	11.9

COLUMN TEMPERATURES

SECTION	1	2	3
TEMPERATURE - F	499.1	534.4	587.0

BASE TEMPERATURE IS 85.4 DEGREES FAHRENHEIT

CONE AND COLUMN THERMAL ANALYSIS

ORBITAL ALTITUDE IS 300.0 MILES ANGLE FROM PLANET - SUN LINE IS 180.0 DEGREES

RADIATION PROPERTIES

INTERIOR OF CONE

SOLAR ABSORPTANCE IS 0.120 SPECULAR REFLECTANCE IS 0.860 DIFFUSE REFLECTANCE IS 0.020 EMITTANCE IS 0.040

EXTERIOR OF CONE

NODE	2	3	4	5	6	7	8	9	10	11	12
SOLAR ABSORPTANCE	0.250	0.250	0.250	0.250	0.250	0.250	0.250	0.250	0.250	0.250	0.250
EMITTANCE	0.900	0.900	0.900	0.900	0.900	0.900	0.900	0.900	0.900	0.900	0.900

COLUMN

SOLAR ABSORPTANCE IS 0.100 SPECULAR REFLECTANCE IS 0.880 DIFFUSE REFLECTANCE IS 0.020 EMITTANCE IS 0.400

BASE PLATE

SOLAR ABSORPTANCE - EXTERNAL IS 0.900 INTERNAL IS 0.900 EMITTANCE - EXTERNAL IS 0.900 INTERNAL IS 0.900

CONE TEMPERATURES

NODE	2	3	4	5	6	7	8	9	10	11	12	AVERAGE
TEMPERATURE - F	-208.2	-207.3	-207.0	-206.7	-206.6	-206.4	-206.3	-206.2	-206.1	-206.0	-205.9	-206.2

COLUMN TEMPERATURES

SECTION	1	2	3
TEMPERATURE - F	-48.4	-35.6	-32.1

BASE TEMPERATURE IS -105.4 DEGREES FAHRENHEIT

CONE AND COLUMN THERMAL ANALYSIS

ORBITAL ALTITUDE IS 300.0 MILES ANGLE FROM PLANET - SUN LINE IS 0.0 DEGREES

RADIATION PROPERTIES

INTERIOR OF CONE

SOLAR ABSORPTANCE IS 0.120 SPECULAR REFLECTANCE IS 0.860 DIFFUSE REFLECTANCE IS 0.020 EMITTANCE IS 0.040

EXTERIOR OF CONE

NODE	2	3	4	5	6	7	8	9	10	11	12
SOLAR ABSORPTANCE	0.900	0.900	0.900	0.900	0.900	0.900	0.900	0.900	0.900	0.900	0.900
EMITTANCE	0.900	0.900	0.900	0.900	0.900	0.900	0.900	0.900	0.900	0.900	0.900

COLUMN

SOLAR ABSORPTANCE IS 0.100 SPECULAR REFLECTANCE IS 0.880 DIFFUSE REFLECTANCE IS 0.020 EMITTANCE IS 0.400

BASE PLATE

SOLAR ABSORPTANCE - EXTERNAL IS 0.900 INTERNAL IS 0.900 EMITTANCE - EXTERNAL IS 0.900 INTERNAL IS 0.900

CONE TEMPERATURES

NODE	2	3	4	5	6	7	8	9	10	11	12	AVERAGE
TEMPERATURE - F	125.4	130.2	135.3	141.5	149.8	161.7	173.8	94.6	93.3	91.4	88.6	112.2

COLUMN TEMPERATURES

SECTION	1	2	3
TEMPERATURE - F	501.3	533.6	585.6

BASE TEMPERATURE IS 147.2 DEGREES FAHRENHEIT

CONE AND COLUMN THERMAL ANALYSIS

ORBITAL ALTITUDE IS 300.0 MILES ANGLE FROM PLANET - SUN LINE IS 45.0 DEGREES

RADIATION PROPERTIES

INTERIOR OF CONE

SOLAR ABSORPTANCE IS 0.120 SPECULAR REFLECTANCE IS 0.860 DIFFUSE REFLECTANCE IS 0.020 EMITTANCE IS 0.040

EXTERIOR OF CONE

NODE	2	3	4	5	6	7	8	9	10	11	12
SOLAR ABSORPTANCE	0.900	0.900	0.900	0.900	0.900	0.900	0.900	0.900	0.900	0.900	0.900
EMITTANCE	0.900	0.900	0.900	0.900	0.900	0.900	0.900	0.900	0.900	0.900	0.900

COLUMN

SOLAR ABSORPTANCE IS 0.100 SPECULAR REFLECTANCE IS 0.880 DIFFUSE REFLECTANCE IS 0.020 EMITTANCE IS 0.400

BASE PLATE

SOLAR ABSORPTANCE - EXTERNAL IS 0.900 INTERNAL IS 0.900 EMITTANCE - EXTERNAL IS 0.900 INTERNAL IS 0.900

CONE TEMPERATURES IN DEGREES FAHRENHEIT

ANGLE AROUND CONE FROM PLANET - DEGREES	- NODE - 2	3	4	5	6	7	8	9	10	11	12	AVERAGE
0	145.1	149.5	154.2	159.9	167.4	178.4	189.6	117.6	116.5	114.8	112.4	133.4
15	143.0	147.6	152.2	158.0	165.6	176.7	188.0	115.3	114.2	112.5	110.0	131.2
30	137.1	141.7	146.5	152.4	160.3	171.6	183.2	108.4	107.3	105.5	102.9	124.9
45	128.2	133.1	138.1	144.3	152.4	164.2	176.2	98.1	96.9	95.0	92.3	115.5
60	117.6	122.8	128.1	134.5	143.1	155.4	167.9	85.7	84.4	82.3	79.4	104.1
75	106.0	111.4	117.0	123.9	132.9	145.8	158.9	71.7	70.3	68.1	64.9	91.5
90	93.8	99.6	105.6	112.8	122.4	136.0	149.6	56.9	55.3	52.9	49.5	78.3
105	81.8	88.0	94.3	102.0	112.1	126.4	140.7	42.0	40.3	37.7	33.9	65.2
120	70.7	77.3	84.0	92.1	102.8	117.8	132.7	27.9	26.0	23.2	19.0	53.0
135	61.3	68.2	75.3	83.8	94.9	110.5	126.0	15.6	13.5	10.5	6.0	42.5
150	54.1	61.3	68.6	77.5	88.9	105.0	121.0	6.0	3.8	0.6	-4.2	34.5
165	49.6	57.0	64.5	73.5	85.3	101.7	117.9	-0.1	-2.3	-5.7	-10.7	29.4
180	48.0	55.5	63.1	72.2	84.0	100.5	116.8	-2.2	-4.4	-7.9	-13.0	27.7
AVERAGE	98.1	103.7	109.6	116.7	126.1	139.4	152.9	62.1	60.6	58.3	54.9	83.0

COLUMN TEMPERATURES

SECTION	1	2	3
TEMPERATURE - F	499.8	533.3	585.6

BASE TEMPERATURE IS 122.1 DEGREES FAHRENHEIT

CONE AND COLUMN THERMAL ANALYSIS

ORBITAL ALTITUDE IS 300.0 MILES ANGLE FROM PLANET - SUN LINE IS 0.0 DEGREES

RADIATION PROPERTIES

INTERIOR OF CONE

SOLAR ABSORPTANCE IS 0.150 SPECULAR REFLECTANCE IS 0.800 DIFFUSE REFLECTANCE IS 0.050 EMITTANCE IS 0.400

EXTERIOR OF CONE

NODE	2	3	4	5	6	7	8	9	10	11	12
SOLAR ABSORPTANCE	0.150	0.150	0.150	0.150	0.150	0.150	0.150	0.150	0.150	0.150	0.150
EMITTANCE	0.050	0.050	0.050	0.050	0.050	0.050	0.050	0.050	0.050	0.050	0.050

COLUMN

SOLAR ABSORPTANCE IS 0.150 SPECULAR REFLECTANCE IS 0.800 DIFFUSE REFLECTANCE IS 0.050 EMITTANCE IS 0.400

BASE PLATE

SOLAR ABSORPTANCE - EXTERNAL IS 0.150 INTERNAL IS 0.150 EMITTANCE - EXTERNAL IS 0.050 INTERNAL IS 0.400

CONE TEMPERATURES

NODE	2	3	4	5	6	7	8	9	10	11	12	AVERAGE
TEMPERATURE - F	303.5	295.9	290.6	286.2	284.8	288.2	294.4	175.8	159.8	138.3	106.2	196.6

COLUMN TEMPERATURES

SECTION	1	2	3
TEMPERATURE - F	606.4	638.1	686.9

BASE TEMPERATURE IS 254.0 DEGREES FAHRENHEIT

CONE AND COLUMN THERMAL ANALYSIS

ORBITAL ALTITUDE IS 300.0 MILES ANGLE FROM PLANET - SUN LINE IS 45.0 DEGREES

RADIATION PROPERTIES

INTERIOR OF CONE

SOLAR ABSORPTANCE IS 0.150 SPECULAR REFLECTANCE IS 0.800 DIFFUSE REFLECTANCE IS 0.050 EMITTANCE IS 0.400

EXTERIOR OF CONE

NODE	2	3	4	5	6	7	8	9	10	11	12
SOLAR ABSORPTANCE	0.150	0.150	0.150	0.150	0.150	0.150	0.150	0.150	0.150	0.150	0.150
EMITTANCE	0.050	0.050	0.050	0.050	0.050	0.050	0.050	0.050	0.050	0.050	0.050

COLUMN

SOLAR ABSORPTANCE IS 0.150 SPECULAR REFLECTANCE IS 0.800 DIFFUSE REFLECTANCE IS 0.050 EMITTANCE IS 0.400

BASE PLATE

SOLAR ABSORPTANCE - EXTERNAL IS 0.150 INTERNAL IS 0.150 EMITTANCE - EXTERNAL IS 0.050 INTERNAL IS 0.400

CONE TEMPERATURES IN DEGREES FAHRENHEIT

ANGLE AROUND CONE FROM PLANET - DEGREES	- NODE - 2	3	4	5	6	7	8	9	10	11	12	AVERAGE
0	303.5	296.3	291.2	287.1	285.9	289.4	295.8	178.3	162.7	141.9	111.0	198.9
15	303.2	296.0	290.9	286.8	285.6	289.2	295.5	177.9	162.3	141.3	110.4	198.5
30	302.4	295.2	290.1	286.0	284.8	288.4	294.8	176.6	160.9	139.8	108.6	197.3
45	301.4	294.1	289.0	284.9	283.7	287.2	293.7	174.7	158.9	137.6	106.0	195.7
60	300.1	292.8	287.7	283.6	282.3	285.9	292.4	172.6	156.6	135.0	103.0	193.7
75	298.8	291.5	286.3	282.2	280.9	284.6	291.1	170.4	154.1	132.3	99.8	191.7
90	297.6	290.2	285.0	280.8	279.6	283.2	289.8	168.1	151.7	129.7	96.6	189.7
105	296.4	289.0	283.8	279.6	278.3	282.0	288.5	166.1	149.5	127.2	93.6	187.8
120	295.4	288.0	282.7	278.5	277.2	280.9	287.5	164.3	147.5	125.0	91.0	186.2
135	294.6	287.1	281.8	277.6	276.3	280.0	286.6	162.8	146.0	123.2	88.9	184.9
150	294.0	286.5	281.2	276.9	275.7	279.4	286.0	161.7	144.8	121.9	87.3	183.9
165	293.6	286.1	280.8	276.6	275.3	279.0	285.6	161.1	144.1	121.1	86.4	183.3
180	293.5	286.0	280.7	276.4	275.2	278.9	285.5	160.9	143.9	120.8	86.0	183.1
AVERAGE	298.0	290.7	285.4	281.3	280.1	283.7	290.2	168.9	152.6	130.6	97.7	190.4

COLUMN TEMPERATURES

SECTION	1	2	3
TEMPERATURE - F	605.3	637.4	686.5

BASE TEMPERATURE IS 243.6 DEGREES FAHRENHEIT

CONE AND COLUMN THERMAL ANALYSIS

ORBITAL ALTITUDE IS 300.0 MILES ANGLE FROM PLANET - SUN LINE IS 45.0 DEGREES

RADIATION PROPERTIES

INTERIOR OF CONE

SOLAR ABSORPTANCE IS 0.150 SPECULAR REFLECTANCE IS 0.800 DIFFUSE REFLECTANCE IS 0.050 EMITTANCE IS 0.400

EXTERIOR OF CONE

NODE	2	3	4	5	6	7	8	9	10	11	12
SOLAR ABSORPTANCE	0.150	0.150	0.150	0.150	0.150	0.150	0.150	0.150	0.150	0.150	0.150
EMITTANCE	0.400	0.400	0.400	0.400	0.400	0.400	0.400	0.400	0.400	0.400	0.400

COLUMN

SOLAR ABSORPTANCE IS 0.150 SPECULAR REFLECTANCE IS 0.800 DIFFUSE REFLECTANCE IS 0.050 EMITTANCE IS 0.400

BASE PLATE

SOLAR ABSORPTANCE - EXTERNAL IS 0.150 INTERNAL IS 0.150 EMITTANCE - EXTERNAL IS 0.400 INTERNAL IS 0.400

CONE TEMPERATURES IN DEGREES FAHRENHEIT

ANGLE AROUND CONE FROM PLANET - DEGREES	- NODE - 2	3	4	5	6	7	8	9	10	11	12	AVERAGE
0	181.7	179.7	179.1	179.0	181.2	187.3	195.1	96.5	86.3	72.8	53.4	114.2
15	181.2	179.2	178.5	178.5	180.7	186.8	194.6	95.6	85.4	71.8	52.4	113.4
30	179.6	177.6	176.9	176.9	179.1	185.3	193.1	93.2	82.9	69.0	49.3	111.2
45	177.3	175.3	174.6	174.6	176.8	183.1	190.9	89.7	79.1	65.0	44.7	108.0
60	174.7	172.6	172.0	171.9	174.2	180.5	188.5	85.6	74.8	60.3	39.4	104.3
75	171.9	169.6	169.2	169.1	171.4	177.8	185.9	81.2	70.1	55.2	33.6	100.3
90	169.2	167.1	166.4	166.3	168.7	175.1	183.3	76.8	65.4	50.1	27.8	96.4
105	166.6	164.5	163.8	163.7	166.1	172.7	180.9	72.7	61.0	45.2	22.2	92.6
120	164.4	162.2	161.5	161.4	163.9	170.5	178.8	69.0	57.1	40.9	17.3	89.3
135	162.6	160.4	159.7	159.6	162.0	168.7	177.1	66.0	53.8	37.4	13.1	86.7
150	161.2	159.0	158.3	158.2	160.7	167.4	175.9	63.7	51.4	34.7	10.1	84.7
165	160.4	158.2	157.5	157.4	159.9	166.6	175.1	62.4	50.0	33.1	8.2	83.5
180	160.1	157.9	157.2	157.1	159.6	166.4	174.9	61.9	49.5	32.6	7.6	83.1
AVERAGE	170.1	168.0	167.3	167.3	169.6	176.1	184.2	78.3	67.1	51.9	29.8	97.7

COLUMN TEMPERATURES

SECTION	1	2	3
TEMPERATURE - F	584.8	621.7	677.6

BASE TEMPERATURE IS 122.2 DEGREES FAHRENHEIT

CONE AND COLUMN THERMAL ANALYSIS

ORBITAL ALTITUDE IS 300.0 MILES ANGLE FROM PLANET - SUN LINE IS 45.0 DEGREES

RADIATION PROPERTIES

INTERIOR OF CONE

SOLAR ABSORPTANCE IS 0.150 SPECULAR REFLECTANCE IS 0.300 DIFFUSE REFLECTANCE IS 0.050 EMITTANCE IS 0.400

EXTERIOR OF CONE

NODE	2	3	4	5	6	7	8	9	10	11	12
SOLAR ABSORPTANCE	0.900	0.900	0.900	0.900	0.900	0.900	0.900	0.900	0.900	0.900	0.900
EMITTANCE	0.900	0.900	0.900	0.900	0.900	0.900	0.900	0.900	0.900	0.900	0.900

COLUMN

SOLAR ABSORPTANCE IS 0.150 SPECULAR REFLECTANCE IS 0.800 DIFFUSE REFLECTANCE IS 0.050 EMITTANCE IS 0.400

BASE PLATE

SOLAR ABSORPTANCE - EXTERNAL IS 0.900 INTERNAL IS 0.150 EMITTANCE - EXTERNAL IS 0.900 INTERNAL IS 0.400

CONE TEMPERATURES IN DEGREES FAHRENHEIT

ANGLE AROUND CONE FROM PLANET - DEGREES	- NODE - 2	3	4	5	6	7	8	9	10	11	12	AVERAGE
0	157.1	156.4	156.6	157.1	159.2	164.0	169.7	106.9	101.5	94.4	84.6	117.3
15	155.7	155.0	155.2	155.8	157.9	162.6	168.4	105.1	99.6	92.5	82.6	115.6
30	151.7	150.9	151.1	151.7	153.9	158.7	164.6	99.8	94.2	86.9	76.7	110.7
45	145.8	145.0	145.2	145.8	148.1	153.0	159.1	92.1	86.2	78.5	67.9	103.4
60	138.9	138.1	138.3	138.9	141.2	146.4	152.6	82.9	76.7	68.6	57.3	94.7
75	131.4	130.5	130.8	131.4	133.8	139.1	145.6	72.7	66.2	57.5	45.4	85.2
90	123.8	122.9	123.1	123.8	126.3	131.8	138.5	62.2	55.2	46.0	33.0	75.4
105	116.5	115.6	115.8	116.5	119.1	124.8	131.8	51.9	44.5	34.6	20.7	65.9
120	109.9	109.0	109.2	109.9	112.6	118.5	125.7	42.4	34.6	24.1	9.1	57.1
135	104.4	103.5	103.7	104.5	107.2	113.3	120.7	34.4	26.1	15.0	-0.8	49.8
150	100.4	99.4	99.7	100.4	103.2	109.5	117.0	28.3	19.7	8.1	-8.5	44.3
165	97.9	96.9	97.2	97.9	100.8	107.1	114.7	24.5	15.7	3.8	-13.3	40.8
180	97.1	96.0	96.3	97.1	99.9	106.3	113.9	23.2	14.3	2.4	-14.9	39.7
AVERAGE	126.4	125.6	125.8	126.5	128.9	134.4	141.0	65.9	59.1	50.0	37.4	78.8

COLUMN TEMPERATURES

SECTION	1	2	3
TEMPERATURE - F	580.2	617.9	675.6

BASE TEMPERATURE IS 101.2 DEGREES FAHRENHEIT